MEASUREMENTS AND REMOTE SESING SESSIONS

CROSS-ACTIVATION OF AIR POLLUTANTS IN URBAN ENVIRONMENT

Krzysztof J. Rudzinski,[1] Józef Ziajka,[1] Lech Gmachowski,[1,2] Edyta Szeremeta [1] - [1] Institute of Physical Chemistry of the Polish Academy of Sciences, Warsaw, Poland, [2] Warsaw University of Technology, Institute of Chemistry, Płock, Poland

DERIVING HIGH RESOLUTION SPATIAL CROSS SECTIONS OF TROPOSPHERIC TRACE GASES FROM AUTOMOBILE MULTI AXIS DIFFERENTIAL OPTICAL ABSORPTION SPECTROSCOPY TECHNIQUE (AUTOMAX-DOAS)

O.W.Ibrahim, T.Wagner ,T.Stein, R.Sinreich and U.Platt - Instiut Für Umwelphysik , Universität Heidelberg, Germany.

AMBIENT AIR LEVELS OF VOLATILE ORGANIC COMPOUNDS (VOC) AND NITROGEN DIOXIDE (NO_2) IN URBAN AIR OF PAMPLONA, SPAIN

Parra, M.A., Bermejo, R., Elustondo, D., Santamaría, J.M. - Laboratorio Integrado de Calidad Ambiental (LICA), Departamento de Química y Edafología, Universidad de Navarra, Irunlarrea s/n, 31080, Pamplona (Spain)

HEAVY METAL CONCENTRATIONS AT THREE FRENCH SITES UNDER INDUSTRIAL AND TRAFFIC INFLUENCES, AND RURAL CONDITIONS
PART I: ATMOSPHERIC PM10 PARTICLES COMPOSITION

A. Gaudry[1], M. Moskura[1], A. Senhou[1], S. Ayrault[2], F. Denayer[3], N. Bernard[4] - 1-Laboratoire Pierre Sue, CNRS/CEA, CEA de Saclay-91191-Gif sur Yvette-France, 2-Laboratoire des Sciences du Climat et de l'Environnement-91198-Gif sur Yvette-France, 3-Institut Lillois d'Ingénierie de la Santé, 59120-Loos-France 4-Laboratoire de Biologie Environnementale, Université de Franche Comté-25030-Besançon-France

TOMOGRAPHIC LP-DOAS MEASUREMENTS OF 2D TRACE GAS DISTRIBUTIONS ABOVE THE CITY OF HEIDELBERG, GERMANY

Denis Poehler, Andreas Hartl and Ulrich Platt - Institute of Environmental Physics, University of Heidelberg, Heidelberg, Germany

SATELLITE-DERIVED DETERMINATION OF AEROSOL OPTICAL THICKNESS FOR AIR POLLUTION MONITORING: A SIMPLIFIED ALGORITHM

Hadjimitsis D.[1, 2, 3], Vryonides P.[1], Themistokleous K.[1, 4], Toulios L.[5]and Clayton C.R.I[2] - [1] Frederick Institute of Technology, Department of Civil Engineering, 7, Y. Frederickou St., Palouriotisa, Nicosia 1036, Cyprus, [2] University of Southampton, Department of Civil & Environmental Engineering, Highfield, Southampton SO17 1BJ, UK, [3] Cyprus Research Centre for Remote Sensing & GIS, Hadjimitsis Consultants, P.O.Box 60055, Paphos, Cyprus, [4]ARCHISYSTEMS LTD, Limassol, Cyprus., [5]National Agricultural Research Foundation (NAGREF) Theofrastou str. 1 41335 Larissa Greece

APPLICATIONS OF SATELLITE REMOTE SENSING & GIS TO URBAN AIR-QUALITY MONITORING IN CYPRUS: POTENTIAL Solutions and Suggestions

Hadjimitsis D.G.[1, 2, 3], Themistokleous K.[4], Vryonides P[1], Toulios L.[5] and Clayton C.R.I[2]
[1] Frederick Institute of Technology, School of Applied Sciences, 7, Y. Frederickou St., Palouriotisa, Nicosia 1036, Cyprus, [2] University of Southampton, Department of Civil & Environmental Engineering, Highfield, Southampton SO17 1BJ, UK, [3] Cyprus Research Centre for Remote Sensing & GIS, Hadjimitsis Consultants, P.O.Box 60055, Paphos, Cyprus, [4]Themistokleous&Associates (ARCHISYSTEMS LTD), Irinis139a, 3022, Limassol, Cyprus, [5]National Agricultural Research Foundation (NAGREF) Theofrastou str. 1 41335 Larissa Greece

DYNAMIC MONITORING OF AIR POLLUTANTS IN ZÜRICH (SWITZERLAND) USING A STREETCAR AS MEASURING PLATFORM

Ph. Kehl[1], J. Staehelin[2], A. Geiger[1], H. -G. Kahle[1] - [1]Institute for Geodesy & Photogrammetry, ETH Zürich, Switzerland, [2]Insitute for Atmospheric and Climate Science, ETH Zürich, Switzerland

STREET VERSUS ROOFTOP LEVEL CONCENTRATIONS OF FINE PARTICLES IN A CAMBRIDGE STREET CANYON

Prashant Kumar, Rex Britter, David Langley - Hopkinson Laboratory, Department of Engineering, University of Cambridge, CB2 1PZ, UK

COMPARISON OF VOLTAMMETRY AND INDUCTIVELY COUPLED PLASMA – MASS SPECTROMETRY FOR THE DETERMINATION OF HEAVY METALS IN PM_{10} AIRBORNE PARTICULATE MATTER

D. Buzica, M. Gerboles, A. Borowiak, P. Trincherini, R. Passarella, V. Pedroni - European Commission – DG Joint Research Centre, Institute for Environment and Sustainability, Transport and Air Quality Unit, 21020 Ispra, Italy.

AEROSOL OPTICAL DEPTH DETERMINATION BY COMBINATION OF LIDAR AND SUN PHOTOMETER

Ts. Evgenieva[1], N. Kolev[1], I. Iliev[2], I. Kolev[1] - [1]Institute of Electronics, Bulgarian Academy of Sciences, 72, Tsarigradsko shosse Blvd., 1784 Sofia, Bulgaria; [2]Central Laboratory of Solar–Terrestrial Influences, Bulgarian Academy of Sciences

THE CARBON DIOXIDE TOWER MEASUREMENTS IN HELSINKI

L. Järvi, S. Launiainen, A. Sogachev, J. Rinne, E. Siivola, P. Keronen, I. Mammarella and T. Vesala, University of Helsinki, Dept. Physical Sciences, P. O. Box 64, 00014 University of Helsinki, Finland

PRELIMINARY RESULTS OF SUSPENDED PARTICLES MEASUREMENTS BY GRIMM ANALYZERS IN INDUSTRIAL AGGLOMERATION IN CZECH REPUBLIC

Josef Keder - Czech Hydrometeorological Institute

APPLICATION OF A NETWORK OF MW-RADIOMETERS AND SODAR FOR THE VERIFICATION OF METEOROLOGICAL FORECASTING MODELS

D. Pernigotti, A. Rossa, M. E. Ferrario, M. Sansone - Istitution for all authors: ARPAV-CMT, Via Marconi 55, 35037 Teolo (PD), Italy.

DOCUMENTATION OF THE DIURNAL CYCLE OF PM10 CONCENTRATION FOR THE URBAN SITE OF VENICE-MESTRE

Rossa Andrea, Pernigotti Denise, Ferrario Massimo E., Sansone Maria, and Benassi Alessandro
Institution for all authors: ARPAV-CMT, Via Marconi 55, 35037 Teolo (PD), Italy.

CROSS-ACTIVATION OF AIR POLLUTANTS IN URBAN ENVIRONMENT

Krzysztof J. Rudzinski,[1] Józef Ziajka,[1] Lech Gmachowski,[1,2] Edyta Szeremeta [1]

[1] Institute of Physical Chemistry of the Polish Academy of Sciences, Warsaw, Poland
e-mail: kjrudz@ichf.edu.pl, tel.: +48-22-3433402
[2] Warsaw University of Technology, Institute of Chemistry, Płock, Poland

ABSTRACT

Cross-activation in the aqueous phase of SO_2 and organic pollutants (isoprene, chlorophenols and dimethylsulphoxide) was shown. Chemistry of metal-catalysed oxidation of S(IV) species was shown to overlap with transformation of organic compounds initiated by sulphate radicals. Rate constants and mechanisms of reactions, formation of secondary products and influence of organic compounds on the oxidation of S(IV) were discussed, with attention paid to reaction rates and mechanisms, formation of secondary pollutants and influence of organics on SO_2 oxidation. Finally, possible implications of discussed cross-activation towards urban air quality were indicated.

1. INTRODUCTION

Cross-activation of pollutants occurs frequently in the environment, when transformation chemistries of two or more polluting species overlap. New transformation pathways are immediately open and unexpected compounds are produced, while lifetimes and transport range of primary pollutants change. Significance of these factors in atmospheric chemistry models can only be judged if kinetics and mechanisms of cross-activation reactions are known. Unrecognized reactions just have no chance to occur in the models, but can proceed in the nature. Urban context offers many opportunities for cross-activation mechanisms, as it gathers many emission sources in relatively small areas – humans and animals, vehicles, heating facilities, waste water systems, incineration facilities, solid waste disposal systems, parks, cemeteries and forests. Air masses coming from neighbouring countryside or sea enrich this environment still more.

Gas-phase example of cross-activation of pollutants is oxidation of dimethylsulphide (DMS) by hydroxyl radicals, with pathways and product distribution controlled by presence or absence of nitrogen oxides, NO_2 and NO (Arsene *et al*., 1999, 2001). Nitrogen oxides support the hydrogen abstraction path and formation of formaldehyde, methanesulphonic acid (MSA) and sulphur dioxide. When no or little nitrogen oxides are present, the OH addition path dominates, that leads to dimethylsulphoxide (DMSO), methanesulphinic acid (MSIA), dimethylsulphone and SO_2. Moreover, NO_x facilitates conversion of DMSO and MSIA to MSA, and conversion of MSIA to dimethylsulphone peroxynitrates. Aqueous phase example of cross-activation of pollutants came from the study of degradation of 2,4-dichlorophenol initiated by sulphate radicals, which are part of SO_2 oxidation chemistry (Anipsitakis *et al*., 2006). Usual products of degradation were higher chlorophenols, chloroacetates and carbon tetrachloride. Only in the presence of nitrate ions 1,1'-sulfonylbis[4-chlorobenzene] was obtained. Cross-activation occurs also during heterogeneous interaction of pollutants. In smog-chamber experiments, sulphur dioxide increased yields of Secondary Organic Aerosol (SOA) formed during photooxidation of isoprene and α-pinene in presence of NO_x (Edney *et al.,* 2005; Kleindienst *et al.,* 2006). Products included organic nitrates and, only in presence of SO_2, organic sulphates (Surrat *et al.* 2006, 2007).

Here, we discuss the cross-activation of pollutants when the aqueous-phase oxidation of SO_2 is brought together with degradation of isoprene, chlorophenols or dimethylsulphoxide (DMSO), the latter in presence of nitrates. We show reactions of these organics with sulphate radicals usually formed during oxidation of SO_2 (Warneck and Ziajka, 1995; Ziajka *et al.*, 1994; Zuo *et al.*, 2005). All considered pollutants are present in urban scenarios. Sulphur dioxide and isoprene are emitted from stationary and mobile sources, chlorophenols are present in chlorinated potable water and are produced in urban waste-treatment facilities, and DMSO is emitted by plants and used as a carrier in medication formulas. Isoprene and chlorophenols are also produced in humans.

2. METHODOLOGY

General principle of our experiments was to place an organic reactant in an isothermal, well mixed solution in which catalytic autoxidation of S(IV) was taking place. For isoprene and DMSO we used a glass reactor of 0.785 dm^3 volume and an $MnSO_4$ catalyst. Reactions were started by adding sulphite solution to solution containing other reactants, and finished when oxygen was used up. Concentration of dissolved O_2 and pH were recorded continuously. UV spectra of reacting solution were taken periodically, from which time traces of concentrations of SO_3^{2-} ions, HSO_3^- ions and isoprene or DMSO were evaluated by decomposition against standards. ESI mass spectra of post-reaction solutions were also recorded. For chlorophenols, we used a 0.060 dm^3 reactor, in which we measured time traces of the O_2 concentration and pH. Reactions were started

by adding solution of $Fe(ClO_4)_3$ catalyst to solution containing other reactants. Rate constants for reactions of chlorophenols with sulphate radicals were determined using the reverse-rate method (Ziajka and Pasiuk-Bronikowska, 2003, 2005).

3. RESULTS AND DISCUSSION

Isoprene

Isoprene influenced the autoxidation of S(IV) in the way depending on the acidity of solutions. Figure 1 shows decay of oxygen measured at three different values of initial pH of solutions, in presence or absence of isoprene. Conversions of oxygen and S(IV) followed the overall stoichiometry of 1:2. Isoprene slowed down the autoxidation in alkaline and in acidic solutions, and accelerated it in solutions close to neutral (pH_o = 6.8 – 7.8).

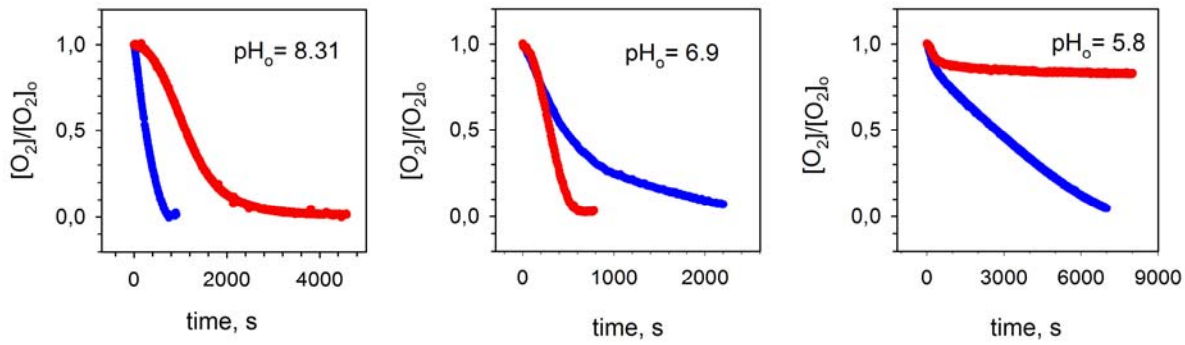

Fig. 1. Normalized decay of oxygen during autoxidation of S(IV) catalysed by $MnSO_4$ in the absence (blue) and presence (red) of isoprene, for different initial acidities of solutions, at 25 °C. Initial concentrations were: 2.5 mM O_2, 9.0 mM S(IV) (added as Na_2SO_3 and $Na_2S_2O_5$ to obtain desired acidity), 2.2 mM C_5H_8, and 0.01 mM $MnSO_4$.

The UV spectra of reacting solutions showed decay of isoprene and formation of weakly absorbing products ($\lambda_{max} \approx 237$ nm). ESI-MS spectra indicated the products could be $(HO_3SO)H_2C\text{-}C(CH_3)=HC\text{-}CHO$ (m/z = 179) and $(HO_3SO)H_2C\text{-}C(CH_3)=HC\text{-}CH_2OH$ (m/z = 181). Computer simulation based on tentative mechanism and rate constant of 2.1×10^9 dm^3 mol^{-1} s^{-1} (25 °C) for reaction of isoprene with sulphate radicals (Rudzinski, 2004) fairly well reproduced the experimental results in basic solutions (Fig. 2). The mechanism incorporated two overlapping chain reactions – one for autoxidation of S(IV) and the other for transformation of isoprene initiated by sulphate radicals.

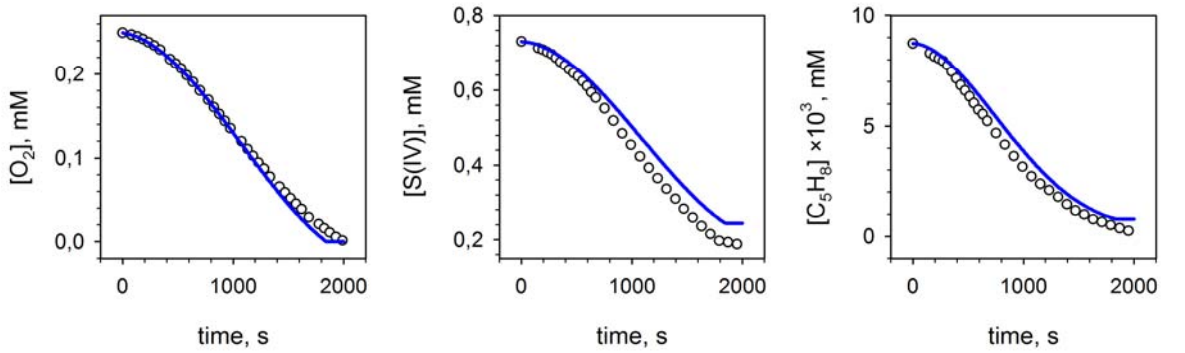

Fig. 2. Experimental and computer-simulated traces of reactant concentrations during autoxidation of S(IV) in presence of isoprene at 25 °C (points and solid curves, respectively). Initial concentrations of reactants were: 2.49 mM O_2, 7.31 mM S(IV) (Na_2SO_3), 0.00874 mM C_5H_8, 0.01 mM $MnSO_4$. Solution pH changed from 8.58 to 8.30.

Chlorophenols

Rate constants of reactions of six chlorophenols with sulphate radicals were determined using the reverse-rate method developed and tested by Ziajka and Pasiuk-Bronikowska (2003, 2005). The method utilises similarity of pseudo-stationary states in chain autoxidation of S(IV) catalysed by Fe(III) salts (sulphate or perchlorate) in presence of single organic compounds (inhibitors) scavenging the sulphate radicals. Classical Steady-State-Approximation analysis showed the reciprocal quasi-stationary rates of inhibited autoxidation depended

linearly on the initial concentration of an organic compound, with slope proportional to the rate constant for reaction this compound with sulphate radicals. The ratio of two slopes for two different compounds was equal to the ratio of respective rate constants for reactions of these compounds with radicals:

$$k_{org1+SO4-} = k_{org\,ref+SO4-} \frac{slope_{org1}}{slope_{org\,ref}} \quad (1)$$

Relation (1) allows determination of rate constants for reactions of various organics with sulfate radicals, which are relative by measurement but placed on the absolute scale, provided an absolute rate constant for a reference compound is used. Figure 3 shows the rate constants determined at 25 °C for phenol, 4-chlorophenol, 2,4- and 2,5-dichlorophenol, 2,4,5- and 2,4,6-trichlorophenol, and 2,3,5,6-tetrachlorophenol, correlated against sum of Hammett substituent coefficients (Ziajka and Rudzinski, submitted). Ethanol was used as a reference compound, with rate constant 4.3×10^7 dm^3 mol^{-1} s^{-1} (Clifton and Huie, 1989). For comparison, literature values of rate constants for reactions of chlorophenols with hydroxyl radicals were included.

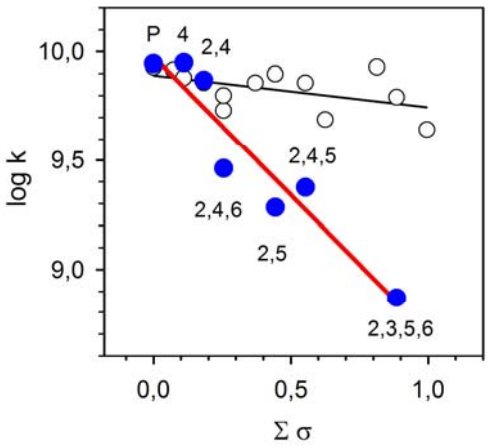

Fig. 3. Correlation of rate constants for reactions of phenol and chlorophenols with sulphate radicals (full points) and with hydroxyl radicals (open points) at 25 °C against sum of Hammett substituent coefficients (Ziajka and Rudzinski, submitted).

In all cases chlorophenols inhibited oxidation of S(IV), but this conclusion is limited to low conversion of chlorophenols we had to observe for the purpose of estimating the rate constants.

Dimethylsulphoxide

Using the method described for isoprene, we carried out experiments on degradation of DMSO during autoxidation of S(IV) in presence of inorganic nitrate. Preliminary results revealed complex behaviour of the system but were not conclusive at the time of writing this paper. Recent studies of Zhu *et al.* (2006), and especially the modelling of cloud processing at remote conditions, clearly show significance of aqueous-phase reactions of DMS, DMSO, MSIA and MSA with inorganic radicals, including $SO_4^{\bullet-}$.

Impact on urban air

We showed isoprene and chlorophenols could react fast with sulphate radicals derived from SO_2 or sulphites in the aqueous phase. Isoprene was transformed into organic sulphate similar to those found in atmospheric aerosols and obtained in aerosol-chamber experiments (Surratt *et al.*, 2006, 2007). Degradation of chlorophenols initiated by sulphate radicals produced other chlorophenols, chloroacetates, chlorocatechols, quinones, hydroxybenzene and carbon tetrachloride (Silva *et al.*, 1996; Anipsitakis *et al.*, 2006). We would like to bring attention to a few points regarding the possible impact of cross-activation of organic pollutants and SO_2 on the quality of urban air.

- Organic compounds can either accelerate or inhibit wet oxidation of SO_2 to sulphates and sulphuric acid. In the latter case, unreacted SO_2 persist in aqueous capsules, apparently inhibited, but in fact converting the inhibitor to some products. Such reactive capsules can be potentially dangerous to living organisms and material surfaces.
- Fast aqueous-phase reaction of sulphate radicals with sparingly soluble isoprene can enhance transfer of

the latter to the aqueous phase. Organosulphates, which are produced in this reaction, become components of wet and dry precipitation, and can affect both living organisms and materials in a way presently unknown.

- Chlorophenols were rarely determined in urban precipitation and aerosols, and are generally considered aquatic rather than air pollutants. However, due to fast reactions with sulphate radicals they can become precursors of potentially dangerous secondary air and water pollutants.
- Urban aerosols and wet precipitation (rain, fog, dew and haze) can contain organosulphates and derivatives of chlorophenols, which can affect living organisms and materials in a way presently unknown.

4. ACKNOWLEDGEMENTS

This work was supported by Polish Ministry of Education and Science (decision nr 71/E-64/SPB/SEF/T-09/DWM 107/2004-2007), in relation to ESF Programme “INTROP”.

5. REFERENCES

Anipsitakis, G. P., Dionysiou, D. D., Gonzalez, M. 2006. Peroxymonosulfate and sulfate radical attack on phenolic compounds. Implications of chloride ions. Environ. Sci. Technol. 40, 1000-1007.

Arsene, C., Barnes, I., Becker K. H. 1999. FT-IR product study of the photo-oxidation of dimethylsulfide: temperature and O_2 partial pressure dependence. PCCP 1, 5463-5470.

Arsene, C., Barnes, I., Becker K. H., Mocanu, R. 2001. FT-IR product study on the photo-oxidation of dimethyl sulphide in the presence of NO_x - temperature dependence. Atmos. Environ. 35, 3769-3780.

Clifton, C. L., Huie, R. E. 1989. Rate constants for hydrogen abstraction reactions of the sulphate radical, $SO_4^{\bullet-}$, with alcohols. Int. J. Chem. Kinet. 21, 677–687.

Edney, E. O., Kleindienst, T. E., Jaoui, M., Lewandowski, M., Offenberg, J. H., Wang, W., Claeys, M. 2005. Formation of 2-methyl tetrols and 2-methylglyceric acid in secondary organic aerosol from laboratory irradiated isoprene/NO*x*/SO2/air mixtures and their detection in ambientPM2.5 samples collected in the eastern United States. Atmos. Environ. 39, 5281-5289.

Kleindienst, T. E., Edney, E. O., Lewandowski, M., Offenberg, J. H., Jaoui, M. 2006. Secondary organic carbon and aerosol yields from the irradiations of isoprene and α-pinene in the presence of NO_x and SO_2. Environ. Sci. Technol. 40, 3807-3812.

Rudzinski, K. J. 2004. Degradation of isoprene in the presence of sulphoxy radical anions. J. Atmos. Chem. 48, 191–216.

Silva, M. I., Burrows, H. D., Graca Miguel, M., Formosinho S. J. 1996. Tris-2,2'bipyridylruthenium(II) peroxydisulphate as a photosensitizer in the oxidative degradation of 4-chlorophenol. Ber. Bunsen-Ges. Phys. Chem. 100, 138-143.

Surratt, J. D., Murphy, S. M., Kroll, J. H., Ng, N. L., Hildebrandt, L., Sorooshian, A., Szmigielski, R., Vermeylen, R., Maenhaut, W., Claeys, M., Flagan, R. C., Seinfeld, J. H. 2006. Chemical composition of Secondary Organic Aerosol formed from the photooxidation of isoprene. J. Phys. Chem. A 110, 9665-9690.

Surratt, J. D., Kroll, J. H., Kleindienst, T. E., Edney, E. O., Claeys, M., Sorooshian, A., Ng, N., Offenberg, J. H., Lewandowski, M., Jaoui, M., Flagan, R. C., Seinfeld, J. H. 2007. Evidence for organosulfates in Secondary Organic Aerosol. Environ. Sci. Technol. 41, 517-527.

Warneck, P., Ziajka, J. 1995. Reaction mechanism of the iron(III)-catalyzed autoxidation of bisulfite in aqueous solution: steady state description for benzene as radical scavenger. Ber. Bunsenges. Phys. Chem. 99, 59-65.

Zhu, L., Nenes, A., Wine, P. H., Nicovich J. M. 2006. Effects of aqueous organosulfur chemistry on particulate methanesulfonate to non-sea salt sulfate ratios in the marine atmosphere. J. Geophys. Res. 111, D05316, doi:10.1029/2005JD006326 (and references quoted therein).

Ziajka, J., Beer, F., Warneck, P. 1994. Iron-catalysed oxidation of bisulphite aqueous solutions: evidence for a free radical chain mechanism. Atmos. Environ. 28, 2549-2552.

Ziajka, J., Pasiuk-Bronikowska, W. 2003. Autoxidation of sulphur dioxide in the presence of alcohols under conditions related to the tropospheric aqueous phase. Atmos. Environ. 37, 3913–3922.

Ziajka, J.; Pasiuk-Bronikowska, W. 2005. Rate constants for atmospheric trace organics scavenging $SO_4^{\bullet-}$ in the Fe-catalysed autoxidation of S(IV). Atmos. Environ. 39, 1431–1438.

Zuo, Y., Zhan, J., Wu, T. 2005. Effects of monochromatic UV-Visible light and sunlight on Fe(III)-catalyzed oxidation of dissolved sulfur dioxide. J. Atmos. Chem. 50, 195–210 (and references quoted therein).

DERIVING HIGH RESOLUTION SPATIAL CROSS SECTIONS OF TROPOSPHERIC TRACE GASES FROM AUTOMOBILE MULTI AXIS DIFFERENTIAL OPTICAL ABSORPTION SPECTROSCOPY TECHNIQUE (AUTOMAX-DOAS)

O.W.Ibrahim, T.Wagner ,T.Stein, R.Sinreich and U.Platt
Instiut Für Umwelphysik , Universität Heidelberg , Germany.

ABSTRACT

We report on the instrumental set-up, application and results of automobile based measurements using the **Auto**mobile **M**ulti **Ax**is **D**ifferential **O**ptical **A**bsorption **S**pectroscopy technique (Auto-Max-DOAS).
Measurements of the air pollutant NO_2 were carried out in urban, industrial areas as well as areas with high traffic density in the local/regional area of the Rhein-Neckar valley in Germany.

The use of UV spectroscopy with the miniature Multi Axis DOAS (MiniMax-DOAS) instrument with a small telescope (f = 40mm) installed on a car roof enables the detection and quantification of the columns of trace gases such as NO_2, SO_2, HONO, and CH_2O in the troposphere. Here we present the results of NO_2 columns from these measurements as an example.

The time resolution of measurements is of the order of 20-30 seconds and the spatial resolution of this method is of the order of several tens of meters to few hundreds of meter depending on the actual integration time and the driving speed of the automobile platform.

The detection limit of NO_2 was about 1 ppb (depending on the length of the light path). Furthermore information about aerosols can be gained from the measurements of the oxygen dimer O_4 combined with radiative transfer modeling. In contrast to in-situ techniques, from continuous Auto-MAX-DOAS observations the integrated amount of trace gases (integrated over the altitude and along the route) is derived. Thus with appropriate driving patterns, it is in particular possible to derive the absolute fluxes of trace gases from an urban area or a point source (e.g. a power plant).
Special measurements strategies can be applied using the Auto-Max-DOAS for encircling specified pollution sources/areas and estimation of the respective emission strengths. Also driving the Auto-Max-DOAS under a large pollution plume can be useful in estimating the spatial extent of pollution overhead and giving some idea also about the vertical extent of the plume.

MOTIVATION:

The Auto-MAX measurements provide a spatial resolution better than that of Satellites and airplanes for city pollution scale and also give more possibilities for measurement strategies than those of stationary ground-based measurements.

INTRODUCTION

Differential Optical Absorption Spectroscopy (DOAS) is Studying the narrow absorption features of atmospheric trace gases in the UV-VIS part of the electromagnetic spectrum, after removal of the broadband signal associated with Rayleigh and Mie scattering processes.

A differential optical thickness is calculated as the logarithm of the ratio between the zenith-sky spectrum and a reference recorded at higher solar elevation (usually at local noon time). Column densities along the optical path, or apparent slant columns, are derived by an iterative least squares procedure, fitting the observed differential optical thickness with high-pass filtered absorption cross sections measured in the laboratory and convolved with the instrument slit function. Interfering species like O_3, O_4 and H_2O are fitted simultaneously within the same spectral window of interest. Slant columns are converted into vertical columns using an optical path enhancement factor, or so-called air mass factor (AMF), which can be calculated by Radiative Transfer models [J-C Lambert et al].

2. METHODOLOGY

2.1 BASIC MAX-DOAS PRINCIPLE

MAX-DOAS utilizes scattered sunlight received from multiple viewing directions. Combining several viewing directions (elevation angles) can derive the spatial (vertical) distribution of various trace gases close to the instrument (trace gas vertical profiles). Ground based MAX-DOAS is highly sensitive to absorbers in the lowest few kilometers of the atmosphere and vertical profile information can be retrieved by combining the measurements with Radiative Transfer Model (RTM) calculations [Hönninger et al., 2004]. This

application is also called “passive” absorption spectroscopy because it is using the scattered sun light as a source, in contrast to active DOAS (i.e. spectroscopy using artificial light sources), for more details about Active DOAS see [Perner et al., 1976; Platt et al., 1979; Perner and Platt, 1979; Platt and Perner, 1980; Platt et al., 1980]. Fig (1) shows the idea of MAX-DOAS, where the telescopes at different elevation angles receive the scattered sunlight.

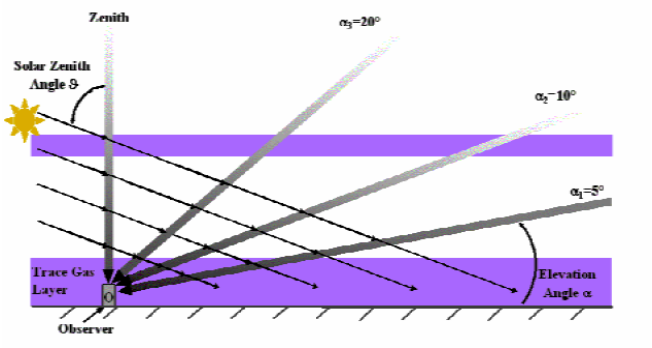

Fig (1): The Multi Axis-DOAS (MAX-DOAS) technique for studying trace gases in the Boundary Layer

2.2 THE EXPERIMENTAL SET-UP

Miniaturized Multi Axis Differential Optical Absorption Spectroscopy (Mini-MAX-DOAS) instrument was used while installed on the top of a car roof. The Mini-MAX-DOAS system consists of an entrance optic (quartz lens, f = 40 mm, d = 20 mm, field of view is approximately ~ 0.6°) coupled to a quartz fiber bundle, which transmits the light into a commercial miniature fiber optic spectrometer (OceanOptics Inc., USB2000) with a spectral resolution of 0.7 nm. This unit is placed inside a metal box, which can be mounted on a tripod or on a metal substrate on the top of a car. One (UG5) filter is used in front of the lens to block the visible light (wavelength > 400 nm) to reduce the stray light in the spectrometer. To prevent direct sun light from being scattered into the fibre and as a protection from rain, a tubular black sunshield (22 mm diameter, 80 mm length) is attached in front of the entrance optics.

In order to reduce the dark current of the CCD detector and to stabilize the optical bench, the complete USB2000 spectrometer was cooled to a temperature of 0 °C during the measurements. Stabilising the temperature of the spectrometer and detector readout electronics also reduced the temperature drift of the electronic offset signal. To avoid water condensation on the spectrometer , the whole unit was made air-tight and silica gel was added to keep the interior dry in case of leakage. The entire system (computer, cooling system, spectrometer and stepper motor) can operate for several hours with a small lead battery (12V). Measurements, stepper motor motion and electronics are controlled by the software DOASIS on a laptop computer (also possible with a hand-held pocket computer). Fig (2) shows the general scheme of the outline of a Mini-MAX-DOAS instrument.

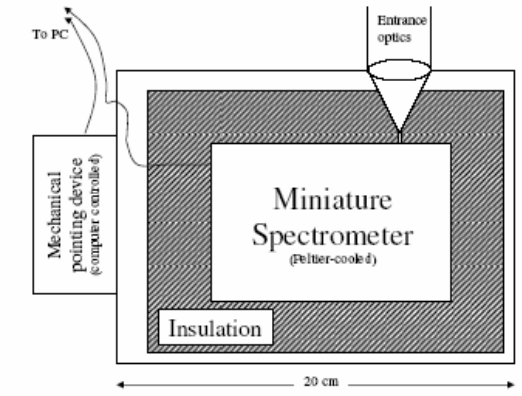

Fig (2): Outline of the Mini-MAX-DOAS instrument. A miniature spectrometer is cooled and temperature stabilized by a 2 stage Peltier cooler. The built-in entrance optics (telescope) provide a narrow field of view (<0.6^{o}). The unit can be pointed in various directions by computer control. The scheme shows a top-view of the Mini-MAX-DOAS so that the motion plane will be perpendicular to the page plane assuming that the horizontal position of the telescope is the zero elevation angle.

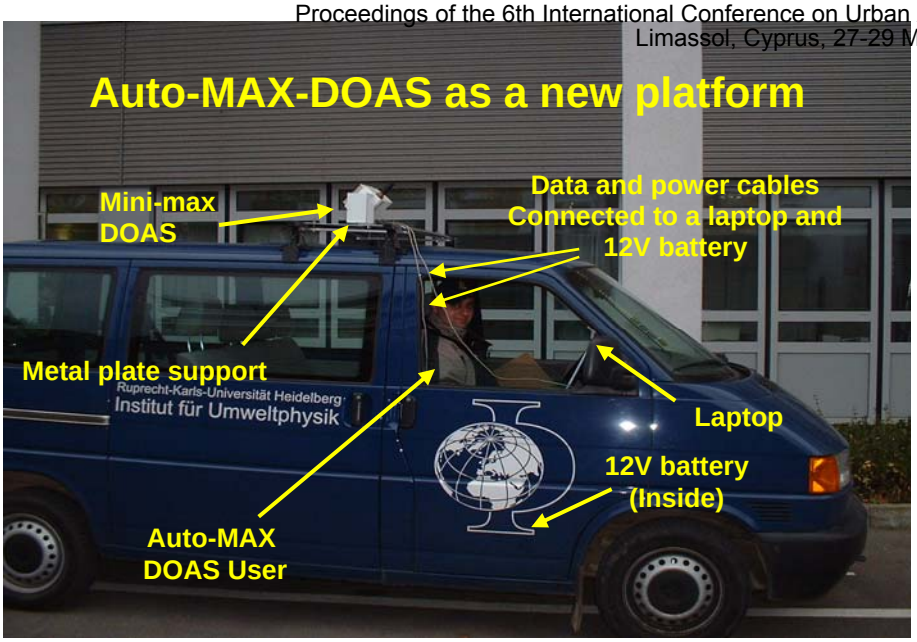

Fig (3): The Auto-MAX-DOAS new platform ready to operate during driving.

3. RESULTS AND DAISCUSSION

Measurements using Auto-MAX-DOAS on the 5th of November 2005 were carried on around the BASF industrial compound in (Ludwigshafen Am Rhein) area . Two concentric circles around the industrial area were done using Auto-MAX-DOAS with continous measurements.
The measurements were taken in sequence of elevation angls of 45° and 90° (zenith) repeatedly and the integration time was of order of few tens of seconds. During the day of measurements the sky was partially cloudy and it was a Sunday so the NO_2 emissions from traffic were minimumso that minimizes the interference between the traffic emissions and the industrial plume emissions during measurements. Figures (4) and (5) show the map of the area and the rout of the driving around the BASF industrial area.

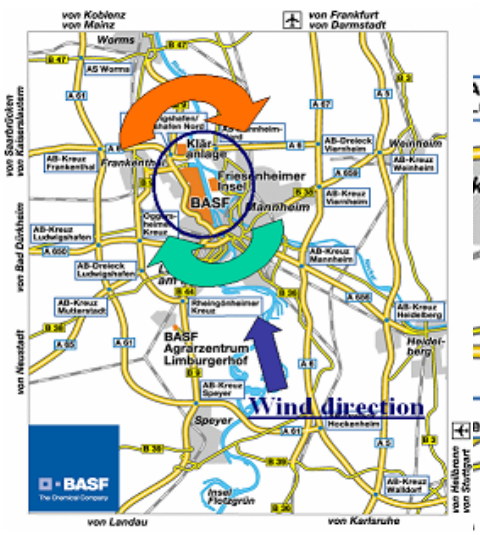

Fig (4) Fig (5)

Fig (4) : The route of encircling the BASF industrial area . The blue arrow shows the prevailing wind direction (SSE)on the day of measurements. The green arrow shows the part of the driving route upwind and the orange arrow shows the part of the driving route downwind which is supposed to have higher concentrations of emitted NO_2.

Fig (5) : The road of driving around the BASF industrial area . The arrows show the route of the two concentric circles around the area.

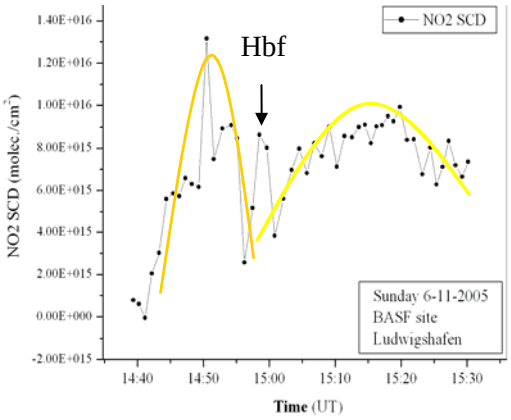

Fig (5) : The NO_2 Slant Column Densities (SCDs) obtaned from the spectral evaluation after the measurements . The two peaks (in yellow) show the elevated SCDs of NO_2 downwind from the BASF indistrial area. Notice that there is a small inter-peak between the two big ones. This small peak corresponds to driving through the main square of the city in front of the main train station (Hbf) which has some heavy traffic activity.

SUMMARY AND CONCLUSION

The Newly established platform Auto-MAX-DOAS was successfully used to encircle a source of NO_2 emissions (BASF industrial area) . Results of evaluation of the collected light spectra shpwed that there are higher concentration of NO_2 downwind from the source as expected.
The Slant Column Densities (SCDs) were up to 1.3E16 Molecule/cm^2 , a quantitiy which should be transformed into the Vertical column Densities (VCDs) (i.e. the concentration of the NO_2 gas in the vertical column overhead at the place of measurements). This calculation is done by Radiative Transfer Modeling (RTM). Then the concentration in terms of absolute units (parts per billion of volume ppbv) can be also calculated later.

OUTLOOK
In the near future, calculations of the Vertical Column Densities (VCDs) is going to be done using the Monte Carlo Radiative Transfer Model (RTM) TRACYII and also some more measurements are going to be done in industrial/urban areas using a new generation of spectrometers (QE6500) which has a better ime resolution and wthus will lead to a better spatial resolution of the measurements.

REFERENCES

Hönninger et al., Multi axis differential optical absorption spectroscopy (MAX-DOAS). Atmos. Chem. Phys., 4, 231–254, 2004.

Lambert J-C. et al: Geophysical validation of SCIAMACHY NO2 columns: Overview of early 2004 results - Proceedings of the Second Workshop on the Atmospheric Chemistry Validation of ENVISAT (ACVE-2).

Perner, D., Ehhalt, D. H., P¨atz, H. W., Platt, U., R¨oth, E. P., and Volz, A.: OH Radicals in the lower Troposphere, Geophys. Res. Lett., 3, 466–468, 1976.

Perner, D. and Platt, U.: Detection of Nitrous Acid in the Atmosphere by Differential Optical Absorption, Geophys. Res. Lett., 6, 917–920, 1979.

Platt, U., Perner, D., Harris, G.W.,Winer, A.M., and Pitts Jr., J.M.: Detection of NO3 in the Polluted Troposphere by Differential Optical Absorption, Geophys. Res. Lett., 7, 89–92, 1980.

AMBIENT AIR LEVELS OF VOLATILE ORGANIC COMPOUNDS (VOC) AND NITROGEN DIOXIDE (NO_2) IN URBAN AIR OF PAMPLONA, SPAIN

Parra, M.A., Bermejo, R., Elustondo, D., Santamaría, J.M.

Laboratorio Integrado de Calidad Ambiental (LICA), Departamento de Química y Edafología, Universidad de Navarra, Irunlarrea s/n, 31080, Pamplona (Spain)

ABSTRACT

Ambient concentrations of VOC and NO_2, collected by means of passive sampling, are being measured at 40 sampling points in Pamplona city from June 2006 to June 2007 (24 biweekly sampling campaigns). VOC and NO_2 air samples are analyzed by thermal desorption and gas chromatography/mass-selective detector and visible spectrophotometry respectively. Concentrations of benzene, toluene, ethylbenzene, xylenes, tetrachloroethene, isopropylbenzene, bromobenzene, propylbenzene, trimethylbenzenes naphthalene and NO_2 have been found to be highly correlated. Their spatial distribution points to traffic as the main emission source of these compounds, since the concentrations of BTEX and NO_2 are their levels negatively associated with road distance. The lowest levels of VOC and NO_2 occur in the summer-time, owing to the occurrence of an increase in solar radiation and lower traffic densities. Mean concentrations for benzene and NO_2 have exceeded the European limits at some of the points monitored.

1. INTRODUCTION

Urban air pollution has become an environmental problem of public concern in the last decades. Volatile organic compounds (VOC) are an important group of air pollutants to study because they can be precursors to the formation of ozone (Atkinson, 2000) and a number of these compounds have been shown to be harmful to human health and atmosphere (WHO, 2000; Hellén et al., 2002).

Large amounts of VOC are emitted from mobile and stationary sources, mainly due to combustions, solvent and fuel evaporation and tank leakage (Fernández-Villarenaga et al., 2004). Motor vehicles are the most important source of VOC especially in locations with few industrial sources, accounting for a 35 % of the total VOC emissions in urban areas (Tran et al., 2000).

The objective of this work is to investigate the VOC and NO_2 levels in Pamplona and the exceedances of the European limits. The temporal and spatial variations of these pollutants are studied and the relations between them, traffic and meteorology.

2. METHODOLOGY

The research is carried out in Pamplona, a medium size city with 193328 inhabitants. This city is located in the northern area of Spain (42º 49' N and 2º 1' W) and covers an extension of 25.1 km^2. It is characterised by a submediterranean climate with a mean annual rainfall of 833 mm and a mean temperature of 12.7ºC, with high differences between winter and summer (20ºC).

Sampling is being carried out from June 2006 to June 2007 at 40 sampling points selected within a sampling grid (450 x 450 m). Perkin Elmer stainless steel tubes (6.3 mm ED x 90 mm, 5.5 mm ID) filled with Tenax TA are used for VOC sampling whereas Radiello passive samplers are used for monitoring NO_2. These samplers are placed at 3 m above ground level and protected from bad weather conditions by polypropylene easily-assembled shelters.

Sampling is performed on a 2-week basis, allowing for a total of 24 exposure periods. Only the first 14 sampling periods are presented in this work. Following exposure, tubes are retrieved and taken to the laboratory in sealed glass jars inside a refrigerated chamber. Field blanks are transported along with samplers to the field and stored in the laboratory during the exposure period.

Measurements of VOC are made using a Markes thermal desorption unit coupled to a gas chromatograph (Agilent 5890) and an Agilent 5970 mass selective detector. NO_2 is determined by visible spectrophotometry. A more detailed description of these methods is described in Parra et al., 2006.

Meteorological data for wind speed and direction, relative humidity, temperature, atmospheric pressure, solar radiation and precipitation are obtained from a meteorological station located in the vicinity of one of the sampling points.

Contour maps have been produced using the kriging method in order to illustrate the spatial distribution of the different variables. All calculations were done with 3DField program. Correlations between pollutants and meteorology were calculated with SPSS v.12.0.

3. RESULTS AND DISCUSSION

A statistical summary of VOC and NO_2 concentration data are presented in Table 1.

Table 1. Summary of VOC and NO_2 concentrations ($\mu g\ m^{-3}$) measured in Pamplona.

	Mean	Median	Range	N
Benzene (BEN)	2.74	2.29	0.05 – 12.67	544
Toluene (TOL)	13.76	12.31	0.14 – 47.05	544
Tetrachloroethene	0.67	0.51	0.01 – 5.10	544
Ethylbenzene (ETB)	2.31	1.86	0.02 – 14.75	544
m/p-Xylene (MPX)	3.70	3.40	0.12 – 12.63	544
o-Xylene (OX)	3.02	2.59	0.12 – 10.55	544
Isopropylbenzene	0.42	0.18	0.11 – 3.66	544
Bromobenzene	9.80	10.62	0.01 – 18.65	544
Propylbenzene	0.49	0.30	0.01 – 11.37	544
1,3,5-Trimethylbenzene	1.38	1.19	0.01 – 5.32	544
Naphthalene	0.18	0.11	0.01 – 6.12	544
NO_2	20.80	18.65	2.10 – 84.64	550

The results clearly indicate the dominance of toluene among all the species investigated, since it exhibits the highest mean concentration with 13.76 $\mu g\ m^{-3}$. This major presence has also been reported in other studies conducted in urban atmospheres (Guo et al., 2004; Ho and Lee; 2002).

According to Directive 2000/69/EC, the annual mean benzene concentrations in air may not exceed 5 $\mu g\ m^{-3}$. Mean values obtained in this study have sometimes exceeded this limit, with a maximum registered value of 5,49 $\mu g\ m^{-3}$ so far. Besides, and although toluene levels are not regulated by European legislation, WHO establishes a guideline value for the protection of human health of 260 $\mu g\ m^{-3}$ expressed as a weekly average, level which indeed remains far above the levels registered to the date in this study. Furthermore, the averaged levels of NO_2 showed that the 1999/30/EC threshold for the protection of human health (40 $\mu g\ m^{-3}$) have been exceeded for three of the points investigated with levels of 53.21, 49.10 and 42.88 $\mu g\ m^{-3}$. Besides, it should be mentioned that these measurements were conducted in autumn and summer, when concentrations are generally lower than in winter season so limits could be exceeded when considering the benzene and NO_2 annual mean at more sampling points.

3.1. Temporal distributions of VOC and NO_2

Figure 1 shows the evolution of the mean concentrations of VOC and NO_2 in the 40 monitored points over the sampling campaigns.

Figure 1. Temporal variation of BTEX and NO_2.

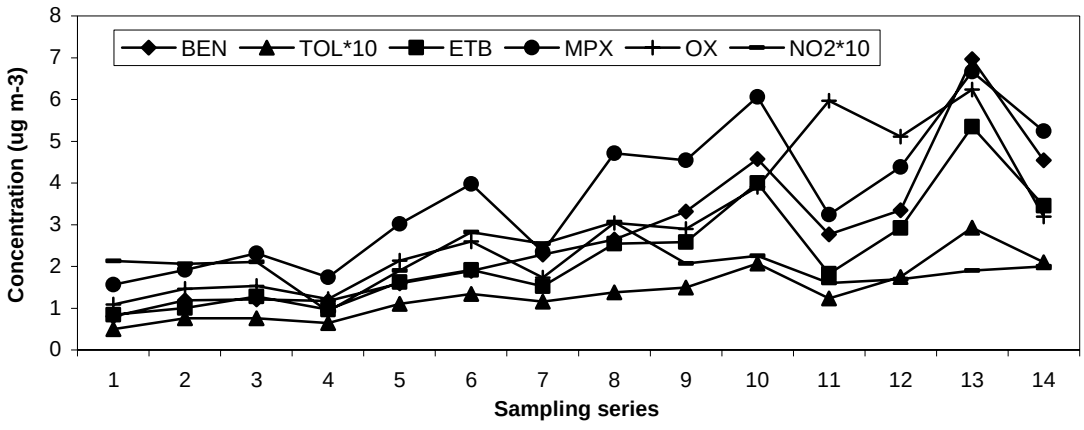

It is interesting to note all the BTEX group has exhibited a similar behaviour trough time, indicating that they likely come from the same emissions sources. The lowest levels of BTEX were recorded in July and August (2^{nd} to 4^{th} sampling), when a lower density of traffic is expected and temperatures were higher, so that a major loss of VOC by photochemical degradation was to be expected. The lowest values of NO_2 in the first fortnight of August (4^{th} sampling), due to the decrease of traffic.

3.2. Spatial distributions of VOC and nitrogen dioxide

Mean concentrations of BTEX (sum of concentrations of benzene, toluene, ethylbenzene and xylenes) and NO_2 for the distinct sampling points are represented in Figure 2.

Figure 2. Contour map for NO_2 (a) and BTEX (b) concentrations (μg m^{-3})

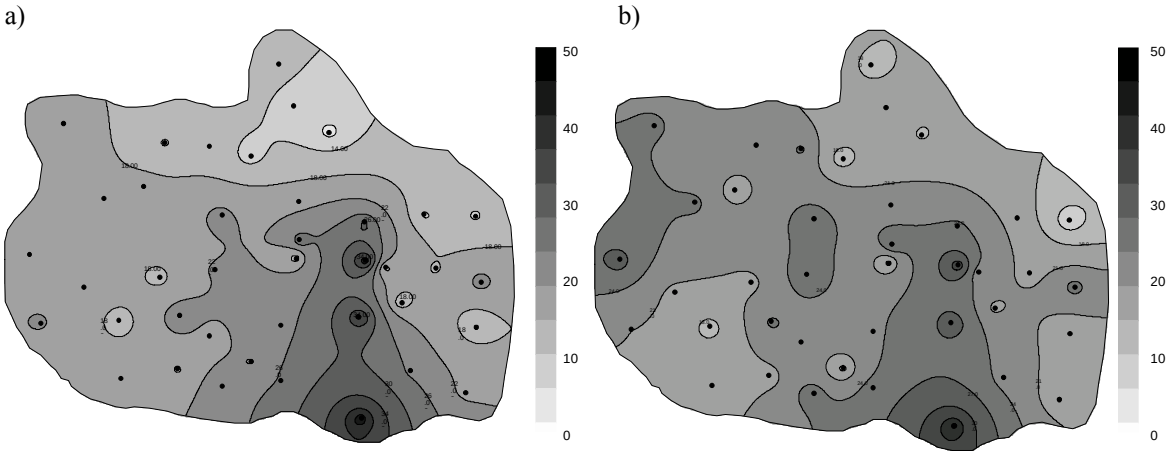

The spatial pattern of BTEX concentrations matches the layout of the main roads in the city. The highest levels have been registered in points: 19, 21, 31 and 38, which correspond to high traffic roads. Points 5, 20 and 14 have showed an opposite behaviour, a predictable fact as these points were located in parks far from sources of pollution such as roads and industries.

3.3. VOC ratios and correlations

The correlation coefficients between the studied compounds are presented in Table 2.

Table 2. Correlation between VOC, NO_2, distance to road and meteorology

	NO_2		BEN	TOL	ETB	MPX	OX
	summer	winter					
BEN	0.900*	0.620*					
TOL	0.856*	0.564*	0.946*				
ETB	0.781*	0.438*	0.815*	0.920*			
MPX	0.816*	0.583*	0.854*	0.936*	0.978*		
OX	0.901*	0.583*	0.967*	0.980*	0.927*	0.949*	
Distance to road	-0.371*	-0.272*	-0.515*	-0.528*	-0.525*	-0.522*	-0.514*
T	0.197		-0.893*	-0.869*	-0.860*	-0.796*	-0.865*
RH	-0.114		0.756*	0.739*	0.750*	0.737*	0.718*
Radiation	-0.032		-0.819*	-0.825*	-0.792*	-0.824*	-0.865*

*Significant with a probability over 99%.

Strong correlations have been found among the BTEX group. They have also exhibited significant correlations with NO_2, fact that points traffic as the main source of these compounds, once more pointing to traffic as the main emission source of these compounds. The fact that this last association is stronger during summer-time than during winter-time points to a different apportionment in winter time due to the contribution of other sources such as house heating. Also, it could be linked to the different chemical nature that can cause a different dynamic reaction. Furthermore, there is a good and negative correlation for BTEX and NO_2 with road distance. This correlation for NO_2 is higher in summer than winter, fact that supports the idea of other sources for NO_2 in winter.

The characteristic ratios of benzene, toluene, ethylbenzene and xylene (BTEX ratio) were 1.19:5.96:1.00:2.91. These ratios are similar to those reported in some roadside studies (Mohamed et al., 2002; Ho and Lee, 2002) and suggest that motor vehicles significantly affect levels of VOC in urban ambient air of Pamplona.

With regards to meteorology, a high and significant negative correlation (Table 2) between temperature and BTEX concentration has been determined. These increases in temperature correspond to higher radiations values in the area, condition that favours the loss of VOC by photochemical degradation, and consequently, a decrease in their concentration (Sillman et al., 1999). Likewise, a significant positive correlation (Table 2) has been found between relative humidity and BTEX concentrations.

4. CONCLUSIONS

The VOC and NO_2 levels registered in Pamplona by the use of passive samplers are up to date similar to others registered in urban atmospheres, exceeding the European limit values at some of the monitored points. The spatial distribution of BTEX and NO_2 indicates an increment in their levels corresponding to areas situated close to principal roads, pointing to traffic as the main source of these pollutants. Pollutants present lower levels in summer linked to a higher intensity of solar radiation which allows a higher loss of VOC by photochemical reactions, and season with lower traffic densities.

5. ACKNOWLEDGEMENTS

This research work was made possible by the permission of Ayuntamiento de Pamplona. Also, authors would like to thank Asociación de Amigos of the University of Navarra for the concession of a research grant.

6. REFERENCES

Atkinson, R. Atmospheric chemistry of VOCs and NO_x. 2000. Atmos Environ. 34, 2063-2101.

Directive 2000/69/EC of the European Parliament and of the Council of 16 November 2000 relating to limit values for benzene and carbon monoxide in ambient air. 13 December 2000. Official Journal of the European Communities.

Directive 1999/30/EC of the European Parliament and of the Council of 22 April 1999 relating to limits values for sulphur dioxide, nitrogen dioxide and oxides of nitrogen, particulate matter and lead in ambient air. 29 June 1999. Official Journal of the European Communities.

Fernández-Villarenaga, V., López- Mahía, P., Muniategui-Lorenzo, S., Prada-Rodríguez, D., Fernández-Fernández, E., Tomás, X. 2004. C1 to C9 volatile organic compound measurements in urban air. Sci Total Environ. 334-335, 167-176.

Guo, H., Wang, T., Simpson, I.J., Blake, D.R., Yu, X.M., Kwok, Y.H., Li, Y.S. 2004. Source contributions to ambient VOCs and CO at a rural site in eastern China. Atmos Environ. 38, 4551-4560.

Hellén, H., Hakola, H., Laurila, T., Hiltunen, V., Koskentalo, T. 2002. Aromatic hydrocarbon and methyl tert-butyl ether measurements in ambient air of Helsinki (Finland) using diffusive samplers. Sci Total Environ. 298, 5-64.

Ho, K.F., Lee, S.C. 2002. Identification of atmospheric volatile organic compounds (VOCs), polycyclic aromatic hydrocarbons (PAHs) and carbonyl compounds in Hong Kong. Sci Total Environ. 289, 145-158.

Mohamed, M.F., Kang, D., Aneja, V.P. 2002. Volatile organic compounds in some urban locations in United States. Chemosphere. 47, 863-882.

Parra, M,A,, González, L., Elustondo, D., Garrigó, R., Bermejo, R., Santamaría, J.M. 2006. Spatial and temporal trends of volatile organic compounds (VOC) in a rural area of northern Spain. Sci Total Environ. 30, 157-167.

Sillman, S. 1999. The relation between ozone, NO_x and hydrocarbons in urban and polluted rural environments. Atmos Environ. 33, 1821-1845.

Tran, N.K., Steinberg, S.M., Johnson, B.J. 2000. Volatile aromatic hydrocarbons and dicarboxylic acid concentrations in airbat an urban site in the Southwestern US. Atmos Environ. 34, 1485-1852.

WHO. 2000. Air quality guidelines for Europe. 2nd edition. Copenhagen: WHO Regional Publications; European Series, No.91.

HEAVY METAL CONCENTRATIONS AT THREE FRENCH SITES UNDER INDUSTRIAL AND TRAFFIC INFLUENCES, AND RURAL CONDITIONS PART I: ATMOSPHERIC PM10 PARTICLES COMPOSITION

A. Gaudry[1], M. Moskura[1], A. Senhou[1], S. Ayrault[2], F. Denayer[3], N. Bernard[4]
1-Laboratoire Pierre Sue, CNRS/CEA, CEA de Saclay-91191-Gif sur Yvette-France
2-Laboratoire des Sciences du Climat et de l'Environnement-91198-Gif sur Yvette-France
3-Institut Lillois d'Ingénierie de la Santé, 59120-Loos-France
4-Laboratoire de Biologie Environnementale, Université de Franche Comté-25030-Besançon-France

ABSTRACT

A whole experiment performed in 2005-2006 in 3 sites of France associated aerosols collections and the biomonitoring of the heavy metals atmospheric pollution in mosses. The present paper concerns the study of the PM10 aerosol composition. Another paper presents the biomonitoring results (Gaudry et al, this conference).

The 3 French locations selected for the experiment are: Montagney, a rural site in East of France, Saclay, a site nearby a highway of the region of Paris, and Dunkerque, an industrial town located at the North Sea coast, and where the pollution can originate mainly from steel and aluminum productions and petroleum refineries. The sampling duration was two months, in order to first, accumulate enough aerosol matter and to smooth variabilities of meteorological conditions, and second, to fit with two months frequencies of bryophyte collections.

More than 50 element concentrations were determined in all samples at all locations, by using neutron activation analysis (INAA) and inductively coupled plasma mass spectrometry (ICPMS).

The Montagney site can be considered a background continental site, because of its remoteness from pollution sources. The relatively low concentration of trace elements and the long period of matter collection enabled to observe iridium, supposed to accompany airborne Pt released from catalytic converters. Enrichment factors (EF) were compared to other rural sites described in the literature.

In Saclay, some elements displayed higher concentrations than in Montagney mainly for Na, Mg, Cl, Cr, Fe, Co, Cu, Nb, Mo, Ag, Sb, Cs, La, Ce and higher EF, mainly for Na, Mg, Cl, Cr, Fe, Co, Cu, Nb, Mo, Sn, Sb, Ba, La, Ce and Bi some of them known to be emitted by the car traffic (fuels, gasoil, oils, tyres, brake-linings).

In Dunkerque, the major pollution observed in aerosols was detected for Fe, Mn, Al. A clear increase of La was also observed, with respect to Ce, suggesting La emissions associated to one or several industries. EF were not possible to calculate, since the reference elements were also emitted by the local industries. However, for all elements, a ratio between the Dunkerque average concentrations and the Montagney average concentrations can be calculated. This gives a pollution index with respect to a background location that reached values higher than 10 for Cl, V, Fe, La, close to 30 for Mn, due to important industrial activities.

Such high concentrations may involve significant depositions of particles at ground and concentrations increases on soils and vegetation. A second work will show the bioaccumulation of heavy metals in mosses, transplanted at the three sites.

1. INTRODUCTION

The atmospheric pollution is recognized to trouble human health when it reaches critical concentrations, in various areas. Toxic compounds are emitted under various forms: gaseous like CO, NO_x, SO_2, or particulate matter containing organic or inorganic species. Small particles with diameters less than 10 µm (PM10 particles) are inhalable and can reach the bronchial system. The smallest, with diameters less than 2.5 µm even can have long residence times in the lungs and sometimes be definitively fixed. Regulatory rules are sometimes defined by states or international agencies (for instance World Health Organization) in order to limit toxic concentrations (SO_2, NO_x, total PM10 particles, Pb).

The present work presents the characterization of heavy metal concentrations in PM10 particles collected at 3 sites representing three kinds of pollutions: urban and industrial pollution, traffic pollution, background continental pollution in a rural site.

2. SITES AND SAMPLING

The site where the pollution was expected the highest is the town of Dunkerque, a city of 220 000 inhabitants, where several industries are working: steel and non-ferrous metal productions, oil refinery, chemical and food industries. This is also an harbour and the pollution by mobile sources like ships, trucks and cars is important.

A second site is located at Saclay (2000 inhabitants), at a 100 meters distance from the high density highway N118, connected to Paris and where 65000 vehicles per day drive. The surroundings are agriculture activities. All kinds of traffic are found from "traffic jam" to fast circulation.

The rural site is Montagney, a small village located 30 km West from the town of Besançon (100000 inhabitants).

PM10 particles were collected on quartz fiber filters by means of a ®Partisol pump, with a flow rate of 0.94 m^3 per hour. The total sampling periods for every sample, did not exceed 2 months and was phased to the sampling of mosses used for the biomonitoring experiment. However, due to pluggings of certain filters

sometimes, two filters were necessary to cover the period. The total experiment was performed between October 26, 2005 and June 7, 2006.

3. ANALYTICAL TECHNIQUES

Filters were stored at 40°C in a closed oven until the preparation for analysis. Each filter was divided in 4 parts, one of them for inductively coupled plasma mass spectrometry (ICPMS) determinations and the 3 other ones for instrumental neutron activation analysis (INAA) determinations. Two first quarters were devoted to short irradiations and long irradiations under thermal neutrons. The third quarter was used for a long irradiation by using epithermal and fast neutrons (ENAA), that improved the sensitivity for the determination of certain elements.

The fourth quarter of filter was dissolved by using an acid mixture composed of HF, $HClO_4$, HNO_3 and H_2O_2, in a closed 35 ml Teflon vessel. Strong acids were evaporated to near dryness and the residual dissolved in regal water (2/3 HCl+1/3HNO_3), then evaporated to 0.3 ml. This last operation was performed three times. Finally the dissolved sample was made up to 50 ml by 2% HNO_3 with 2 ppb internal standards (Be, In, Re). That solution was diluted 10 times and ready for ICPMS measurements. The ICPMS device was a ®Thermo-Optek "X7 series".

Both techniques were controlled by using various reference materials: NIST2783 filter, NIST 2789 dust, and spiked filters (A3) certified by the Department of Occupational Hygiene (Norway).

A study of the 54 elements was performed but results for 30 of them are given here : Na, Al, Cl, Ca, Sc, V, Cr, Mn, Fe, Co, Ni, Cu, Zn, As, Se, Br, Rb, Mo, Ag, Cd, Sn, Sb, La, Ce, Ir, Au, Pb, Tl, Bi and Th.

4. RESULTS

The two month time intervals involved that every site was submitted to a wide range of air trajectories. From such an experiment it is not possible to assess the various pollution origins. However, it was possible to define an average situation attached to every site and to make determination on an important amount of matter accumulated on filters, representing from 454 of m^3 until 1360 m^3.

The Table 1 gives the average concentration at each site for 30 elements, among with the relative standard deviation that defines the variability.

Table 1. Heavy metal concentrations recorded in PM10 particles at Dunkerque, Saclay and Montagney. Values with the symbol * are in 10^{-4} ng m^{-3}.

	MONTAGNEY (ng m^{-3})				SACLAY (ng m^{-3})				DUNKERQUE (ng m^{-3})			
	Avera-ge	mini	maxi	S.D%	Avera-ge	mini	maxi	S.D. %	Avera-ge	mini	maxi	S.D.%
Na	251	139	397	39	641	356	890	35	1420	1180	1920	20
Al	87	43	113	54	106	59	151	28	244	152	325	27
Cl	204	5	565	109	390	22	815	77	1761	612	2432	39
Ca	234	134	453	59	309	159	404	30	1090	741	1563	30
V	1.5	0.84	3.0	58	2.7	2.3	3.1	14	16	8	28	48
Sc	0.017	0.0076	0.029	58	0.020	0.013	0.026	31	0.055	0.037	0.081	48
Cr	1.2	0.83	2.2	49	2.2	1.9	2.4	11	5	3.4	6.9	28
Mn	3.8	2.4	7.7	57	5.1	4	7.3	25	99	80	122	17
Fe	105	72	166	39	290	230	333	13	1752	1141	2272	23
Co	0.04	0.015	0.054	40	0.15	0.085	0.21	37	0.3	0.25	0.35	11
Ni	1.5	0.84	2.8	54	1.9	1.3	2.5	23	9.4	5.8	13	34
Cu	4.5	2.2	9.9	71	14.5	10	17	18	16	7	36	75
Zn	23	13	45	56	27	21	33	17	131	92	176	23
As	0.57	0.24	1.3	73	0.56	0.31	1	48	2.5	2	3	18
Se	0.7	0.42	1.6	74	0.77	0.56	1.25	36	1.8	1.2	2	20
Br	3.2	2.4	6.2	53	3.5	2.1	5.2	34	9.6	4.9	13	33
Rb	0.74	0.40	1.5	62	0.41	0.34	0.51	21	1.9	1.2	3	37
Mo	0.81	0.4	2.2	95	1.5	1	2	27	2.1	1.5	2.7	22
Ag	0.037	0.013	0.12	131	0.03	0.018	0.05	49	0.12	0.08	0.15	25
Cd	0.25	0.09	1.6	74	0.24	0.17	0.3	22	1.3	0.9	1.9	41
Sn	1.5	0.7	3.5	74	3.1	2.3	3.8	19	2.9	1.6	3.7	36
Sb	1.1	0.7	2	51	2.7	2.1	3.3	18	2.2	1.3	3	33
La	0.16	0.082	0.32	63	0.35	0.22	0.53	34	1.6	0.9	2.4	39
Ce	0.18	0.096	0.33	54	0.42	0.32	0.49	20	0.46	0.37	0.54	15
Ir	12*	4*	28*	90	6*				16*			
Au	8*	1.5*	1*	58	15*	5*	43*	126	13*	1*	17*	19
Pb	9.7	3.8	22	75	10	7	12	22	34	24	40	17
Tl	0.06	0.012	0.17	115	0.021	0.012	0.032	40	0.57	0.35	1	17
Bi	0.12	0.05	0.28	75	0.13	0.1	0.15	17	0.32	0.24	0.38	17
Th	0.017	0.004	0.05	106	0.018	0.01	0.023	30	0.041	0.027	0.060	34

Comparison between Saclay and Montagney:
Average concentrations are similar in Saclay and Montagney for Al, Ca, V, Sc, Mn, Ni, Zn, As, Se, Br, Cd, Sn, Pb, Ir, Tl, Th. Thus, it is not possible to attribute to those elements a possible traffic origin. Their variability is rather linked to other kinds of sources, like remote pollution giving a continental background pollution and fine particles from wind erosion origins. It is worth noting that the Pb concentrations found in Saclay particles are very similar to those in Montagney. It seems that the prohibition to use Pb compounds additives in fuels gives convicing effects on Pb atmospheric concentrations near a high traffic area. Concentrations in PM10 particles of Saclay are higher than in Montagney for Na, Cl, Cr, Fe, Co, Cu, Mo, Ag, Sb, La, Ce, Bi. For some of them, the role of the traffic may explain such an increase. Fe can be emitted from mechanical wearing in various part of mobiles (Garg et al, 2000). Cu and Sb are emitted from brake-linings wearing (G.C. Lough et al, 2005). Br, Cu, Pb, Sb, Ba, Cr and Fe were also mentioned as originating from the traffic as observed in tunnel experiments (Stechmann and Dannecker, 1990). Zn, Mo, Cu and Sb were assumed to be associated to diesel-soot in the urban environment of Cologne (Weckwerth, 2001). La and Ce are present in converters of recent vehicles as coatings supporting platinum group elements used as catatysts in order to decrease NO_x emissions. Fuels and diesel fuels contain also various elements that are emitted in particles of car exhausts.

Comparison between Dunkerque and Montagney:
All concentrations are higher in PM10 particles collected in Dunkerque, than in Montagney by factors varying from at least 2.4 for (Th) to a factor of 32 (for Mn). Thus, all elements are emitted in hot sources working in Dunkerque, including crustal elements usually present in fine soil dust. For elements like Na, Cl and Br, a possible marine source was expected. A study of ratios between element concentrations Cl/Na, Na/Br, Na/Ca and Na/K, that are major element in sea water with conservative concentrations, shown a good correlation between Na and Cl with values close to the sea water ratio, except for the individual sample taken in summer 2006, for which an important loss of chlorine was observed. However, the other elements Br, K and Ca need other contributions than sea water. The important production of steel and non-ferrous alloys explains the increase at Dunkerque of the concentrations of Mn, Fe, Co, Ni, Zn, Mo, Sn, Al, Cr, Cu, As. The existence of carbon in steel, involves also the introduction of coal in the process, that can explain also the increase of elements like Sc, Th, Se, As. Petroleum refining is rather responsible of increases of element concentrations of V, La and some rare earth elements, either existing in the crude oil or used as cracking catalysts (Kulkarni et al, 2005).

Enrichment factors:
A comparison between PM10 contents and a reference upper continental crust (UCC) content (Taylor and Mac Lennan, 1985), for most elements, and Wedepohl (1995) for halogens was used in the past by many authors after having calculated an enrichment factor, EF. Here such a comparison appears in Fig 1, by using Sc as a reference element. EF is defined by the relation $EF=(Y_x/Sc_x)/(Y_{UCC}/Sc_{UCC})$, where EF is calculated for the element Y in a sample X, referring to the same element in UCC, and using Sc as a reference element in the same sample X and UCC.

Fig 1: Enrichment factors (EF) of heavy metals in PM10 particles at 3 french sites

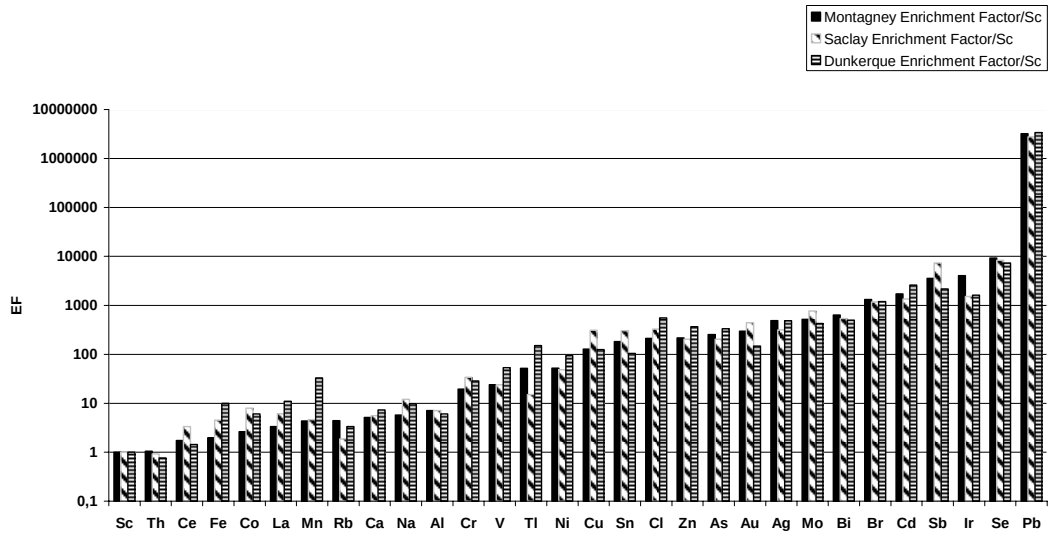

At Montagney, EF is less than 5 for Sc, Th, Ce, Fe, Mg, La, Mn, that can be considered as originating mostly from the upper crust by wind erosion. When EF is higher than 10, that is the case for Cr, V, W, Tl, Ni, some other sources are needed. EF values higher than 100 are also observed at Montagney for Cu, Sn, Cl, Zn, Au, Ag, Mo, Bi, I and even higher than 1000 for Br, Cd, Sb, Ir, Se. For all of them, other sources like hot sources or material wearing (most of them anthropogenic) are needed. This defines a background pollution on the continental areas, where human activities are highly developed, then able to invade remote locations. The highest enrichment factor 10^6 was observed for Pb, despite its prohibited use as an additive in car motor fuels. The existence of a significant enrichment for Ir, was not expected. A possible explanation should be the existence of Ir as an impurity in platinum of the new converters. Platinum is emitted in the atmosphere and concentrations of the order of 0.36 to 3 $pg.m^{-3}$ were measured in the city of Dortmund (Alt et al, 1993). Ir was observed in soils located in roadsides with concentrations of the order to 1% those of Pt (Ely et al, 2001). Impurities at a % level of Ir in Pt catalysts should explain concentrations and enrichment factors in PM10 particles collected in Montagney. In Saclay enrichment factors higher than in Montagney are observed for Ce, Fe, Co, Mg, La, Na, Cr, Cu, Sn, Cl, Au, Mo, Sb. For some of them, the traffic is expected to be the main cause (Mg, Fe, Co, Ce, Mg, La, Cr, Cu, Sb) as above mentioned. For some other elements, other causes should be evoked like transports of urban pollution (from Paris at 30 km, Versailles at 20 km, or a smaller town Les Ulis at 7 km). At Dunkerque, the increase of Sc concentrations due to local sources, made wrong the enrichment factor. The values indicated in Fig 1 have to be considered as minor values with respect to the real enrichment compared to natural dust. It is worth to note a particular enrichment for La with respect to Ce in Dunkerque, denoting a local significant source of that element. Presently, the most likely is the emission from the petroleum refinery. The case of Tl has also to be mentioned because it is a very toxic element and a regional source is made conspicuous. Some further studies may be developed in order to precise the source intensity and the potential impact on the environment.

5. CONCLUSION

The present work provides data on the background pollution by heavy metal fixed on PM10 particles, observed at a French continental rural site. The sensitivity of the analytical techniques enabled to detect elements like Ir in remote areas and Tl in an industrial area. At a site located near a highway, other elements are dispayed enrichments attributed to mobile sources. The site of Dunkerque displays much higher concentrations for most of heavy metals, making necessary further impact studies of the pollution on the environment and on human health.

Acknowledgements: This work is supported by the Primequal contract. We thank C. Mariet, and F. Carrot for their technical assistance, and J. Fabure for helpful discussion.

REFERENCES

F. Alt, A. Bambauer, K. Hoppstock, B. Mergler and G. Tölg, Platinum traces in airborne particulate matter. Determination of whole content, particle size distribution and soluble platinum, Fresenius J. Anal. Chem. (1993), 346, 693-696.

J.C. Ely, C.R. Neal, C.F. Kulpa, M.A. Schneegurt, J.A. Seidler and J.C. Jain, Implications of platinum-group element accumulation along U.S. roads from catalytic-converter attrition, Environ. Sci. Technol. (2001), 35, 19, 3816-3822.

B. D. Garg, S.H. Cadle, P. A. Mulawa and P.J. Groblicki, Brake-wear particulate matter emissions, Environ. Sci. Technol. (2000), 34, 24, 4463-4469.

A.Gaudry, M. Moskura, A. Senhou, S. Ayrault, F. Denayer, N. Bernard, Heavy metal concentrations at three french sites under industrial and traffic influences, and rural condition. Part 2: Biomonitoring by using mosses, 6th International Conference on Urban Air Quality, March 27 to 29, (2007), Limassol, Cyprus.

P. Kulkarni, S. Chellam, M.P. Fraser, Lanthanum and lanthanides in atmospheric fine particles and their apportionment to refinery and petrochemical operations in Houston, TX, Atmos. Environ. (2006), 40, 508-520.

G. C. Lough, J.J. Schauer, J.-S. Park, M.M. Shafer, J.T. Deminter and J.P. Weinstein, Emissions of metals associated with motor vehicle roadways, Environ. Sci. Technol. (2005), 39, 826-836

H. Stechman and W. Dannecker, Characterization and source analysis of vehicle-generated aerosols, J. Aerosol Sci., (1990), 21, 1, S287-S290

S.R.Taylor and S.M. Mac Lennan, The continental crustes: its composition and evolution. An examination of the geochemical record preserved in sedimentary rocks, (1985), Blackwell Scientific, Oxford.

G. Weckwerth, Verification of traffic emitted aerosol components in the ambient air of Cologne, Atmos. Environ. (2001), 35, 5525-5536

K.H.Wedepohl, The composition of the continental crust, Geochimica and Cosmochimica Acta, (1995), 59, 7, 1217-1232

TOMOGRAPHIC LP-DOAS MEASUREMENTS OF 2D TRACE GAS DISTRIBUTIONS ABOVE THE CITY OF HEIDELBERG, GERMANY

Denis Poehler, Andreas Hartl and Ulrich Platt -
Institute of Environmental Physics, University of Heidelberg, Heidelberg, Germany

ABSTRACT
In this work we present the first outdoor tomographic measurements using the Tomographic LP-DOAS technique. They were performed in the city of Heidelberg, Germany over an area of about 4 * 4 km². The instruments could detect the trace gases NO_2, SO_2, O_3, HCHO and HONO. For the first investigation period in February 2006 we discover high accuracy for NO_2 and SO_2 mean concentrations. They allow deriving two-dimensional distributions for these trace gases above the city. The best achieved time resolution for tomographic inverted distribution was 30 minutes. Different emission sources varying strongly in space and time can be identified. The results demonstrate that tomographic DOAS measurements can be used to study emissions and transport of trace gases.

1 INTRODUCTION
The measurement principle is based on the Long Path Differential Optical Absorption Spectroscopy (LP-DOAS) determining the absorption of different trace gases along an extended light path in the open atmosphere [e.g. Platt, 1994]. For the chosen measured wavelength range from 285 to 365 nm the trace gases NO_2, SO_2, O_3, HCHO and HONO feature strong absorptions in urban areas. These gases play a major role in the chemistry of the polluted atmosphere, e.g. photo smog, acid rain. In order to retrieve information of the spatial trace gas distribution tomographic LP-DOAS measurements are useful. This is especially important if small-scale variations exist or transport is significant. The application of tomographic techniques on outdoor measurements was recently investigated [Pundt et al., 2005; Laepple et al., 2004]. They reflect the necessity of multitude intersecting light paths for tomographic measurements. The development of the "Multibeam" LP-DOAS instrument [Pundt and Mettendorf, 2005], with a modified LP-DOAS telescope from Axelsson et al. [1990], allows the measurement along several light paths simultaneously with one instrument, and therefore higher time resolution than typical LP-DOAS instruments.
With the suitable combination of three "Multibeam" LP-DOAS instruments and the use of tomographic reconstruction techniques good quality 2D reconstructions of the measured trace gases can be achieved. The obtained information from the experiment is not only helpful for pollution monitoring, but also to validate chemical transport models.

2 METHODOLOGY
2.1 Basic LP-DOAS principle
Typical LP-DOAS instruments emit the light of an artificial light source (typically Xe-Arc lamp) as a parallel light beam to a cube retro reflector and simultaneously receive the reflected light. The received light contains information of the trace gas absorptions, typically in the UV and visible wavelength range. Quantitatively the absorption of radiation is expressed by Lambert-Beers Law:

$$I(\lambda) = I_0(\lambda)\exp\left(-\int_0^L \sum_i \sigma_i(\lambda)\cdot c_i \cdot dl\right) \tag{1}$$

Where $\sigma_i(\lambda)$ denotes the absorption cross section at the wavelength λ, while $I_0(\lambda)$ is the initial intensity emitted from the source and $I(\lambda)$ is the radiation intensity after passing through an air volume with a length L. Since atmospheric scattering and broad-band absorption can hardly be separated, the absorption cross section σ is divided in two parts:

$$\sigma(\lambda) = \sigma_{broad}(\lambda) + \sigma'(\lambda) \tag{2}$$

$\sigma'(\lambda)$describes only the characteristic narrow band absorption structures of different trace gases. For a DOAS setup Lambert-Beers Law can be expressed as:

$$I(\lambda) = I_0(\lambda)\exp\left(-\int_0^L \sum_i \sigma_{i,broad}(\lambda)\cdot c_i \cdot dl\right)\times\exp\left(-\int_0^L \sum_i \sigma_i'(\lambda)\cdot c_i \cdot dl\right) \tag{3}$$

$$I(\lambda) = I_0'(\lambda)\exp\left(-\int_0^L \sum_i \sigma_i'(\lambda)\cdot c_i \cdot dl\right) \tag{4}$$

$I_0'(\lambda)$ contains the initial intensity and the broad band absorption structures and is computed from the measured spectrum $I(\lambda)$ by applying a low pass filter. The in laboratory measured absorption cross sections $\sigma_i(\lambda)$ have to be treated with the same high pass filter algorithm to achieve the differential absorption cross sections $\sigma_i'(\lambda)$.

With this technique it is possible to determine average concentrations along the investigated light path of many different trace gases simultaneously like O_3, SO_2, NO_2, HONO, HCHO, BrO, NO_3, ClO, IO [e.g. Platt, 1979, 1994]. Our measurements were performed over a wavelength range from 285 to 365 nm and allow the determination of NO_2, SO_2, O_3, HONO and HCHO.

2.2 LP-DOAS Tomography

LP-DOAS Tomography is a combination of multiple LP-DOAS measurements with tomographic inversion techniques. 10 to 30 or even more light beams are used to probe the concentration field from different directions [e.g. Laepple, 2004; Hartl et al., 2006]. With the use of a "Multibeam" LP-DOAS instrument it is possible to measure up to four light beams simultaneously. With moving external mirrors more light paths can be investigated. Combining three of these instruments at different locations and belonging reflectors, a good coverage of an investigating area can be achieved.

2.3 Multibeam LP-DOAS instrument

For tomography the Axelson et al. [1990] telescope typically used for LP-DOAS measurements has been modified to a "Multibeam" LP-DOAS telescope which emits four light beams. Figure 1 shows a sketch of a complete system with four emitting beams.

The telescope **A** has a main mirror of f=1500mm and 300mm diameter and is similar to a coaxial Newton telescope. The crucial change was realised inside the lamp housing **B**. Up to four small mirrors (two in vertical and two in horizontal direction) inside the lamp house produce one virtual light source each in the focal plane of the main mirror. They emit light beams in specific directions, depending on the position and orientation of the lamp housing mirror.

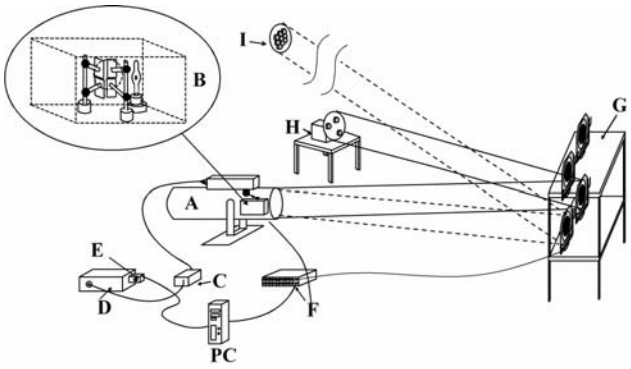

Figure 1. Experimental setup of an entire Multibeam system [Pundt and Mettendorf, 2005]

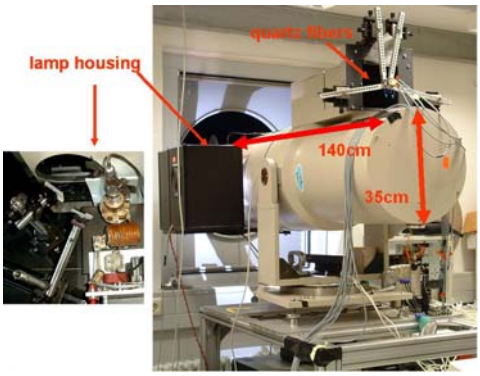

Figure 2. "Multibeam" LP-DOAS instrument (Hydra) with extended view: inside of the lamp housing from above.

In front of the telescope plane mirrors (360 x 320 mm^2) are positioned on the tower **G** in a distance of minimum 15m. They redirect each beam into the desired direction, for example to a retro reflector array **I**. The mirrors can be turned in horizontal and vertical direction with stepper motors by the controller **F**. After reflection at the cube retro reflectors the light is received with the same telescope. For each beam the received light is focused on a quartz fiber and than sent over a mode mixer **C** to an imaging Czerny-turner spectrograph where a 2D CCD chip **E** measures the spectrally analysed signal. The lamp reference spectrum can be measured over a reflector array **H** close by the instrument**.** [Pundt and Mettendorf, 2005]

3. THE MEASUREMENT SETUP OF HEIDELBERG

For the measurements in Heidelberg three "Multibeam" instruments were installed on the buildings labeled "IUP", "SAS" and "HD-Druck" (Figure 3). Additionally different in-situ monitors were used at the "IUP" and at an environmental measurement station DEBW009 (in north-west of Heidelberg) to compare the results.

4. TOMOGRAPHIC MEASUREMENTS AND RESULTS - FEBRUARY 2006

First tomographic measurements were performed in February 2006. In this period the detected concentrations of NO_2 and SO_2 were significant above the detection limit and could be used for tomographic reconstructions. Before a reconstruction could be applied the detected column densities need to be averaged and interpolated to synchronous time intervals. Due to a measurement cycle time of 15 to 30 minutes the best achievable time resolution was limited to 30 minutes. To give a better overview of the change of distribution over a day, 3 hour averaged data are used for the reconstruction as well and presented below. The resulting average concentrations along all 18 light paths, including measurements with in-situ monitors, are displayed in Figure 4. The concentrations display strong variability in time, but only slight differences between the

investigated light paths. They are dominated by the background concentrations. This is driven by the weather conditions and the local emissions, for NO_2 mainly from traffic during the rush hours and for SO_2 mainly from small heating systems.

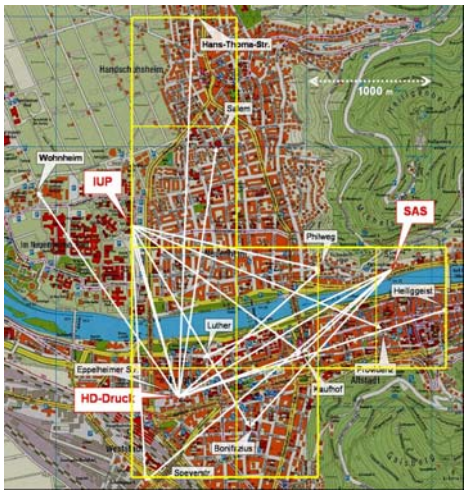

Figure 3: Measurement geometry in Heidelberg with three Multibeam telescopes located at the top of the buildings "IUP", "SAS" and "HD-Druck". The light beams (white lines) are redirected to 18 retro reflector arrays. The yellow lines indicate the boxes used for the tomographic 2D reconstruction of the trace gases displayed in Figure 5.

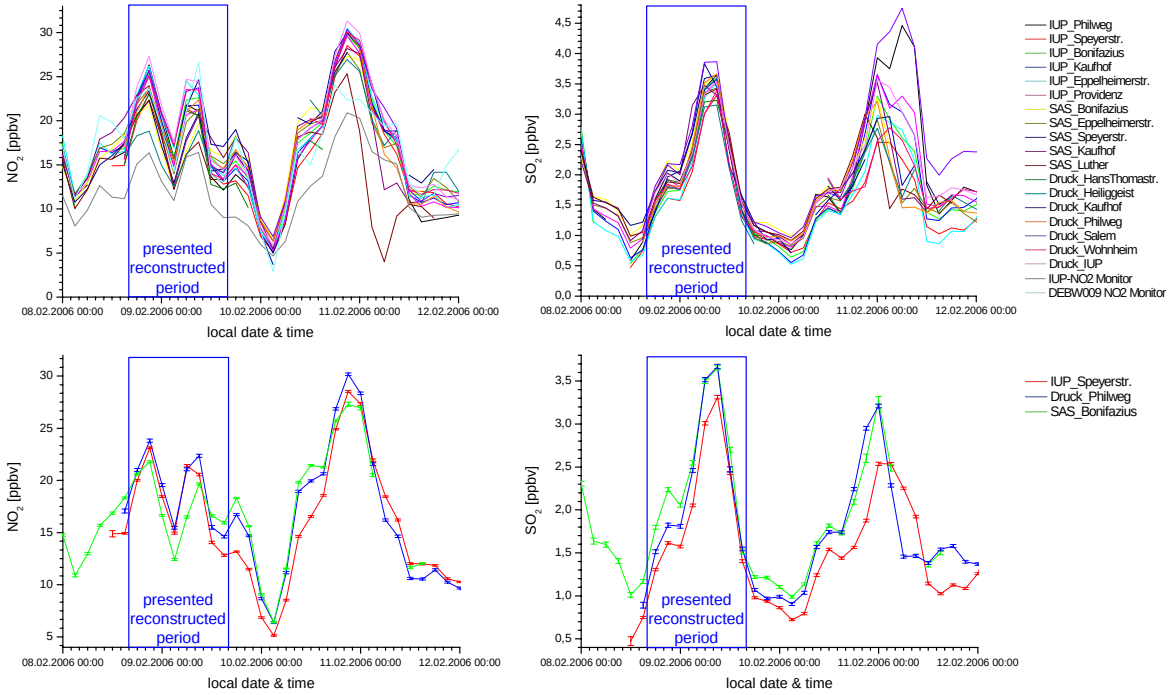

Figure 4: Upper plots: Average concentration along all 18 light paths and in-situ monitors averaged over 3 hours (left: NO_2, right SO_2). Lower plots: Example for the measurement errors for 3 light paths.

To obtain spatial fluctuations the differences in concentration for different light paths need to be larger than the measurement error. The accuracy of this measurement technique is adequate good to achieve this condition. The lower plots in Figure 4 display as an example the concentrations of three light paths including the measurement error.

Due to the underdetermined system the reconstruction is made with a linear parametrisation using a least square minimum norm solution (Hartl et al., 2006). The used grid for the reconstruction is displayed as yellow lines in Figure 3. The reconstruction tool determines the concentration at each grid knot and performs a bilinear interpolation between the knots. The discretisation produces some artefacts. First the maximum or minimum concentration can only be located at the grid knot. Second the concentration peaks and valleys are shifted to the next grid knot. Fluctuations smaller than the grid size, e.g. between two grid knots, can not be resolved. The reconstructed distributions of NO_2 and SO_2 for 24 hours (8^{th} to 9^{th} February 2006) are displayed in Figure 5. This period is highlighted with a blue frame in Figure 4.

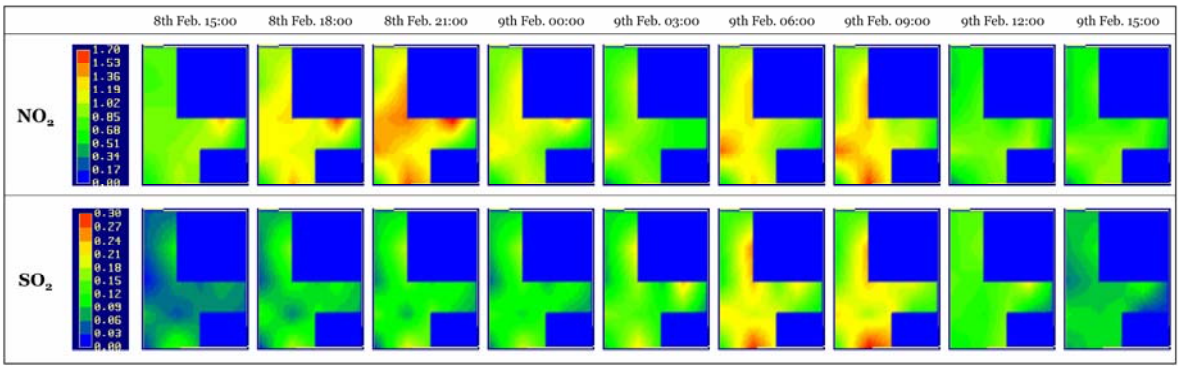

Figure 5: Tomographic reconstructed distributions for one day using 3 hour averaged data. The area and the used reconstruction grid is indicated with yellow lines in the map of Figure 3. The main wind direction during this period was from south-west.

The distributions of both trace gases display strong temporal and spatial variations. Highest NO_2 concentrations occur in the late evening and morning hours especially in the regions of high traffic roads. The high way end in the west and many roads divert from there to the south, to the north over the river Neckar and along the river to the east. Considering the wind direction to the north-east, the emissions are dispersed in this direction. We can conclude that the local high concentrations occur due to emissions from traffic during rush hours.
The highest SO_2 concentrations arise in the early morning hours when most small heating systems start to work after the night break and warm up the water reservoir and the flats. The highest concentrations occur in the south. This is an area with older residential houses, where still many heating systems using oil. These energy sources are mainly hold responsible for the SO_2 emissions. In areas using heat from a district heating network or gas as energy source feature no locally increased SO_2 concentration. This is the case in the north and north-west. The concentrations are as well lower along the river due to missing emission sources. We conclude that the spatial high concentrations arise mainly due to emissions from small oil heating systems. This example of tomographic measurements shows that it is a useful tool to monitor spatial variations of trace gas distributions.

5. OUTLOOK

The system measured continuously over several weeks in winter 2005 / 2006 and summer to winter 2006 / 2007. Most of the data are not jet evaluated. The time resolution was increased for the last measurements to 10 minutes. Additionally the reconstruction quality can be increased due to further optimization of the grid. We intend to compare the tomographic measurements with the results from 2D and 3D chemical transport models.

6. ACKNOWLEDGEMENTS

We thank the companies “Heidelberger Druckmaschinen AG” and “SAS Institute GmbH, Germany” for the possibility to install a telescope on the roofs of their buildings and all organizations which allow us to mount retro reflector arrays at their building.

7. REFERENCES

Axelsson, H., Galle, B., Gustavsson, K., Regnarsson, P. and Rudin, M. 1990. A transmitting/ receiving telescope for DOAS-measurements using retroreflector technique. Dig. Top. Meet. Opt. Remote Sens. Atmos. OSA, 4, p. 641-644.

Hartl, A., Song, B.C. and Pundt, I. 2006. 2D Reconstruction of Atmospheric Concentration Peaks from Horizontal Long Path DOAS Tomographic Measurements: Parametrisation and Geometry within a Discrete Approach. ACP-0263.

Laepple T., Knab, V., Mettendorf, K. U. and Pundt, I. 2004. Longpath DOAS tomography on a motorway exhaust plume: Numerical studies and application to data form BABII campaign. Atmospheric Chemistry and Physics Discussion. Vol. 4, 2435-2484

Platt, U., 1994. Differential Optical Absorption Spectroscopy (DOAS), Monitoring by Spectroscopic Techniques, M. W. Sigrist, J. Wiley, New York.

Platt, U., Perner, D. and Pätz, H. 1979. Simultaneous measurements of atmospheric CH2O, O3 and NO2 by differential optical absorptions. J. Geophys. Res., (84), p. 6329-6335.

Pundt, I. and Mettendorf, K. U. 2005. Multibeam long-path differential optical absorption spectroscopy instrument: a device for simultaneous measurements along multiple light paths. Appl. Opt., 44, 23, 4985-4994.

SATELLITE-DERIVED DETERMINATION OF AEROSOL OPTICAL THICKNESS FOR AIR POLLUTION MONITORING: A SIMPLIFIED ALGORITHM

HADJIMITSIS D.[1, 2, 3], VRYONIDES P.[1], THEMISTOKLEOUS K.[1, 4]
TOULIOS L.[5]and CLAYTON C.R.I[2]
[1] Frederick Institute of Technology, Department of Civil Engineering, 7, Y. Frederickou St., Palouriotisa, Nicosia 1036, Cyprus.
[2] University of Southampton, Department of Civil & Environmental Engineering, Highfield Southampton SO17 1BJ, UK.
[3] Cyprus Research Centre for Remote Sensing & GIS, Hadjimitsis Consultants, P.O.Box 60055, Paphos, Cyprus.
[4]ARCHISYSTEMS LTD, Limassol, Cyprus.
[5]National Agricultural Research Foundation (NAGREF) Theofrastou str. 1 41335 Larissa Greece
E-mail: dhadjimitsis@cytanet.com.cy ; eng.vp@fit.ac.cy, kt33@cytanet.com.cy, nagref@lar.forthnet.gr, c.clayton@soton.ac.uk

ABSTRACT
In this study, a new algorithm for estimating the aerosol optical thickness from satellite image data alone without the use of any other auxiliary data is presented. In this new algorithm, the aerosol optical thickness has been determined using the basics of the radiative transfer equations and the simplified version of the 'darkest-pixel' atmospheric correction algorithm. The algorithm works on two scenarios (a) by considering that the reflectance values of the selected dark targets is zero (b) by inserting a specific value of the reflectance value of the proposed darkest targets. Both scenarios are used to determining the corrected aerosol optical thickness value by investigating the contrast values of the sub-images before and after atmospheric correction. As for the algorithm validation, the simultaneous meteorological data with the LANDSAT/TM and SPOT overpass, respectively, shows that the satellite-derived aerosol optical thickness is well correlated with the one extracted by considering the visibility values. The determined aerosol optical thickness has been used as a tool of assessing air pollution in several areas in Cyprus and UK regions. Based on the fact that almost a Landsat TM scene covers mostly the whole Cyprus, the proposed algorithm can be used in conjunction with a GIS system for locating the suitable positions of mobile air pollution stations.

1. INTRODUCTION

Air quality monitoring stations have been established in major cities and provide means for alert. The measuring stations are scarcely distributed and they do not provide sufficient tools for mapping atmospheric pollution since air quality is highly variable. Air quality monitoring has typically been taken place using ground based instrumentation, which has restricted the area of land that can be monitored and investigated. The ground instruments are designed to monitor specific pollutants and a lot of these instruments cannot provide an accurate description of the total concentration of all pollutants at a citywide level. For these reasons, satellite remote sensing has been widely used to assist in air quality monitoring of urban areas. Satellite remote sensing is certainly a valuable tool for assessing and mapping air pollution due to their major benefit of providing complete and synoptic views of large areas in one image on a systematic basis due to the sufficient temporal resolution of various satellite sensors. Indeed, satellite observations can show the major sources of pollution and the distribution pattern can assist in determining where the effort should be focused to decrease the level of pollution; and determine any relationship between the city features and the air pollution distribution (Wald and Baleynaud, 1999).

Tulloch and Li (2004) provide an overview of the four major satellite remote sensing techniques that are used by various researchers to determine air quality in urban areas. The first method is measuring the aerosol thickness in the atmosphere, second is black particle measurement, third is a visual inspection of satellite imagery, and the last one is the land-use/land-cover change analysis.

A basic understanding of how aerosol thickness can be measured is required before any case studies can be reviewed. Aerosol thickness is an indicator of the overall pollution of an area. There have been many methods used over the past 30 years to determine and monitor aerosol thickness, the major four of which are:-

- 'ocean method'
- 'brightness method',
- 'contrast-reduction method',
- 'Dark vegetation method' (Sifakis *et al*., 1998).

The proposed method is based on the use of the darkest pixel in the scene. The spectral blue band (e.g. Landsat TM band 1) is used in the proposed method since water vapour absorption is found from the literature to have negligible effects in this wavelength region (Forster, 1984; Kaufman, 1989). Guoyong et al. (1999) shows that the aerosol optical thickness of the *blue band*, estimated from the dark object approach, agrees quite well with the Sun photometer measurements. Since the surface reflectance of a dark object is

small, then the error retrieved aerosol optical thickness is also relatively small compared to errors over bright surfaces. The assessment of atmospheric pollution is explained by changes of aerosols. Aerosols are generated in industrial and urban areas from gases like SO_2 and NO_2 in chemical reactions in the humid air environment (Forster, 1984).

2. METHODOLOGY

The proposed methodology is shown in Figure 1 and is briefly described below:

- Choose the suitable dark-target in the scene
- Select a sub-image from the desired scene
- Check the image contrast for the selected sub-image
- It is recommended to divide the image under investigation into different sub-regions. In the case where many dark objects appeared in the scene it is necessary to calculate separately the darkest pixel for every sub-region. This is more important for hazy atmospheres with spatial variability.
- By applying the principle of the DP method, every dark pixel in the sub-region represents the atmospheric path radiance in this region. The atmospheric path radiance is a function of the aerosol optical thickness which is the term used to define the prevailing atmospheric conditions.
- Input parameters: Ozone transmittance (t_{O3}) =1, Water vapour transmittance (t_{H20}) =1, Aerosol single scattering albedo=1 (perfectly scattering aerosol); Surface reflectance of the dark-target: use standard values (from spectral library files or consider it as zero value).
- Run the algorithm and determine the aerosol optical thickness

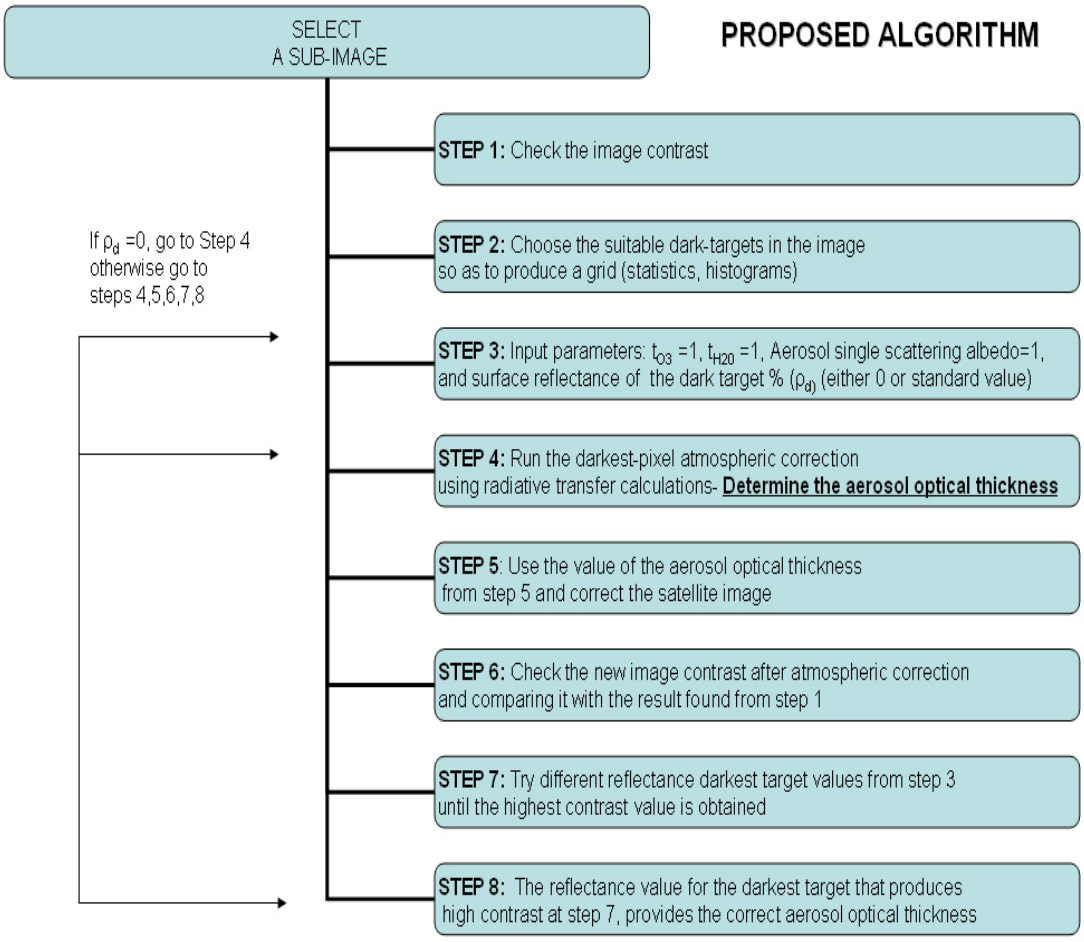

Figure 1. Proposed algorithm for determining the aerosol optical thickness

3. RESULTS AND DISCUSSION

3.1 London Heathrow Area (UK)

The proposed approach was applied to Landsat-5 TM band 1 (0.45-0.52 μm) images of the London Heathrow area acquired on 17th of May, 2nd of June 1985, 4th of July 1985, 28th of September 1985 and 28th of June 1986. By relating the determined aerosol optical thickness with the visibility values shown in Table 1, a logarithmic regression was fitted with a correlation coefficient r^2=0.82. The observed significance for the regression model was 0.02<0.05. The authors reproduced the plots obtained from Forster (1984) and Tanre *et al*. (1990) and those data have been plotted on the same plot so as to compare their results. The author's results show an agreement with Forster's *aerosol optical thickness Vs visibility results* and a small deviation from Tanre's model (Hadjimitsis and Clayton, 2006).

Table 1. Calculated aerosol optical thickness for the three Landsat-5 TM band 1 images of Heathrow Airport area

Image Date	Determined Aerosol Optical Thickness	Visibility (km)	RH %
2-June-1985	**0.13**	**26.2**	55
17-May-1985	0.58	13.2	54.1
28-September-1985	0.60	6.9	68.4
28-June-1986	0.70	5.4	51.6
4-July-1985	0.76	7.5	60.4

3.2 Cyprus

The proposed algorithm was applied to: (a) Landsat-5 TM band 1 images of the Paphos Airport area acquired on the 11/5/2000, 11/9/98 and 3/6/1985 and (b) SPOT-5 sub- image of Larnaca area acquired on 11/4/2003 (see Figure 2). A positive high correlation of between the visibility data measured at Paphos Airport and the deduced aerosol optical thickness for each Landsat TM image has been found. This clearly indicates the potential of the proposed method for assessing the prevailing atmospheric conditions. Table 2 shows the prevailing meteorological data as well the determined atmospheric path reflectance component for each satellite Landsat TM overpass. It is apparent that a hazy atmosphere was occurred on the 3rd of June 1985 (visibility=15 km); and clear atmospheric conditions were found for the 11th of May 2000 (30 km). For the SPOT band 1 image, the determined aerosol optical thickness 0.18.

Figure 2. (a) Landsat TM image of Cyprus (11/9/98)

Table 2. The atmospheric path reflectance indicates the type of the prevailing atmospheric conditions (aerosol optical thickness+Rayleigh optical thickness) (Paphos Airport Region)

Image Date	Visibility	Mean RH (%)	Atmospheric Path (reflectance)
11-5-2000	30	69.5 %	0.094
11-9-1998	20	77.5 %	0.135
3-6-1985	15	69.5	0.148

4. CONCLUSIONS

The proposed algorithm shows how to determine the aerosol optical thickness for a certain area of interest using only the image itself without any auxiliary data (except from the case whether the user wants to run the algorithm with certain values of the dark target reflectance value). Visibility data have been used to support our determined values of the aerosol optical thickness. Further validation is needed to support our proposed algorithm using simultaneously the following data: air pollution data, meteorological data, sun-photometer data and satellite image data. The method was also straightforward and easy to apply for potential users of QuickBird and IKONOS data.

5. ACKNOWLEDGEMENTS

The authors acknowledge the support of the Hadjimitsis Consultants in Cyprus (www.cyprusremotesensing.net).

6. REFERENCES

Forster, B.C. 1984. Derivation of atmospheric correction procedures for Landsat MSS with particular reference to urban data. International Journal of Remote Sensing, 5(5), 799-817.

Fraser, R. S., Gaut, N. E., Reifenstein, E. C., and Sievering, H. 1983. Interaction mechanisms within the atmosphere. In Manual of Remote Sensing, edited by R. G. Reeves (Falls Church, VA: American Society of Photogrammetry).

Guoyong W., Tsay Si., Cahalan R and Oreopoulos L. 1999.Path radiance technique for retrieving aerosol optical thickness over land.Journal of Geophysical Research, vol. 104, no. d24, pages 31,321–31,332.

Hadjimitsis D.G and Clayton C.R.I. 2006. Detecting Air pollution from Space Using Image-based method, *International Conference: Protection and Restoration of the Environment VIII, Crete*, July, 2006, organized by the: Technical University of Crete, Stevens Institute of Technology, p.313.

Kaufman, Y.J., Fraser, R.S., and Ferrare, R.A.1990. Satellite measurements of large-scale air pollution methods. Journal of Geophysical Research, 95, 9895-9909.

Sifakis N, Soulakellis N and Paronis D.1998. Quantitative mapping of air pollution density using Earth observations: a new processing method and application to an urban area, International Journal of Remote Sensing, 19 (17), 3289-3300.

Tanre D., Deroo C., Dahaut P., Herman M., and Morcrette J.J. 1990. Description of a computer code to simulate the satellite signal in the solar spectrum: the 5S code, International Journal of Remote Sensing, 11, 659-688.

Tulloch M. and Li J. 2004. Applications of Satellite Remote Sensing to Urban Air-Quality Monitoring: Status and Potential Solutions to Canada. Environmental Informatics Archives, Volume 2, 846-854,

Wald, L., Basly, L., and Balleynaud, J.M. 1999. Satellite data for the air pollution mapping. Proceedings of the 18th EARseL symposium on operational sensing for sustainable development (Enschede, Netherlands, 11-14 May 1998), *In: Operational Remote Sensing for Sustainable Development* (edited by Nieeuwenhuis, G.J.A, Vaugham, R.A., Molenaar, M.), pp.133-139.

APPLICATIONS OF SATELLITE REMOTE SENSING & GIS TO URBAN AIR-QUALITY MONITORING IN CYPRUS: POTENTIAL SOLUTIONS AND SUGGESTIONS

HADJIMITSIS D.G.[1, 2, 3], THEMISTOKLEOUS K.[4], VRYONIDES P[1] , TOULIOS L.[5] and CLAYTON C.R.I[2]
[1] Frederick Institute of Technology, School of Applied Sciences, 7, Y. Frederickou St., Palouriotisa, Nicosia 1036, Cyprus.
[2] University of Southampton, Department of Civil & Environmental Engineering, Highfield, Southampton SO17 1BJ, UK.
[3] Cyprus Research Centre for Remote Sensing & GIS, Hadjimitsis Consultants, P.O.Box 60055, Paphos, Cyprus.
[4]Themistokleous&Associates (ARCHISYSTEMS LTD), Irinis139a, 3022, Limassol, Cyprus.
[5]National Agricultural Research Foundation (NAGREF) Theofrastou str. 1 41335 Larissa Greece
E-mail: dhadjimitsis@cytanet.com.cy ; kt33@cytanet.com.cy, eng.vp@fit.ac.cy, nagref@lar.forthnet.gr, c.clayton@soton.ac.uk,

ABSTRACT
Urban air quality has traditionally been monitored with networks of ground monitoring stations and the use of predictive models. The increasing availability of satellite imagery together with advances in digital image processing techniques and the GIS tools, provide a new avenue to monitor urban air quality at large-scale and regional levels. This paper presents on overview of the beneficial use of both satellite remote sensing and GIS tools for air-quality monitoring in several areas around Cyprus. Practical solutions for developing an up-to-date system for mapping air-pollution levels are also suggested and presented. Landsat TM satellite images are used in this study to explore the potential of satellite remote sensing in conjunction with GIS to systematically monitor air quality in the urban areas.

1. INTRODUCTION

The use of geographic information systems (GIS) has created a new area of environmental modelling. More powerful computers have the ability to run air quality models at global and local spatial scales possible. Generally, the modeling system should consist of other subsystems such as information regarding point and area sources of air pollution, spatial description of terrain elevations, meteorological data, air quality monitoring networks etc. Indeed, the use of GIS can assist in: air pollution modeling; can be further extended to processing the surface data (as shown by Longley *et al*., 2001; Matejicek *et al*., 2005) and should be extended to include temporal variations of three-dimensional spatial data.

As it has been found in the literature, several methods are used for small scale and large scale air quality modeling in conjunction with GIS analysis. Interpolations, integrations of land cover surface data, and the GIS analyses are used on small scale spatial models carried out in the kilometer grid as shown by Matejicek (2002) However, in the case of large scale air quality modelling, more detailed spatial data are needed to include the impact of buildings and other manmade barriers on the distribution of air pollutants, (Civis, 2001). Statistical theory is also used to indicate spatio-temporal interactions as shown by Briggs *et al.* (2000).

Using the recommendations made on the 'Executive Summary VII, Preliminary Assessment of Ambient Air Quality in Cyprus', the proposed pilot study has been performed to assist the local authorities as well the governmental sector to formulate a Strategic Plan for the management and monitoring of air pollution in Cyprus. The first measure for an effective improvement of the air quality is the implementation of an air quality management and control system which is hosted at the Government of Cyprus. Indeed, the use of GIS and remote sensing will be ideal tools to achieve the following tasks and provide up-to-date data for any user:
This management will be responsible for:

- Establishing of an emissions remote control centre
- To complete the air quality monitoring network
- To provide an online information of the public: online data transfer, Internet and TV connection
- Development of plans and programmes for air pollution abatement measures and air quality assessment and management strategies
- Number and location of monitoring stations for an air quality monitoring network

Based on the fact, that one of the main requirements for the integrated spatial modelling of air quality in the framework of GIS is to represent a common geospatial coordinate system, vector themes for description of surface objects (supported by raster and surface data (digital elevation models), and vector themes for representation of air pollution inputs (local point, line and area sources of pollution, long-distance transport of air pollution), the authors suggest the following methodology for assisting the Cyprus Government to establish a complete system for managing air pollution.

2. METHODOLOGY

The basic task of the proposed project is to develop a complete network system using suitable in a timely and cost-effective manner techniques for managing systematically the air pollution activities in the Cyprus region and providing up-to date related information. Indeed, satellite remote sensing and Geographical Information Systems (GIS) techniques are found to be the most effective tools for such case.

Satellite Remote Sensing

Satellite remote sensing is used to locate the monitoring stations on a synoptic map as well to suggest future suitable areas for locating the monitoring stations based on their determined aerosol optical thickness found from the proposed new algorithm shown by Hadjimitsis *et al* (2007). Based on the fact that almost a Landsat TM scene covers mostly the whole Cyprus, the proposed algorithm can be used in conjunction with a GIS system for locating the suitable positions of mobile air pollution stations. Then the GIS can be used to insert all the databases automatically from the monitoring stations or from other sources.

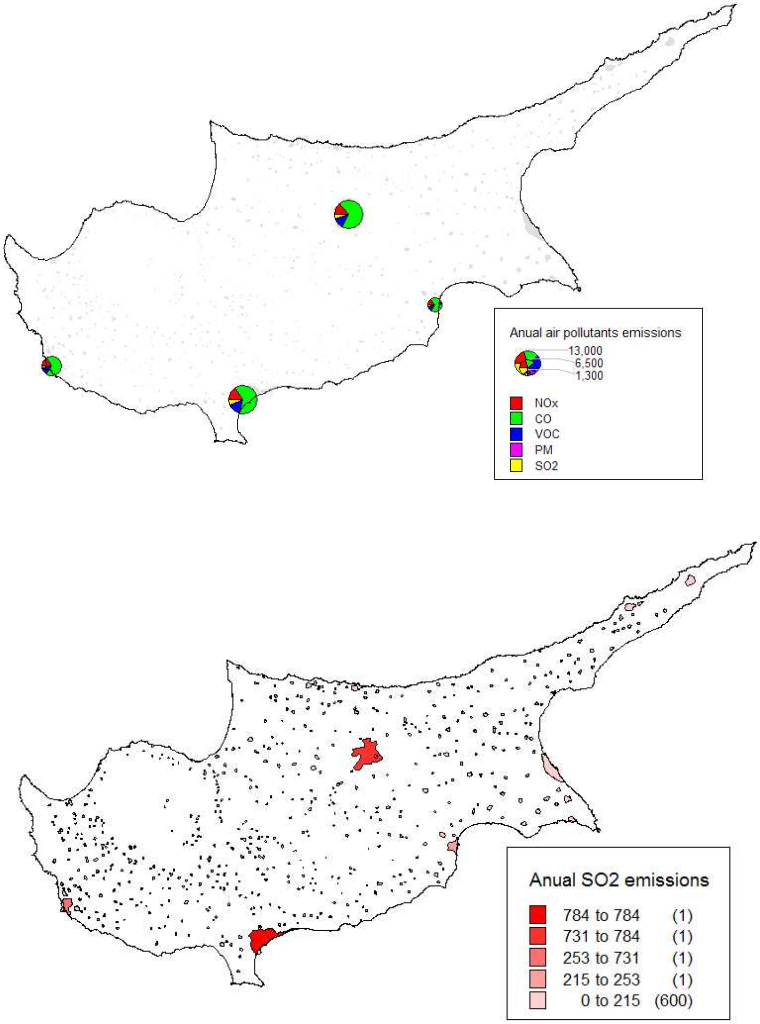

Figure 1. Annual air pollution data used in a GIS system for the Cyprus Island.

GIS data:

The GIS database will consist of base data, input and output data.

Base data include: (a) map base-data (for use initially as a layer to locate any other data that to be stored in the system; (b) air pollution data from the stations (data can be obtained from: http://www.airquality.dli.mlsi.gov.cy/); (c) detailed survey, topographical data and any available thematic mapping information (d) meteorological data from the airports or stations (e) aerosol optical thickness data as determined from the satellite images.

Input data include: (a) Distribution maps for each of the monitoring stations; (b) Constraint data as may be readily available in digital form or relatively easily digitised (buildings, roads etc); (c) Locations of each

station
Output data will be provided in the form of maps for the individual air-pollutant reports and papers and site specific data as required.

Figure 1 shows how air quality data obtained from the Ministry of Labour (2005) are used in a GIS system for the Cyprus region. Figure 2 shows the overlay of GIS locational information of air pollution stations in different areas in Cyprus on a Landsat-5 TM image of Cyprus acquired on 3/6/85. It is important to mention that since a Landsat TM satellite image of Cyprus mostly covers the whole island, by using the proposed algorithm shown by Hadjimitsis *et al*. (2007), it can be more efficient proposed location of the air pollution stations based on the determined aerosol optical thickness using the algorithm shown by Hadjimitsis *et al*. (2007).

3. RESULTS AND DISCUSSION

The following data are used to demonstrate the potential of using GIS for assisting air-pollution studies in Cyprus. The data shown in Table 1 are used to create a database for the Paphos Airport site. It is apparent that the haziest atmosphere (most polluted) is occurred for the image acquired on the 3/6/1985 as can be easily supported from the visibility data.

Table 1. Input data on a GIS (Paphos Airport area/Cyprus)

Image Date	Visibility	Mean RH (%)	Atmospheric Path : found from the satellite image data (REFLECTANCE)	NO2 average in μg/m³	SO2 average in μg/m
				(15)	(5.1)
11-5-2000	30	69.5 %	0.094		
11-9-1998	20	77.5 %	0.135		
3-6-1985	15	69.5	0.148		

The atmospheric path component (parameter used for assessing atmospheric pollution) has been extracted by using the Landsat TM image of Cyprus acquired on 3/6/1985 for three different areas around Cyprus as shown in Table 2 after using the proposed algorithm shown by Hadjimitsis et al. (2007). It is apparent from Table 2, that Kouklia area which is very near to the Paphos International Airport has higher value of atmospheric path radiance than the other two areas in Limassol (Germasogia and Kalavassos) (see Figure 2). This shows that since the Mie Scattering is related with the aerosol optical thickness (part of atmospheric path radiance component); the higher value of atmospheric path radiance indicates high concentrations of particulate matter (PM10). Such pilot study can be further expanded by dividing into grids the future Landsat TM image acquisitions of Cyprus and using the determined aerosol optical thickness (or atmospheric path component); air pollution stations can be installed to the right positions.

Table 2. Input data on a GIS (Kouklia, Kalavassos, and Germasogia)

	Atmospheric Path Radiance Component ($mWcm^{-2}\ sr^{-1}\ \mu m^{-1}$)
Kouklia	0.86
Germasogia	0.50
Kalavasos	0.73

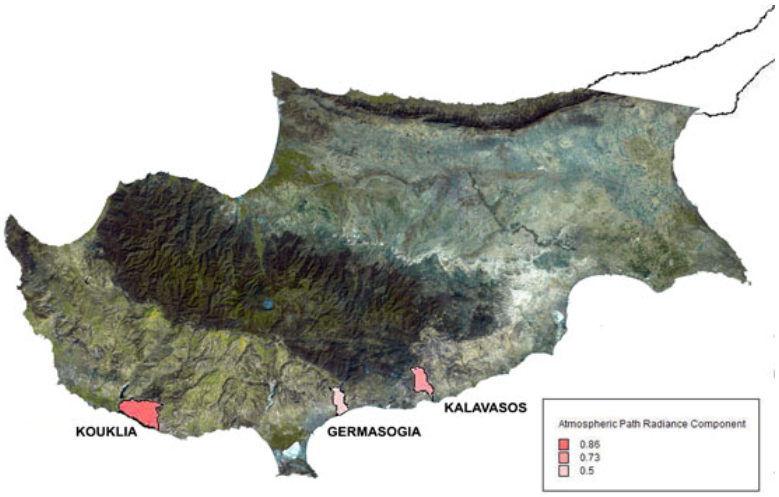

Figure 2. Overlay of GIS/Landsat TM image and determined values of the atmospheric path radiance. Kouklia area has a more polluted atmosphere than Germasoyia and Kalavasos areas.

4. CONCLUSIONS

In this paper is mainly focused on the integration of a wide range of data in the framework of the GIS spatial database for the Cyprus region. This method of data management and analysis is also promoted by the Landsat TM data, which represent measurements of atmospheric path component (Rayleigh + Mie Scattering). Despite the complexity of the spatial data management, analysis, and visualization, modeling of air pollution has to be solved independently in the framework of standalone computer systems (mathematical modeling or physical scaled models). The GISs therefore serve as the data stores, which can manage all the data together with model outputs to carry out future risk assessment analysis and map compositions. Future actions consist of inserting all the data acquired simultaneously such as: air pollution data, meteorological data, determined aerosol optical thickness (part of the atmospheric path component) from the satellite images, sun-photometer atmospheric data.

5. ACKNOWLEDGEMENTS

The authors acknowledge the support of the Archisystems Ltd and Hadjimitsis Consultants in Cyprus.

6. REFERENCES

Briggs, D. J.2000. A regression-based method for mapping traffic related air pollution: application and testing in four contrasting urban environments, The science of the total environment, 253, 151–167.

Civis, S., Zelinger, Z., Strizik, M., and Janour, Z. 2001. Simulation of Air Pollution in a Wind Tunnel, in: Spectroscopy from Space, edited by: Demaison, J., Kluwer Academic, Dordrecht, 275–299.

Hadjimitsis D.G., Themistokleous K., Vryonides P., and Clayton C.R.I.2007. Satellite-derived determination of aerosol optical thickness for air pollution monitoring: a simplified algorithm. AIR POLLUTION 2007 Fifteenth International Conference on Modelling, 6th International Conference on Urban Air Quality Cyprus, 27-29 March 2007.

http://www.airquality.dli.mlsi.gov.cy/ (Cyprus Government)

Longley, P. A., Goodchild, M. F., Maguire, D. J., and Rhind, D. W. 2001: Geographic Information Systems and Science, John Wiley & Sons, 27–58, New York.

Matejicek, L. 2002. Environmental Modelling in Urban Areas with GIS, Integrated Assessment and Decision Support, Proceedings of the 1st biennial meeting of iEMSs, Lugano, 60–65.

Ministry of Labour. 2005. Executive Summary VII, Preliminary Assessment of Ambient Air Quality in Cyprus.

Tulloch M. and Li J. 2004. Applications of Satellite Remote Sensing to Urban Air-Quality Monitoring: Status and Potential Solutions to Canada. Environmental Informatics Archives, Volume 2, 846-854.

Proceedings of the 6th International Conference on Urban Air Quality
Limassol, Cyprus, 27-29 March 2007

DYNAMIC MONITORING OF AIR POLLUTANTS IN ZÜRICH (SWITZERLAND) USING A STREETCAR AS MEASURING PLATFORM

Ph. Kehl[1], J. Staehelin[2], A. Geiger[1], H. -G. Kahle[1]

[1]Institute for Geodesy & Photogrammetry, ETH Zürich, Switzerland,
[2]Insitute for Atmospheric and Climate Science , ETH Zürich, Switzerland

ABSTRACT

The project «Dynamic Environmental Monitoring» aims at providing a dynamic and real-time assessment of ambient air quality and at improving the understanding of the interaction between road traffic emissions and urban air quality. The data analysed are based on the autonomous operation of a measuring system on a streetcar in regular service. The streetcar is equipped with instruments to measure air pollutant concentrations of nitrogen oxides (NO and NO_2), aerosol particles and ozone. The measurements represent the various characteristics of an urban environment, such as busy places and parts of the city without private road traffic. GPS has been used for precise positioning and timing. Urban sites often degrade navigation accuracy and availability. Therefore techniques involving filtering and map-matching have been developed to provide precise positioning. First results clearly show varying concentrations of air pollutants along the streetcar track as well as characteristic hot-spots near busy streets.

1. INTRODUCTION

Despite the substantial decrease in road traffic emissions (mainly because of the introduction of catalytic converters in gasoline vehicles) ambient air concentrations of air pollutants such as nitrogen dioxide, particulates and ozone still often exceed the limiting values at urban sites in Switzerland [Ordonez et al., 2005]. The project «Dynamic Environmental Monitoring» (http://www.ggl.ethz.ch/research/wg59/) has been launched as an interdisciplinary project, funded by the department «Bau, Umwelt und Geomatik» (D-BAUG, Construction, Environment and Geomatics) of the Swiss Federal Institute of Technology Zürich (ETH Zürich). It pursues three research topics. These include satellite based traffic modeling, air quality monitoring and the influence of traffic on the air quality. The project aims at improving the understanding of the interaction between road traffic emissions and on urban air quality in Zürich and at demonstrating the feasibility of dynamic and real-time measurements and its limitations.

2. THE MEASUREMENT PLATFORM

To achieve the project goal of dynamic monitoring, a suitable mobile platform had to be found. A pilot survey had been carried out [Schneebeli and Wegmann, 2002] to investigate the technical and metrological demands for the mobile platform. To measure ambient air concentrations of nitrogen oxides (NO and NO_2), Ozone, and particulates, the technical requirements are manifold and include: *space* (appr. $1m^3$), *load capacity* (appr. 200kg), *electrical power* (appr. 1000W) and the possibility to *position* the carrier. The metrological demands are a *regular uptime* as long as possible. The *platform* has to move along roads and above ground and operate at least on daytime (covering morning and evening rush hours and the time in between) for a longer time period (months or more). Since the technical demands made it impossible to use or build a dedicated vehicle, the focus soon moved on the vehicles in use by public transport. While busses were found unusable, certain types of streetcars met the requirements. The public transport operator (Verkehrsbetriebe Zurich, VBZ) agreed to provide a suitable streetcar and to operate it on a regular basis on a desired line. The measurement system has eventually been installed on the roof of a relatively modern streetcar constructed in the years 1992/1993. Since it relies on semiconductor technology, there are no heat-producing breaking current resistors on the roof which might falsify the measurements. Of course the pantograph produces arcing and abrasion, but the placement of the sensors at the other end of the wagon minimizes these influences.

The streetcar travels on tracks that cross the city in north-south or east-west direction. The lines are characterised by interesting height profiles and encounters various different traffic situations. The streetcar and the measurement system, respectively pass many different places, such as busy places and parts of the city without private road traffic. Therefore it is assumed that the measurements represent the various characteristics of an urban environment. Figure 1 features a map of the general situation and the three lines used.

3. THE MEASUREMENT SYSTEM

The sensors have been built into a measurement system (figure 2) that has been purpose-built to meet regulations, terms and metrological demands. The structure gage and the available space on the roof of the

vehicle defined size and form of the box. A commercially available roof box for cars has been chosen as the housing for the measurement equipment. To improve the stability and to provide mounts for the equipment, the box has been fortified. A high-grade steel framework has been assembled and fitted into the box. New mountings of the same steel have been added. On the streetcar itself supporting notches have been welded on the roof.

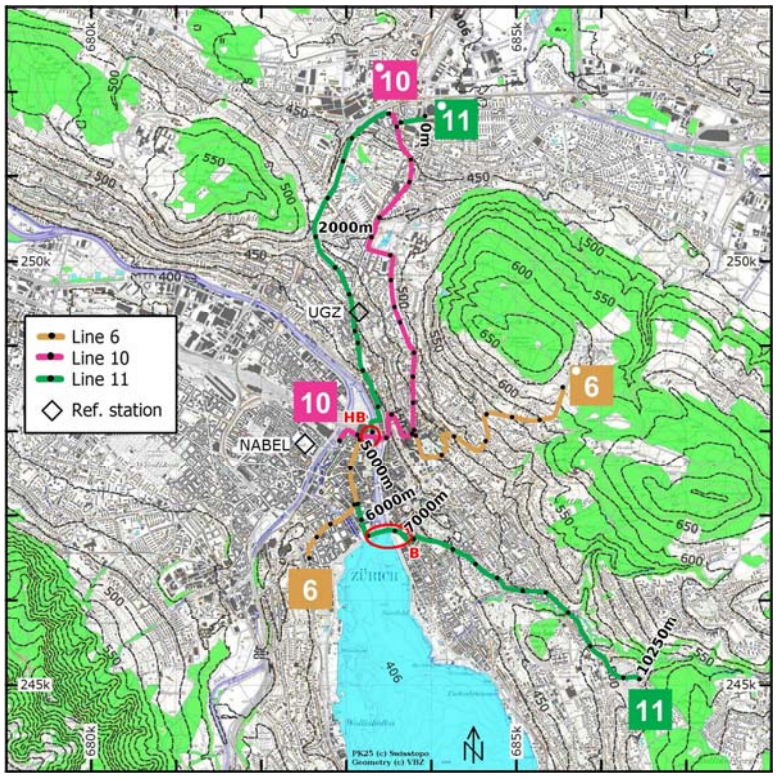

Figure 1: Topographic map of Zürich and surroundings (9x9km^2) with emphasised contour lines (25m equidistance). The three streetcar lines used in this project are indicated with their number and colour. Two places of interest (see figure 3) are marked in red. Positions along the track (chainage) are indicated in metres.

3.1. The Sensors

There are three pollutant sensors integrated into the measurement system. These are a trace-level NO-NO_2-NO_X analyzer, an ozone monitor and a particle sensor. The measuring principle of the nitrogen oxides sensor is chemiluminescence of NO formed by reactions with O_3. NO_2 is measured after conversion to NO. It has a measurement range of 0 – 200 ppbv with an averaging time of 10 seconds. The used instrument is a Thermo Environmental Instruments Model 42C TL. The ozone sensor measures the UV absorption of O_3 at a wavelength of 254 nm. The maximum measurement range is 0 – 100 ppmv, although a narrower range of 0 – 250 ppbv is used. The used instrument is a 2b Technologies Ozone Monitor Model 202. Particulate matter is detected by a diffusion charging particle sensor. Unlike the traditional weighting of particles of a certain size class (e.g. PM2.5 or PM10) this sensor determines the total active surface of all particles, the so called Fuchs surface. The device features a measurement range from 0 - 2000 $\mu m^2 \cdot cm^{-2}$. The sensor reacts quickly on a change in ambient air concentration of particles (better than 1 Hz). The used instrument is a Matter Engineering Diffusion Charging Particle Sensor Type LQ 1-DC. Meteorological data of the ambient air are acquired as well. A combined sensor measures the temperature (-30 – +70 °C) and the relative humidity (0 – 100 %RH). An absolute pressure sensor measures the pressure in a range from 950 – 1020 hPa.

3.2. Power Supply & Control

The requirements for the power supply of the measurement system are multifaceted. The tram itself nominally provides 36 volts direct current which goes up to 42 VDC and might contain voltage peaks. The maximum power output is 1500 watts. This power source is not uninterruptible and may fail for short periods (seconds) due to the nature of the pantograph or for longer periods (minutes) due to re-starts of the street car which occasionally occur. Based on these facts a custom-built uninterruptible power supply has been built Attached to this controlled power supply, different of-the-shelf converters had been installed to provide the various voltages needed for the sensors and other devices. In total the complete measurement system draws

between 400 and 750 watts, depending on the operation state of the sensors (normal operation versus heating/powering up).

An industrial computer based on Linux and custom software controls the measurement system. It decides to power on or shut down the system based the operational state of the streetcar. It monitors the sensors for alarms and takes action accordingly. And it also logs the measurement data.

3.3. Positioning with GPS

GPS has been chosen as a position and time reference. An investigation on the performance of various GPS receiver in urban areas has showed that it is possible to navigate in urban areas, even in pronounced street canyons with buildings up to circa 30m height with a reasonable precision using certain receivers [Heller, 2003]. The chosen receiver has been examined on the streetcar in further detail [Forster and Landtwing, 2004]. The results have showed the reliability of the receiver on most parts of the track. Few parts of the track showed poor GPS reception because of the signal blockage of buildings and trees or degraded accuracy due to multi-path effects. The used sensor is a μ-Blox Antaris EvalKit (SBR-LS) with a standard active GPS patch antenna. For this project the receiver's maximum navigation rate of 1Hz has been selected. All relevant navigation, time and satellite information is logged to the computer.

The GPS data is post-processed to provide reliable and precise information to position the measurement data. This processing involves two steps. The raw navigation solutions are filtered to exclude faulty data and then transformed into precise positions using a projective map-matching technique which takes the limited mobility of the streetcar and the known track geometry into account. Missing positions have been interpolated using standard position-time relations for the streetcar. The outages last a few seconds up to a few dozens of seconds and the interpolation provides sufficient quality [Rossinelli, 2006; Kehl et al., 2006].

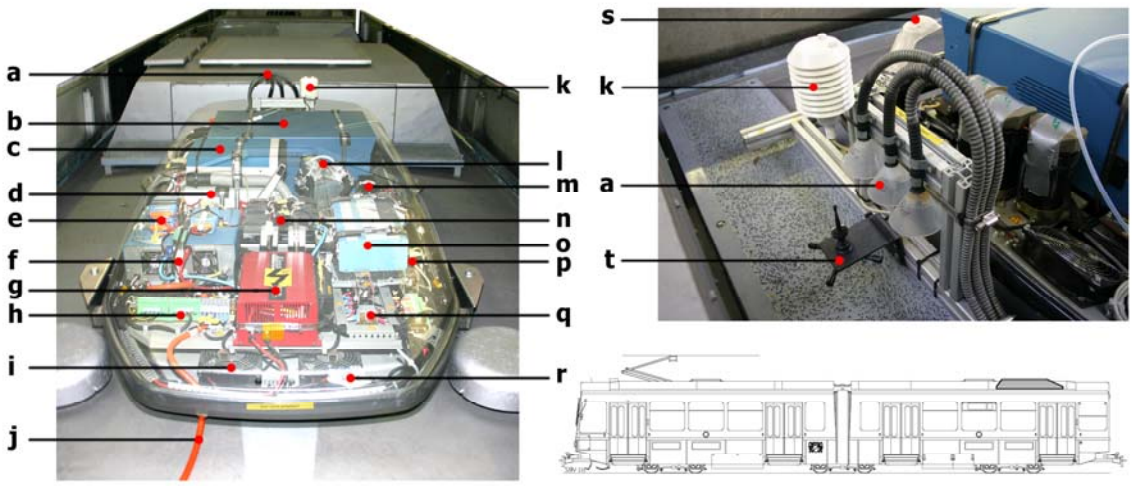

Figure 2: The measurement system (box) on the roof of the streetcar (left), a detailed view of the sample inlets (right) and the position of the box on the streetcar (bottom right).
Legend:
a) sample inlets, *b)* NO_X analyser, *c)* ozone sensor, *d)* particle sensor, *e)* A/D converters, *f)* power supply, *g)* 230 VAC inverter, *h)* power terminals, *i)* ventilation, *j)* power input lead, *k)* meteorological sensors, *l)* vacuum pump, *m)* networking equipment, *o)* data logger and computer, *p)* GPS receiver (not visible), *q)* power relays, *r)* thermostat, *s)* GPS antenna, *t)* GSM antenna

4. RESULTS

Figure 3 is a showcase of an analysis of data from ten sunny work days in June/July 2005. The position of the measurements is defined through the position along the streetcar track in metres (also known as *chainage*). The streetcar has usually been operated from early morning to late night. These two parameters are the x axis and y axis, respectively in the plots. The data has been interpolated to a grid with 100m x 60 minutes resolution using the kriging technique. NO_X as a primary pollutant directly emitted by road transport correlates with the amount of traffic at specific places. Two notoriously busy places in the inner city of Zürich are represented by the measurements. The area around Hauptbahnhof (central station) is busy

throughout the day. The area from Bürkliplatz to Bellevue place is an intersection of two major streets connecting to each side of the lake and high capacity lanes connecting down town and near quarters. See figure 1 for the location of the places (red circles labeled "HB" and "B", respectively).

Besides of this traffic-pollution correlation three meteorological and chemical effects can be seen. In the morning hours the NO_X concentrations are rather high all along the track. When the inversion dissolves in the later morning the concentrations generally decrease but at busy places. The ozone concentrations increase with the position of the sun and reach the maximum in the afternoon. The third effect, best visible at the busy places, shows the titration of O_3 by NO below the inversion layer.

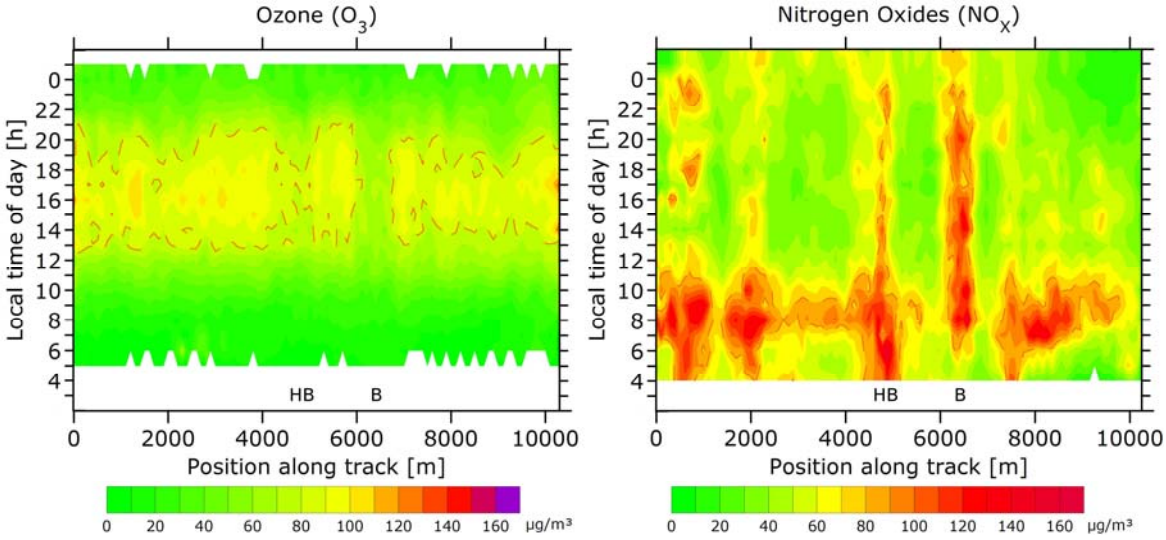

Figure 3: The plots show the diurnal change of air pollutant concentrations along the track (nr. 11, see figure 1) for days with fair weather (more than ten hours of sunshine). The dashed lines represent 80 µg/m^3. The data has been interpolated to a grid (100m by 60' spacing) using the kriging technique.

5. CONCLUSIONS

The feasibility of dynamic and real-time measurements and its limitations have been shown by carrying out two measurement campaigns lasting 18 and 20 weeks in spring 2005 and winter/spring 2005/2006. The analysis clearly show varying concentrations of air pollutants along the streetcar track as well as characteristic hot-spots near busy places. The data set also allows retrieving diurnal variations for various seasonal conditions.

6. ACKNOWLEDGEMENT

This study is conducted under grants from the department «Umwelt, Bau und Geomatik» (D-BAUG) of the Swiss Federal Institute of Technology (ETH Zürich).

7. REFERENCES

Forster, M. and Landtwing, S. (2004). *GPS-Sensoren im öffentlichen Verkehr*. Technical report, Geodesy & Geodynamics Lab., Institute for Geodesy & Photogrammetry.

Heller, O. (2003). *Low-Cost GPS im städtischen Raum.* Technical report, Geodesy & Geodynamics Lab., Institute for Geodesy & Photogrammetry. ETH Zürich

Kehl, P., Geiger, A., Kahle, H.-G., and Stähelin, J. (2006). «Labor im Tram» Dynamische Umweltmessungen zur Erfassung der Luftverschmutzung in Zürich mit GPS als Positionssensor und Zeitreferenz. *Geomatik Schweiz,* 2006 (11):602-607.

Ordonez, C., Prevot, A., and Staehelin, J. (2005). Emissions from road traffic and surface ozone in Switzerland. In Eichsleder, U.-P. D. H., editor, *14th Symposium Transport and Air Pollution*, volume 85/I, pages 4150. Institute for Internal Combustion Engines and Thermodynamics.

Rossinelli, S. (2006). *GPS Sensoren zur genauen Navigation und Fahrtenkontrolle im öffentlichen Verkehr.* Technical report, Geodesy & Geodynamics Lab., Institute for Geodesy & Photogrammetry.

Schneebeli, H. and Wegmann, M. (2002). *Dynamisches Verkehrs- und Umweltmonitoring.* Technical report, Geodesy & Geodynamics Lab., Institute for Geodesy & Photogrammetry, ETH Zürich.

Proceedings of the 6th International Conference on Urban Air Quality
Limassol, Cyprus, 27-29 March 2007

STREET VERSUS ROOFTOP LEVEL CONCENTRATIONS OF FINE PARTICLES IN A CAMBRIDGE STREET CANYON

Prashant Kumar, Rex Britter, David Langley
Hopkinson Laboratory, Department of Engineering, University of Cambridge, CB2 1PZ, UK

ABSTRACT

A newly developed instrument was deployed to measure the particle number distribution in the 5-1000 nm range in a Cambridge street canyon. Measurements were taken for 7 weekdays between 08 and 21 June 2006 at three different heights and on another weekday at rooftop level. This article compares roof top (22 June) and street level (16 June) particle number concentration (PNCs) since meteorological and traffic conditions were similar on these days. The results showed that traffic was the main source of particles in the vicinity of the measurement site. The ratio between the street and rooftop level PNCs was about 6.5. However, this ratio changed significantly when the PNCs in various size ranges at these two heights were compared. Rooftop PNCs were near constant throughout the measurements and seemed unaffected by changes in rooftop wind speed. Conversely, street level PNCs decreased with the increased rooftop wind speed due to dilution with background air.

1. INTRODUCTION

Current regulations address the atmospheric particulate matter (PM) level as PM_{10} and $PM_{2.5}$ mass concentration rather than number concentration (QUARG, 1996). Fine particles (below 1000 nm) are not included in the regulatory limits since they contribute very little to the particle mass. The case for using the particle number concentration (PNC) as markers of potential health hazards has been made by several researchers (Pope III et al., 1995). Progress has been hampered by the lack of proven methods to measure PNC. Zones of high pollutant concentration are common in urban street canyons because of tall buildings and heavy traffic flow. These concentrations can be several times higher than those in unobstructed locations depending on traffic characteristics, street canyon geometry, advection of emissions from adjacent streets and turbulence produced by wind, atmospheric instability and traffic, making pollutant dispersion in the urban street canyons a complex problem. Several studies such as Shi et al. (1999), Vardoulakis et al. (2002), Longley et al. (2003) reported the measurements of particle mass and number concentrations at different heights in urban street canyons. Few studies (Bauman et al., 1982; Vakeva et al., 1999) could be found in the literature that reports a comparison between the street and rooftop level measurements of fine particles. Our study is somewhat different in two ways; firstly we used a newly developed instrument, the 'fast response differential mobility spectrometer DMS500', to measure the PNCs and this provides near real time continuous measurements unlike other studies that used the scanning mobility particle sizer, the electrical low pressure impactor, the ultra particle condensation particle counter or the optical particle counter alone or in combination. Secondly, we measured a broad range (5-1000 nm) of particles at a high frequency (10 Hz output data rate). However to ensure maximal data quality, our experiments recorded particle number distributions (PND) with a 1 Hz output data rate. The main aims of the measurements were the investigation of the effect of the rooftop wind speed, direction and traffic flow on the street and rooftop level PNDs and the comparison of PNCs in various size ranges between the two levels.

2. EXPERIMENTAL

2.1 Site Description and Particle Measurements

PNDs in the 5-1000 nm range were measured on a 200 m long section of a Cambridge road (Fen Causeway). The height *H* and width *W* of this street canyon were about 20 m giving an aspect ratio around unity. Measurements were taken for 7 weekdays between 8-21 June 2006 (from 09:00 to 19:00 h) on each day at 0.20 m, 1.0 m, and 2.60 m above road level (called A, B and C). Further measurements were taken on another weekday (22 June 2006) at rooftop level, about 20 m above road level (called R). It should be noted that only the street level measurements for 16 June have been compared with the rooftop measurements; the wind speed, wind direction, temperature, humidity and traffic conditions were similar on these days, as shown in Table 1. Other results from the street level measurements are reported elsewhere (Kumar and Britter, 2006). Sampling was performed on the north side of the road and street level sampling points were about 0.3 m away from the wall of Department of Engineering building and 3.05 m away from kerb while the rooftop sampling point was on the roof of Department building and 3.35 m away from the kerb.

2.2 Measurement Methodology

Street and rooftop level PNDs were measured at a frequency of one spectrum per second, every second for 10 hours between 09:00 to 19:00 h. Street samples were taken for 20 minutes in an hour on two different occasions (i.e. 2 samples per hour, 10 minutes per sample) at each height by manually re-positioning the sampling point every 10 minutes. Roof top measurements were taken continuously for one day. The specially designed 'conductive' rubber sampling tubes (5.85 mm internal diameter) were 5 m long for street level measurements and 15 m long for rooftop measurements. The estimated sample residence time in these tubes at 0.25 bars was 0.3 and 0.8 seconds respectively. Particle losses due to the diffusion and inertial impaction were estimated (Hinds, 1999), found to be modest and therefore not considered further. Kumar and Britter (2006) give further detail on the site and methodology. Meteorological data (wind speed hereafter called reference wind speed, wind direction, temperature, and relative humidity) were taken from University-operated AT&T weather station on the roof of the Department of Engineering. It is about 40 m above the street at a point some 100 m from the sampling site. This location is above the average height for Cambridge buildings and is not overlooked. The traffic volume on the road was typically 1623 vehicle h^{-1} with a standard deviation of 165 vehicle h^{-1}, of which cars and vans (gasoline), cars and vans (diesel), buses, light duty vehicles (LDV), heavy duty vehicles (HDV) and motorcycles were about 74.85%, 19.15%, 1%, 3%, 1% and 1% respectively.

Table 1: Comparison of meteorological parameters

	Date	Wind speed (m s^{-1})	Relative humidity (%)	Temperature (^{0}C)	Wind Direction
Hourly average	16 June	6; Standard dev. 1.8	39; Standard dev. 2.6	25; Standard dev. 0.6	South West (SW)
	22 June	6; Standard dev. 1.6	44; Standard dev. 5.9	20; Standard dev. 0.9	South West (SW)

3. RESULTS AND DISCUSSIONS

3.1 Particle Number Distributions at Street Level and Rooftop Level

The hourly averaged PNDs at street and rooftop level are shown in Fig. 1a. Street level PNDs at each height were similar but showed a consistent and discernible decrease with height. However, significant differences can be seen between street and rooftop level PNDs. Street and rooftop level PNDs showed a typical bi-modal distribution. Street level PNDs showed a peak about 30 nm and other peak at about 100 nm while the rooftop PNDs peaked at about 20 nm and 100 nm showing the presence of gasoline and diesel engined vehicles which were about 75.85% and 24.15% respectively. If we treat the rooftop PNDs as background and subtract them from street level PNDs, the resulting PNDs should reflect local traffic (Fig. 1b). These showed an additional peak at about 10 nm presumably due to the fresh emissions from traffic and/or atmospheric formation from various precursor gases. In order to show the correlation of particle number concentrations (PNC) with reference wind speed, direction and traffic volume the PNDs were divided into four broad ranges i.e., 5-10 nm, 10-30 nm, 30-300 nm and 300-1000 nm based on the observed peaks, and the PNCs in these respective ranges were referred to as $N_{5\text{-}10}$, $N_{10\text{-}30}$, $N_{30\text{-}300}$ and $N_{300\text{-}1000}$ respectively. PNCs in each range were obtained by integrating the area under the PND curves in that given size range.

3.2 Effect of Reference Wind Speed on Street and Rooftop level PNDs

We used the half-hourly averaged reference wind speed and direction in order to show their effect on street and rooftop level PNDs at the micro scale. The RWS were categorized in various ranges i.e., 2.5-3.5, 3.5-4.5, 4.5-5.5, 5.5-6.5, 8.5-9.5 m s^{-1} and plotted with the half-hourly averaged PNDs in each RWS ranges (Figs. 2 a and b). The street level PNDs were found to be acutely dependent on the RWS since the largest PNDs were at the time of smallest RWS and vice-versa. The rooftop PNDs were less affected by the RWS. The changes in the street level PNDs seem mainly due to the RWS rather than changes in rooftop PNDs. Moreover, wind direction was SW throughout the measurement period and the street level sampling points were situated in the windward side of the canyon, and the changes in street level PNDs can be attributed to the dilution due to vortex circulation in the canyon. This can occur in a regular street canyon when the RWS is greater than 1.5 m s^{-1} (Depaul and Sheih, 1986) and at an angle of more than 30^0 to the street axis (Oke, 1998), as shown in Fig. 3.

3.3 Street Level versus Rooftop Level Particle Number Concentrations in Various Size Ranges

Street level PNCs in the $N_{5\text{-}1000}$ range decreased with increased sampling height and the maximum differences among A, B and C were between 15-20 %. Closer inspection of the data indicated that concentration differences between the two lower sampling positions were consistently smaller than those between the two upper sampling positions. For simplicity, the street level PNCs (average of A, B and C) in various size ranges were compared

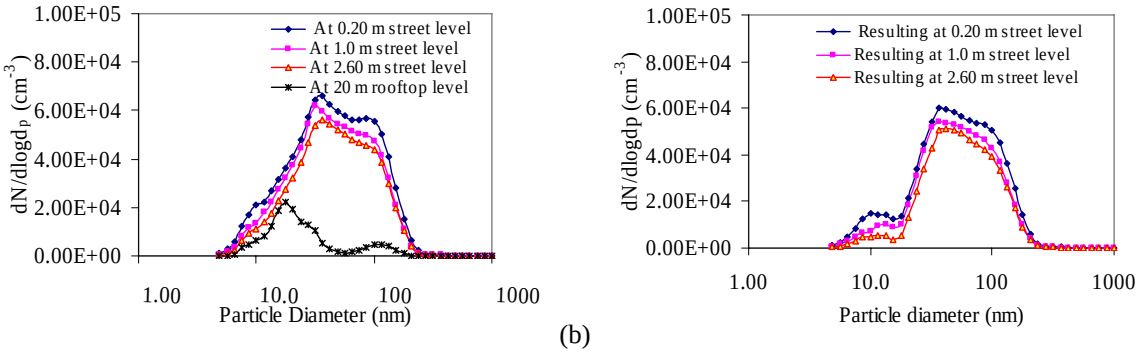

(a) (b)

Fig. 1 (a) Street and rooftop level PNDs. The PND data is the hourly average over the whole sampling duration during both the days. (b) Resulting PNDs after the subtraction of roof top level PNDs from street level PNDs.

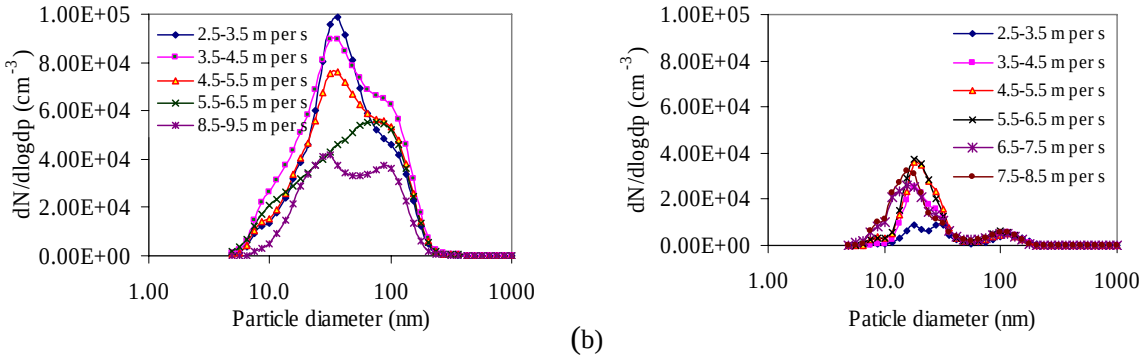

(a) (b)

Fig. 2 Effect of RWS on (a) street level PNDs (averaged over A, B and C) (b) rooftop level PNDs. In both the figures, half-hourly averaged RWS and PND data is divided into the various categories of wind speed.

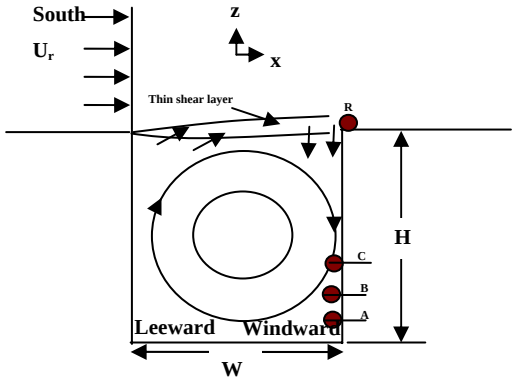

Fig. 3

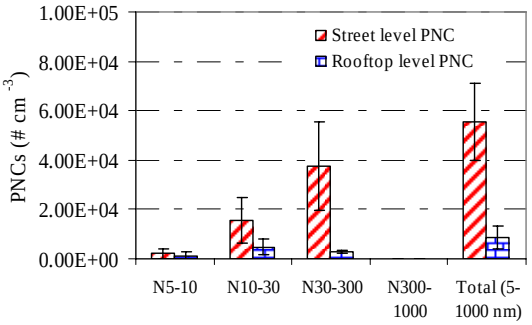

Fig. 4

Fig. 3. Sketch of flow inside the street canyon representing the vortex circulation inside the canyon.
Fig. 4. Street versus rooftop level PNCs in various size ranges. The street level PNCs is averaged over the sampling positions A, B and C.

with the rooftop PNCs. Clear differences between the street level and roof top level PNCs were seen in each size range (Fig. 4). A ratio of about 6.5 was observed for street and rooftop level PNCs in the $N_{5\text{-}1000}$ range. This ratio changed significantly when the comparison was made in various size ranges; it was about 2.4, 3.2, 12.8 and 6.6 for the particles in $N_{5\text{-}10}$, $N_{10\text{-}30}$, $N_{30\text{-}300}$ and $N_{300\text{-}1000}$ range respectively. This ratio was highest (~13) for the accumulation mode ($N_{30\text{-}300}$) particles and this was expected because the primary emissions from the traffic are formed during combustion or thereafter at the street level. The ratio for nucleation mode ($N_{5\text{-}10}$ and $N_{10\text{-}30}$ or $N_{5\text{-}30}$) particles was not very high (~3). One explanation for this was that particle production in the nucleation mode at rooftop level would be favoured by the higher concentrations of condensable species and the smaller concentrations of pre-existing particles (Vakeva et al., 1999). Moreover, higher street level PNCs in the accumulation mode could suppress growth of nucleation mode particles since suppression depends on the surface

area available for the adsorption and dilution history (Kittelson et al., 2004). Diurnal analysis showed that street level particles in the accumulation mode followed directly from traffic activity but inversely with the RWS. Rooftop level particles in this mode did not show any strong evidence of such changes. The growth of street level particles in the nucleation mode was found to be suppressed by the street level accumulation mode. Also, the nucleation mode particles at both the levels showed some nucleation events and they were observed during the midday hours and this could possibly be due to photochemical induced nucleation (Vakeva et al., 1999).

4. CONCLUSIONS

Particle number distributions were measured at rooftop level and at three different heights in an urban street canyon. The diurnal variations in the street level PNDs were related to the variations in reference wind speed and traffic volume. Unlike the street level PNDs, rooftop PNDs were found to be less affected by the variation in reference wind speed. Street level PNCs were dominated by the accumulation mode particles while the nucleation mode particles dominated the rooftop level PNCs. The main results of the study were the differences of PNCs between the street and rooftop levels. A ratio of about 6.5 was observed for street and rooftop level PNCs in the $N_{5\text{-}1000}$ range. However the transformation of nuclei mode particles and direct emissions of accumulation mode particles changed this ratio significantly when the comparison was made in various size ranges. At rooftop level the formation of nucleation mode particles was favored presumably due to the lower concentration of pre-existing particles, higher concentration of condensable species and photochemical induced nucleation. Conversely, at street level the presence of higher pre-existing particles and precursor gases could have suppress the growth of nucleation mode.

5. ACKNOWLEDGEMENTS

Prashant Kumar thanks Cambridge Commonwealth Trust and Overseas Research Scholarship award for providing the financial support for his PhD. The authors also thank Dr. Paul Fennell to help in setting up the DMS500 and initial discussions, and Prof. A.N. Hayhurst and Dr. J.S. Dennis for lending it for the study.

6. REFERENCES

[1] Bauman, S. E., Ferek, R., Williams, E. T, Finston, H. L., Ferrand, E.F., Santowski, J., 1982. Street level versus rooftop sampling: carbon monoxide and aerosol in New York city. Atmos. Environ. 16, 2489-2496.
[2] Caton, F., Britter, R.E., Dalziel, S., 2003. Dispersion mechanisms in a street canyon. Atmos. Environ. 37, 693-702.
[3] De Paul, F.T., Sheih, C.M., 1986. Measurements of wind velocities in a street canyon. Atmos. Environ. 20(3), 455-459.
[4] Hinds, W.C., 1999. Aerosol technology: Properties, behaviour and measurement of airborne particles (ed). John Wiley & Sons, UK.
[5] Kittelson, D.B., Watts, W.F., Johnson, J.P., 2004. Nanoparticle emissions on Minnesota highways. Atmos. Environ. 38, 9-19.
[6] Kumar, P., Britter, R., 2006. Measurements of the particles in the 5-1000 nm range close to road level in an urban street canyon. (Submitted to Atmos. Environ.).
[7] Longley, I.D., Gallagher, M.W., Dorsey, J.R., Flynn, M., Allan, J.D., Alfarra, D., Inglish, D., 2003. A case study of aerosol (4.6nm-Dp-10microns) number and mass size distribution measurements in a busy street canyon in Manchester, U.K. Atmos. Environ. 37, 1563-1571.
[8] Oke, T.R., 1988. Street design and urban canopy layer climate. Energy and Buildings 11, 103–113.
[9] Pope III, C.A., Dockery, D.W., Schwart, J., 1995. Review of epidemiological evidence of health effects of particulate air pollution. Inhal. Toxicol. 7, 1-18.
[10] QUARG, 1996. Airborne particulate matter in the United Kingdom. Third report of the quality of the of urban air review group. Department of Environment, UK.
[11] Shi, P.J., Khan, A.A., Harrison, R.M., 1999. Measurements of ultra fine particle concentration and size distribution in the urban atmosphere**.** Scien. of the Tot. Environ. 235, 51-64.
[12] Vakeva, M., Hameri, K., Kulmala, M., Lahdes, R., Ruuskanen, J., Laitinen, T., 1999. Street level versus rooftop concentrations of submicron aerosol particles and gaseous pollutants in an urban street canyon. Atmos. Environ. 33, 1385-1397.
[13] Vardoulakis, S., Gonzalez-Flesca, N., Fisher, B.E.A., 2002. Assessment of traffic-related air pollution in two street canyons in Paris: implications for exposure studies. Atmos. Environ. 36, 1025-1039.

COMPARISON OF VOLTAMMETRY AND INDUCTIVELY COUPLED PLASMA – MASS SPECTROMETRY FOR THE DETERMINATION OF HEAVY METALS IN PM_{10} AIRBORNE PARTICULATE MATTER

D. Buzica*, M. Gerboles*, A. Borowiak, P. Trincherini, R. Passarella, V. Pedroni
European Commission – DG Joint Research Centre, Institute for Environment and Sustainability, Transport and Air Quality Unit, 21020 Ispra, Italy.

ABSTRACT

Voltammetry was examined for the determination of heavy metals in ambient air particulate matter (PM_{10}) on quartz filter. Cd, Pb, Cu, Zn, As were determined by anodic stripping voltammetry (ASV) while adsorptive stripping voltammetry (AdSV) was used for Ni (Buzica et al., 2006). The method detection limit and recovery of the voltammetric method were evaluated and found to satisfy the requirements of the EN 14902. A comparison between voltammetry and Inductively Coupled Plasma – Mass Spectrometry (ICP-MS) on a NIST Certified Reference Material and PM_{10} filters was carried out. Here also the differences between the measurements by ICP-MS and voltammetry remained consistent with the level of uncertainty requested in the European Directives for heavy metals (European Council, 1994, 2004). As such, one may expect voltammetry to provide a reliable alternative to the European laboratories in charge of ambient air monitoring at the time when the European Directives require to measure heavy metals in PM_{10} on a regularly basis.

1. INTRODUCTION

Heavy metals are of concern as atmospheric pollutants due to their toxic effects. Current European Directives (European Council, 1999 and 2004) set limit and target values for heavy metals in ambient air with the aim of minimising the harmful effects on human health. The Directives also established reference methods for the sampling and analysis of heavy metals *e.g.* Graphite Furnace Atomic Absorption Spectroscopy (GFAAS) and Inductively Coupled Plasma - Mass Spectrometry (ICP-MS) described in EN 14902 (European Standard, 2005). Other methods could be used if demonstrated to give results equivalent to the reference ones. An alternative method for the determination of heavy metals is voltammetry. This technique is becoming more popular for heavy metals analysis because it can be used for multi-element analysis, it can be fully automated and it only requires low investment costs.
Hereafter the results of a study in which voltammetry was examined to measure zinc (Zn), cadmium (Cd), copper (Cu), lead (Pb), nickel (Ni) and arsenic (As) in ambient particulate matter (PM_{10}) are presented. The aim was to evaluate the analytical method as compared to ICP-MS under the same sampling and liquid-extraction conditions. The capacity of voltammetry to meet the data quality objective of the Directives (expanded uncertainty less than 25 % for Pb and 40 % for Cd, As and Ni) and the analytical requirements of EN 14902 (the method detection limits, the average recovery rates) were evaluated.

2. METHODOLOGY

PM_{10} was sampled according to EN 12341 (European standard, 1998) on two filters in the Krakow area (PL) in January 2005. PM_{10} containing heavy metals were collected on Quartz filters (Quartz filter QMA 4.7 cm - Whatman), using a Low Volume Sampler (LVS) with PM_{10} head (Derenda LVS version 3.1). The sampling flow rate was 2.3 m^3 h^{-1} and the sampling time was 24 h.
The filters were digested according to the procedure given in the EN 14902 using a micro-wave oven (Millestone ETHOS TC). Each filter was placed in a Teflon vessel in which 8 ml nitric acid 70 % (J.T. Baker Ultrex II) and 2 ml hydrogen peroxide (J.T. Baker Ultrex II) were added. After cooling down to room temperature, the solution was transferred in a PFA-volumetric flask (VIT-LAB GmbH) which was previously cleaned and dried with purified air. Five ml of ammonia 25% (NH3, Merck Suprapur) was added into the PFA-volumetric flask, which was then completed to 25 ml using MilliQ water (Millipore).
The voltammetric analysis were carried out with a Metrohm 797 VA Computrace and 813 Compact Autosampler. Only high purity grade (Merck Suprapur) reagents and MilliQ water were used. For calibration, the standard addition method was applied to limit the matrix effects. The calibration standards were prepared

Corresponding authors Daniela Buzica Tel.: +39-332-789851, Fax: +39-332-789931, E-mail: daniela.buzica@jrc.it
Michel Gerboles Tel.: +39-332-785652, Fax: +39-332-789931, E-mail: michel.gerboles@jrc.it

using RimAg-xtra CRMs (Romil) at 1000 ppm of Pb, Cd, As, Ni, Cu and Zn. All elements were quantified using linear regression based on the height of the peaks of the voltamogramms. Anodic stripping voltammetry (ASV) was used to determine Zn, Cd, Pb, Cu and As while adsorptive stripping voltammetry (AdSV) was used for the determination of Ni.

3. RESULTS AND DISCUSSION

Estimation of the method detection limit, quantification limit and instrumental detection limit. To determine the Method Detection Limit (MDL) and quantification limit (QL), six blank filters, Whatman QMA, were digested and analysed with 3 repetitions. The MDL of voltammetry is at least five times smaller than the requirement for all the pollutants of interest. The quantification limit is well below the mass of heavy metals found on filter exposed for 24 hours at the limit and target values of the Directives (Table 1). A portion of the NIST 1648 CRM (4.36 mg) was digested according to the procedure given before. Aliquots of 1 ml were taken out of the sample of 25 ml and were analysed to evaluate the recovery of the method. It can be seen that the recovery rates (Table 1), defined as the percentage ratio of the measured value out of the certified one are always within the required range define by EN 14902 (Buzica et al., 2006). In EN 14902, it is required to establish the Instrumental Detection Limit (IDL) to be used to detect potential analytical anomalies if this limit changes over time. Six solutions of blank reagent were prepared and analysed following the same procedure as for filters with 4 repetitions. The results, calculated according to EN 14902, are shown in Table 1 (Buzica et al., 2006)

Comparison between ICP-MS and voltammetry on CRM and PM10 on filters
As an example, Figure 1 shows the voltammograms corresponding to the determination of Zn, Cd, Pb, Cu, Ni and As found on the PM10 accumulated on the outdoor filter. The peaks are well defined and the positions correspond to the standard potential of the metals of interest.
In order to compare ASV/AdSV and ICP-MS while having a SI traceable reference value, a portion of 6.93 mg of the NIST-1648 was digested and analysed. The results of the analysis of the CRM are given in Table 2. All the voltammetric determinations were found to fall within less than 15% of the certified values for all the metals for the heavy metals of interest. This demonstrated the ability of the developed ASV/AdSV methods to measure Cd, Pb, Ni and As concentrations with an adequate accuracy.
The results of the two filters analysis performed using both ICP-MS and ASV/AdSV are shown in Table 2. The method of the normalized deviation, according to ISO Guide 43-1 (ISO, 1997), was used to evaluate whether the differences between ICP-MS and ASV/AdSV remained within the accepted uncertainty set by the European Directives. $|E_n|$ numbers were far smaller than 1 and therefore it is confirmed that the difference between ICP-MS and ASV/AdSV values remained within requested uncertainty and are consistent with the DQO of the Directives (Buzica et al., 2006).

4. CONCLUSION

The implementation of voltammetry for the determination of heavy metals in PM_{10} sampled with LVS for 24 hours has been described. Cd, Pb, Cu, Zn, As and Ni were determined. This study has shown that voltammetry provides a reliable alternative to ICP-MS, the reference method, for determination of heavy metals in PM_{10} and do comply with the analytical requirements of the Directives and EN 14902. Therefore, voltammetry becomes of big interest, taking into account its low investment costs, for European laboratories in charge of ambient air monitoring at the time when the European Directives require to routinely measure heavy metals in PM_{10}.

5. ACKNOWLEDGEMENT

The authors are grateful to Dr. Jean-Luc Widlowski of the Institute for Environment and Sustainability, Joint Research Centre for his helpful discussion and suggestion.

6. REFERENCES

Buzica, D., Gerboles, M., Borowiak, A., Trincherini, P., Passarella, R., Pedroni, V. 2006. Comparison of voltammetry and inductively coupled plasma-mass spectrometry for the determination of heavy metals in PM10 airborne particulate matter. Atmos. Environ. 40, 4703 – 4710.

European Council – Directive, 1999, Official Journal of European Communities 1999/30/CE, L 163/41.

European Council – Directive, 2004, Official Journal of European Communities 2004/107/EC, L 23/3.

European standard, 1998, Air quality - Determination of the PM 10 fraction of suspended particulate matter - Reference method and field test procedure to demonstrate reference equivalence of measurement methods, EN 12341**,** Brussels.

European standard, 2005, Ambient air quality - Standard method for the measurement of Pb, Cd, As and Ni in the PM10 fraction of suspended particulate matter, EN 14902, Brussels.

International Organisation for Standardisation, 1997, *Proficiency testing by interlaboratory comparisons - Part 1 Development and operation of proficiency testing schemes*, ISO Guide 43-1, Geneva.

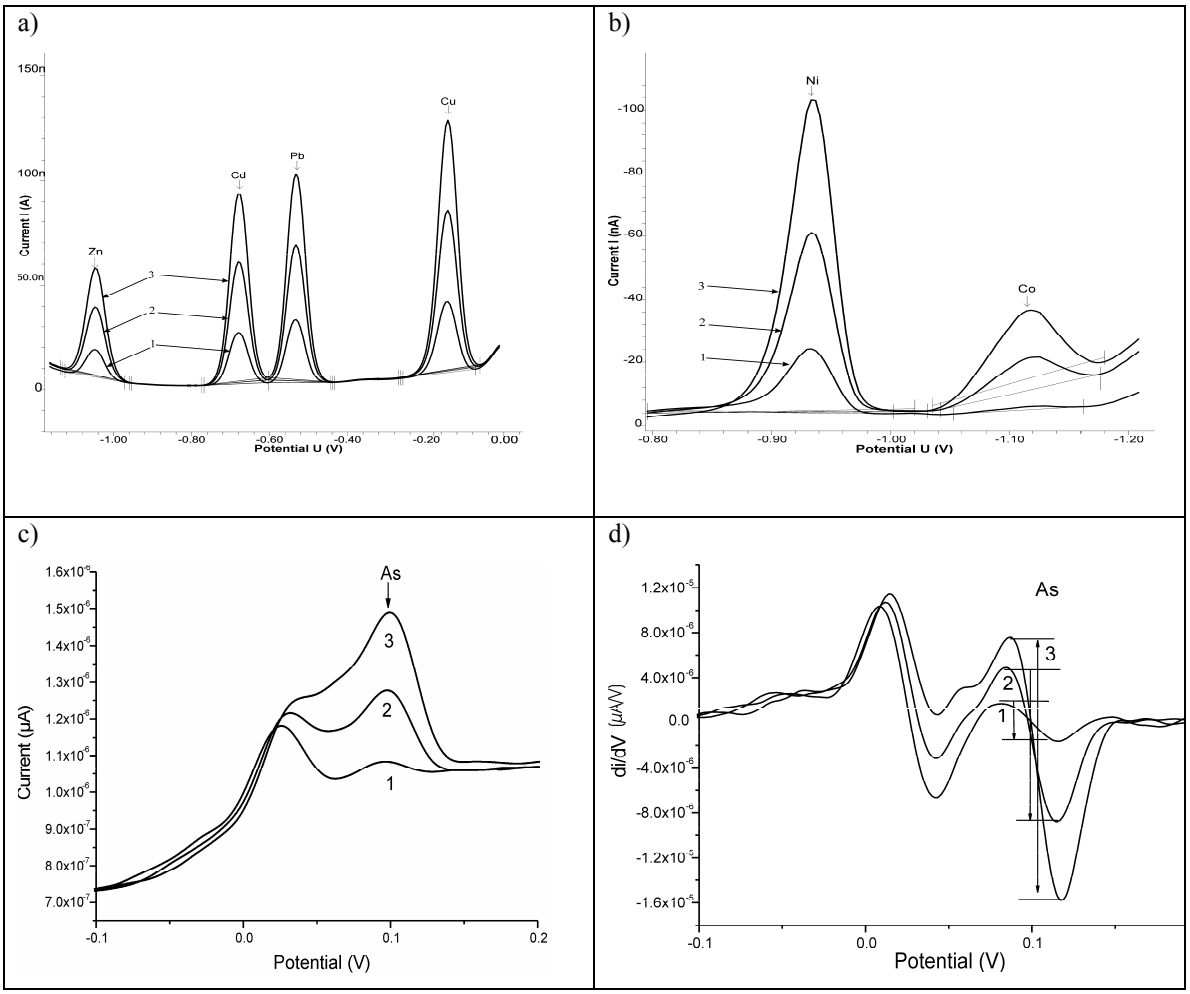

Figure 1 Voltammogram for the determination of Zn, Cd, Pb, Cu (a), Ni (b) and As (c) in PM_{10} samples; d) first derivative of the current for As used for the calibration line for As. The lines labelled 1 correspond to the samples while the lines labelled 2 and 3 correspond to the 1st and 2nd standard additions (Buzica et al., 2006)

Table 1 Analytical features of the voltammetric determination. The requirements for recovery and method detection limit come from EN 14902. Method detection limit is the concentration in ng m^{-3} in a blank filter, instrumental detection limit is the concentration in ng ml^{-1} of blank reagent, RSD is the relative standard deviation. (Buzica et al., 2006)

	Method detection limit: measured/required, ng m^{-3}	Quantification limit/limit value, ng	Recovery: measured/ required, %	Instrumental detection limit, ng ml^{-1}	% RSD
Zn	9.3/ - (n = 6)	2000/ - (n = 6)	100/ - (n = 4)	9.0 (n = 6)	2.0
Cd	0.1/0.5 (n = 6)	20/276 (n = 6)	92/90-110 (n = 4)	0.72 (n = 6)	4.0
Pb	0.8/50 (n = 6)	180/27600 (n = 6)	103/90 – 110 (n = 4)	0.8 (n = 6)	3.0
Cu	0.3/ - (n = 6)	50/ - (n = 6)	99/ - (n = 4)	2.0 (n = 6)	3.0
Ni	0.4/2 (n = 6)	90/1100 (n = 6)	97/85 – 115 (n = 3)	0.60 (n = 6)	4.6
As	0.1/0.6 (n = 13)	20/330 (n = 13)	98/85 – 115 (n=3)	0.059 (n = 5)	4.9

Table 2 Comparison between measurements on 3 samples performed using ASV/AdSV and ICP-MS. (Buzica et al., 2006)

	NIST 1648					Filter 1				Filter 2				U_X	U_s	U_e
	Gravimetry, ng	ICP-MS, ng	ASV/AdSV, ng	ICP/ Grav	ASV/ Grav/	ICP-MS, ng m^{-3}	ASV/AdSV, ng m^{-3}	E_n	Grav/ ICP	ICP-MS, ng m^{-3}	ASV/AdSV, ng m^{-3}	E_n	Grav/ ICP	U_{X_0}	(sampling)	(digestion)
Ni	568 ± 9%	600	529 ± 9 (n=3)	105%	93%	7.7	7.0 ± 0.7 (n=5)	-0.18	0.91	5.1	4.5 ± 0.3 (n=4)	-0.24	0.88	36%	15%	8%
Cu	4222 ± 9%	3540	3699 ± 222 (n=5)	84%	88%	90	94 ± 5 (n=4)	0.07	1.04	51	56 ± 9 (n=3)	0.20	1.10	35%	15%	13%
Zn	32999 ± 9%	26173	32249 ± 1469 (n=5)	79%	98%	579	822 ± 18 (n=4)	0.70	1.42	424	560 ± 20 (n=3)	0.56	1.32	35%	15%	13%
As	797 ± 12%	771	815 ± 27 (n=4)	97%	102%	6.4	7.1 ± 1.5 (n=2)	0.30	1.12	4.4	4.8 ± 0.3 (n=3)	0.25	1.10	26%	15%	26%
Cd	520 ± 12%	491	453 ± 32 (n=5)	94%	87%	69	86 ± 3 (n=4)	0.42	1.23	34	41 ± 4 (n=3)	0.36	1.20	35%	15%	11%
Pb	45408 ± 8%	39981	43299 ± 4050 (n=5)	88%	95%	180	202 ± 7 (n=4)	0.43	1.12	134	157 ± 16 (n=3)	0.60	1.17	19%	15%	7%

AEROSOL OPTICAL DEPTH DETERMINATION BY COMBINATION OF LIDAR AND SUN PHOTOMETER

Ts. Evgenieva[1], N. Kolev[1], I. Iliev[2], I. Kolev[1*]

[1]Institute of Electronics, Bulgarian Academy of Sciences, 72, Tsarigradsko shosse Blvd., 1784 Sofia, Bulgaria;
E-mail: blteam@ie.bas.bg, Tel.: +359 (2) 71 44 696, Fax: +359 (2) 975 32 01
[2]Central Laboratory of Solar–Terrestrial Influences, Bulgarian Academy of Sciences

ABSTRACT

Two campaigns of investigation of the atmosphere over the urban area of the Sofia City were carried out. Active (lidar) and passive (sun photometer) remote sensing were used to study various optical characteristics (extinction coefficient, aerosol optical depth and Angstrom parameters) during the convective boundary layer formation. The aerosol optical depth values obtained from the two devices during simultaneous measurements performed in clear sunny days are juxtaposed. The results show that the values of the aerosol optical depth taken by the sun photometer exceed those retrieved from the lidar data.

1. INTRODUCTION

Atmospheric aerosols play an important role in many atmospheric processes. Most aerosols of anthropogenic origin are found in the lower troposphere and contribute significantly to the haze often visible during early morning and after sunset near to the ground surface (Balis et al., 2000). This study aimed at: (i) determining the atmospheric boundary layer (ABL) height over an urban area situated in a mountain valley using the aerosol as a tracer; (ii) determining the variation in the aerosol optical characteristics over the area in question during the ABL development (convective and stable boundary layer formation) using a lidar and a sun photometer.

2. APPARATUS AND METHODOLOGY

The main parameters of the two devices are: **Specifications of the lidar:** transmitter – a standard Nd-YAG laser (operational wavelength 532 nm, pulse duration and energy 15–20 ns and 10–15 mJ, repetition rate 12.5 Hz; receiving antenna – a Cassegrainian telescope (main mirror diameter 150 mm, equivalent focal length 2250 mm); photodetector – a PMT with an interference filter (1 nm FWHM); data acquisition and processing set – 10 bit 20 MHz ADC and a PC (Kolev et al., 2000). **Specification of the sun photometer:** optical channels: $\lambda = 380$ nm, $\lambda = 500$ nm, $\lambda = 675$ nm, $\lambda = 936$ nm and $\lambda = 1020$ nm, viewing angle – 2.5°, dynamic range > $3x10^5$, computer interface – RS 232 (Solar Light Company, 2003).

The extinction coefficient of atmospheric aerosol is determined from the lidar data using common inversion Fernald method (Fernald, 1984) for solving of the lidar equation. One of the most basic parameters of the aerosols is the optical depth obtained from solar extinction measurement with sun photometers. The calculations are based on the Beer – Lambert – Bouguer law (Devara, 1996).

3. RESULTS AND DISCUSSION

The experiments were carried out in the south-eastern part of the city of Sofia, where the Institute of Electronics (aerosol lidar) and the Central Laboratory for Solar-Terrestrial Influences (sun photometer) are located. In the present work, as we have already mentioned, we present experimental data from two experimental campaigns – autumn (2006) and winter (2006/2007).

3.1. Lidar data

The synoptic situation during the whole period of the present autumn campaign was almost constant, without significant changes, and we had the possibility to make observations in the second half of October 2006. Taking into account the mixing layer height (MLH) the data from this campaign shows two different types of convective

* Corresponding author

boundary layer (CBL): CBL with maximum height H_{CBL} = 600m and CBL with maximum height H_{CBL} = 1000m.

Fig.1 shows the lidar data obtained on 04.10.2006. Twelve images were constructed from the lidar data. The data from 07:30 LST to 08:30 LST are given on the first three height-time images (HTIs) where the stable boundary layer (SBL) formed during the previous night is seen. One can also see the typical for the region multilayer inversion at heights H = 100m, H = 200m and H = 400m as well as the height of the residual layer (RL) formed during the previous day. On the next four HTIs one can see the beginning of the formation of the new mixing layer (ML) which starts after 10:00 LST, while the full destruction of the SBL takes place around 11:00 LST. The residual layer height (RLH) decreases gradually and reach H_{RL} = 450m at 11:30 LST. The full formation of the ML between 12:30 LST and 14:00 LST is shown on the next four HTIs. The MLH reaches about H_{ML} = 600m at 14:00 LST. There are fluctuations in the MLH between 12:30 LST and 14:00 LST. The RL is completely destroyed at 12:30 LST.

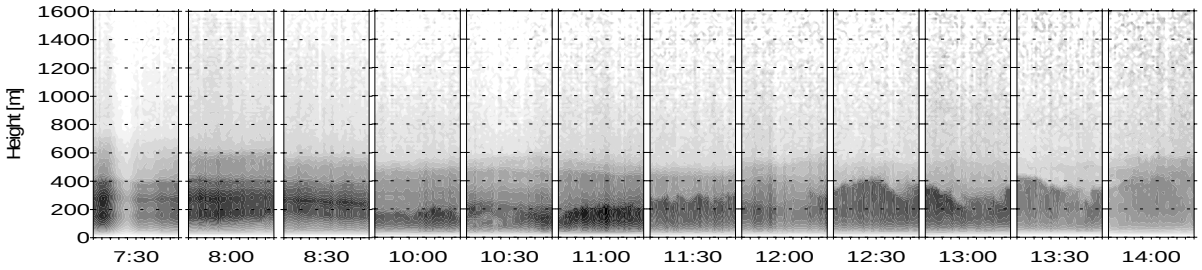

Fig.1. Height – time images obtained from the lidar data on 04.10.2006

The experimental lidar data for one day obtained in the second half of October, namely 18.10.2006, are shown on the next figure (Fig.2). The experiment started at 08:45 LST and finished at 13:30 LST. On the first HTI, the SBL with H_{SBL} = 150-200m remaining from the previous day is seen, as well as the RL with height H_{RL} = 1050m. The new ML begins to form at 09:10 LST and its height is about H_{ML}=100m; its height is about H_{ML}=200m at 10:30 LST and reaches H_{ML}=500-550m at 11:00 LST. The next few images show that the MLH reaches H_{ML} = 750m at 12:00 LST, decreasing to H_{ML} = 600m at 13:00LST. In the next half hour MLH reaches H_{ML} = 1000m.

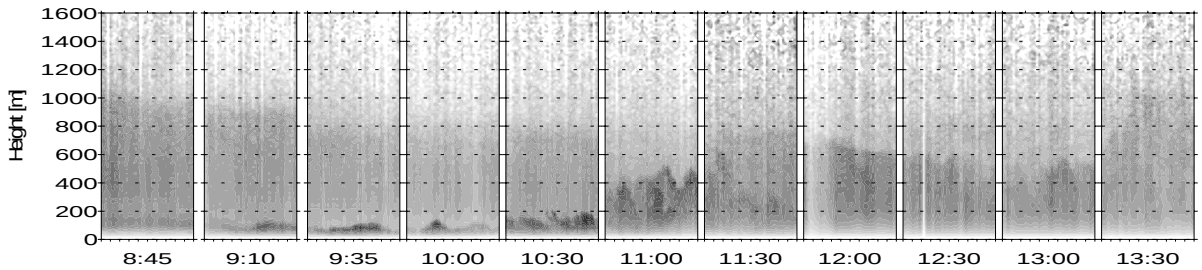

Fig.2. Height – time images obtained from the lidar data on 18.10.2006.

In the next part of the study we present the lidar data obtained on one day of the winter campaign 2007.

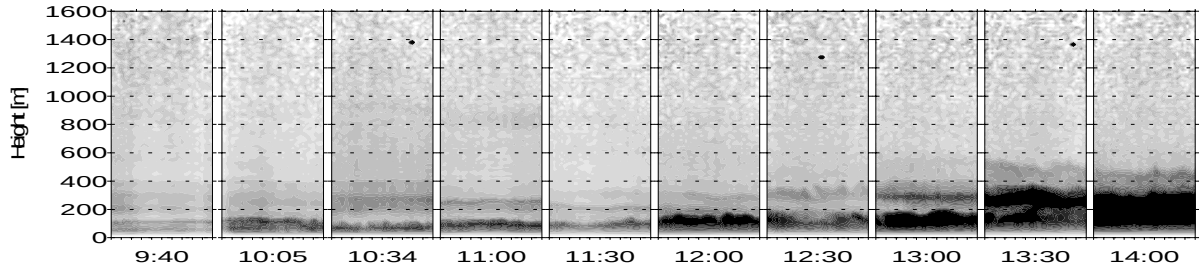

Fig.3. Height – time images obtained from the lidar data on 10.01.2007

Fig.3 shows 10 HTIs obtained on 10.01.2007. The experiment started at 09:40 LST and was completed at 14:00 LST. On the first two HTIs one can see the SBL remaining from the previous evening with height H_{SBL}=400m, with four layers being situated in it. Two of them are located in the first 100-150m and the others are at heights ranging from H = 200m to H = 350m. The RLH is H_{RL} = 1200-1400m and stays constant during the experiment. The beginning of the formation of the new ML occurs at 10:34 LST and the first two aerosol layers are destroyed. The MLH remain constant around H_{ML} = 100m until 11:30 LST, and reaches H_{ML} = 200m at 12:30 LST. The SBL is destroyed completely at 13:30 LST when the MLH reaches H = 550m and remains about H_{ML} = 500m at 14:00 LST.

3.2. Sun photometer data

We present here the experimental data for AOD obtained by using a Microtops II sun photometer. Generally, the data from the autumn campaign show constant decrease of the AOD at the various wavelengths used, especially at wavelength λ = 500nm. The comparison with the lidar data given below is precisely for that wavelength λ = 500nm which is the closest to the laser operational wavelength λ = 532nm.

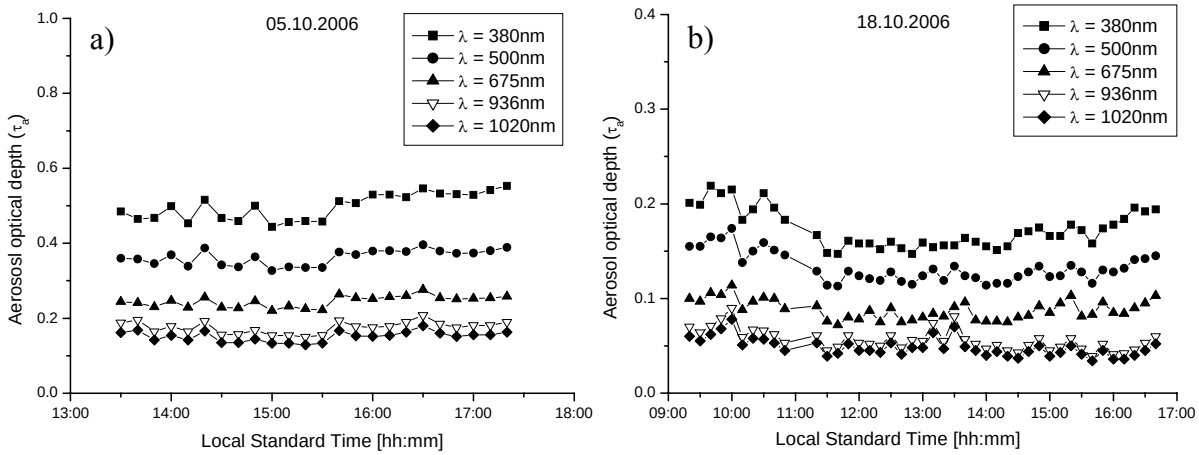

Fig.4. Variations in the AOD at λ = 380nm, λ = 500nm, λ = 675nm, λ = 936nm and λ = 1020nm obtained from sun photometer on a) 05.10.2006 and b) 18.10.2006.

Fig.4 a) shows variations in the AOD at five wavelengths on 05.10.2006. The experiment started at 13:30 LST and finished at 17:20 LST. The mean value at λ = 500nm is τ_a^{mean} = 0.36. AOD has similar behaviour on 04.10.2006 when the mean AOD at λ = 500nm is τ_a^{mean} = 0.26. The experiment started at 08:40 LST and finished at 18:20 LST. On Fig.4 b) variations in the AOD on 18.10.2006 are shown. The experiment started at 09:20 LST and finished at 16:20 LST. The mean value at λ = 500nm is τ_a^{mean} = 0.13. Fluctuations in AOD between 09:20 LST and 11:30 LST are observed. In this period AOD at λ = 500nm varies between τ_a = 0.18 and τ_a = 0.13. AOD has similar behaviour on 19.10.2006. The experiment started at 12:30 LST and finished at 16:30 LST. The mean value for the whole period of observation at λ = 500nm is τ_a^{mean} = 0.17. The mean AOD for the rest of the days in October varies from τ_a^{mean} = 0.25 to τ_a^{mean} = 0.33. In November the mean AOD values are τ_a = 0.22 and τ_a = 0.30. In January the mean AOD varies from τ_a = 0.15 to τ_a = 0.27. Actually, the weather in January was dry and warm which resulted in the formation of an ABL that is not typical for this season characterizing by aerosol pollution in the whole layer.

We present below a comparison between the AOD values obtained from the lidar and the sun photometer data for two days during the ABL formation. Fig.5 a) shows the experimental data obtained on 04.10.2006. In the beginning of the experiment at 07:30 LST the RLH is H_{RL} = 600m. The RL is fully destroyed at 12:00-12:30 LST at height H_{RL} = 400m. The beginning of the formation of the new ML takes place around 09:30 LST. The MLH reaches a maximum value H_{ML} = 600m at 14:00 LST. The values of the AOD retrieved from the lidar data are lower than AOD values taken by the sun photometer. The AOD obtained from the lidar varies from τ_{al} = 0.17 to τ_{al} = 0.22. For the same period the AOD obtained from the sun photometer varies from τ_{as} = 0.3 to τ_{as} = 0.25. The maximum AOD value measured by the sun photometer in the period between 14:30 LST and 18:00 LST

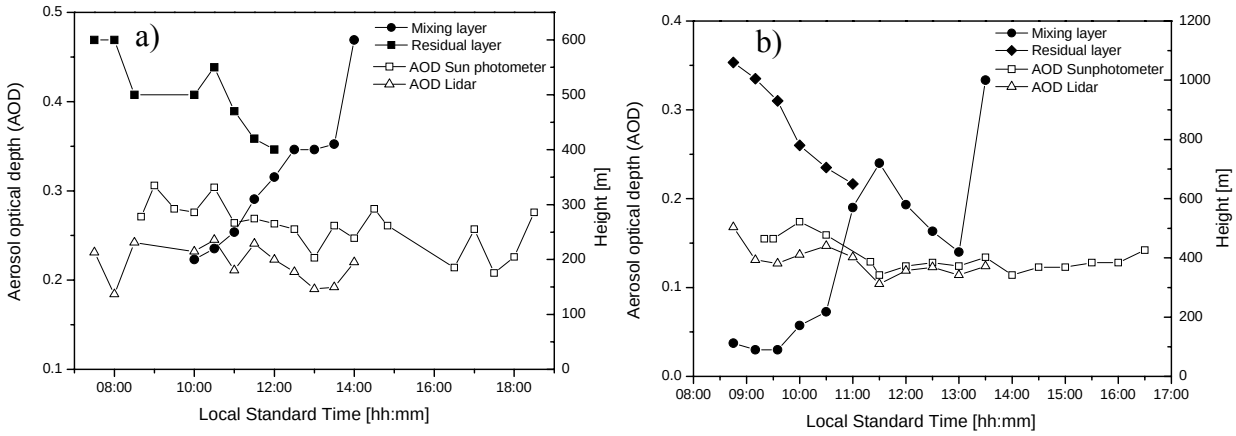

Fig.5 Variations in the height of the different layers and in the aerosol optical depth determined from the lidar, and sun photometer data on a) 04.10.2006 and b) 18.10.2006.

is $\tau_{as} = 0.2$. Fig.5 b) shows the experimental data obtained on 18.10.2006. In the beginning of the experiment the RLH is $H_{RL} = 1050$m. The RL is fully destroyed at 11:00 LST at height $H_{RL} = 650$m. The formation of the new ML starts around 08:30 LST at height around $H_{ML}=100$m and reaches maximum height $H_{ML}=1000$m at 13:30 LST. The AOD values obtained from the lidar data are lower but close to sun photometer one. The maximum values obtained from the two devices are around $\tau_a = 0.17$. The minimum values are $\tau_{al} = 0.10$ and $\tau_{as} = 0.11$ obtained from the lidar and the sun photometer, respectively. The behaviour of the AOD obtained from the two devices is similar.

It is clearly seen, that when lower values of the MLH $H_{ML}=600$m are seen on 04.10.2006 and on 05.10.2006, the AOD values obtained by both the devices are higher than those obtained on 18.10.2006 and 19.10.2006 when the MLH exceeds $H_{ML}=1000$m. The first two days can be characterised with a stronger lidar signal due to the higher humidity in the ML in comparison with the days in the second half of October 2006.

4. CONCLUSIONS

Despite of the preliminary character of the analysis, the data obtained by simultaneous measurements using a lidar and a sun photometer reveal a relation between the ML development, the atmospheric aerosol optical characteristics and the concrete meteorological parameters of the atmosphere over the observed region.

5. REFERENCES

Balis, D., Papayannis, A., Galani, E., Marenco, F., Santaceraria, V., Hamonov, E., Chazette, P., Ziomas, I, Zarefos, C. 2000. Tropospheric lidar aerosol measurement and sun photometric observations at Thessaloniki, Greece. Atmos. Environ. 34, 925-932.

Devara, P.C.S., Pandithurai, G., Raj, R.E., Sharma, S. 1996. Investigations of aerosol optical depth variations using spectroradiometer at an urban station, Pune, India. J. of Aerosol Science 27 (4), 621-632.

Fernald F.G. 1984. Analysis of atmospheric lidar observations: some comments. Appl. Opt. 23, 652-653.

Kolev, I., Savov, P., Kaprielov, B., Parvanov, O., Simeonov, V. 2000. Lidar observation of the nocturnal boundary layer formation over Sofia, Bulgaria. Atmos. Environ. 34, 3223–3235.

Solar Light Company, Inc. 2003. User's guide MICROTOPS II Sunphotometer Version 5.5. USA.

THE CARBON DIOXIDE TOWER MEASUREMENTS IN HELSINKI

L. Järvi, S. Launiainen, A. Sogachev, J. Rinne, E. Siivola, P. Keronen, I. Mammarella and T. Vesala

University of Helsinki, Dept. Physical Sciences, P. O. Box 64, 00014 University of Helsinki, Finland

ABSTRACT

The CO_2 concentrations and fluxes were studied in heterogeneous environment in Helsinki during one year. The surrounding area was divided to different land use sectors (urban, road and vegetation), which enabled us to study the effect of different land use to CO_2 exchange. The highest concentrations were measured during colder seasons, most probably caused by increased domestic activity. Large proportion of CO_2 emissions were traffic related, and the highest fluxes were measured in the road sector during all seasons. The daytime fluxes were around 30 μmol/m^{2}s in the road sector and somewhat lower in the urban sector during all seasons, indicating equal emissions during whole year. The CO_2 exchange was lowest in the vegetation sector where the anthropogenic sources can be expected to be limited. The CO_2 vegetation uptake had a clear influence balancing the anthropogenic sources at summertime.

1. INTRODUCTION

Urban areas are significant source of carbon dioxide (CO_2), which has an important role in global climate change. CO_2 is emitted from fossil fuel combustion with great importance in traffic emissions (e.g. Gratani and Varone, 2005). Even so, the direct measurements of CO_2 exchange between urban surface and atmosphere are restricted in few cities (e.g. Coutts et al., 2007). The CO_2 concentration and flux measurements were started in Helsinki at the end of year 2005. In Helsinki Metropolitan area (pop. 1 million), the total CO_2 emissions were 7108 kT in 2005 and largest sources were energy plants with contribution of 72 % and traffic with contribution of 17 % (Myllynen et al., 2006).

The CO_2 measurements are made at 31 m high tower which is a part of the SMEAR III measuring station (*Stations for Measuring Ecosystem – Atmosphere Relationships*). The tower is located on a hill (26 m above the sea level) about three kilometres north-east from the downtown of Helsinki. The surroundings of the tower are very heterogeneous consisting of buildings, patchy forest and low vegetation, parking lots and roads. Thus, the effect of different land use covers to CO_2 exchange can be studied by dividing the surroundings to three sectors: Urban, road and vegetation (Table 1). The average land use fractions inside a circle of 250 m around the tower are listed in table 1 for the whole circle and separately for all sectors. The urban sector is mainly covered by University of Helsinki buildings with an average height of 20 m and by roads and parking lots. One of the main roads leading to downtown of Helsinki is passing the road sector and the distance between the tower and road is 150 m. On the road, the average daily traffic rate was 58 600 vehicles in 2005, concentrating especially to rush hours (Lilleberg and Hellman, 2006). The vegetation sector is mainly covered with vegetation including both deciduous trees and greenspace with grasses and garden cultivation.

Table 1. The land use fractions around the measuring tower within a circle of radius 250 m separately for all three sectors.

	Land use type	Building fraction (λ_b)	Road fraction (λ_r)	Vegetation fraction (λ_v)
320 - 40°	Urban	0.42	0.51	0.07
40 - 180°	Road	0.10	0.60	0.30
180 - 320°	Vegetation	0.02	0.13	0.85
Full circle		0.14	0.40	0.46

2. METHODOLOGY

The measurement system included a Metek ultrasonic anemometer (USA-1, Metek GmbH, Germany) and an open-path gas analyzer (LI-7500, Li-Cor, Lincoln, Nebraska, USA) which were measuring wind components and temperature, and CO_2 mixing ratios, respectively. The CO_2 fluxes were calculated according to the eddy covariance technique given by (e.g. Balcocchi, 2003)

$$F_c = \rho_a \overline{w' c'} \quad (1)$$

where ρ_a is the density of dry air, w is the vertical wind component and c is the mixing ratio of CO_2. Overbar denotes time average and prime fluctuations around the average. A linear trend removal and 2-dimensional coordinate rotation were applied before the flux calculations. Data with friction velocity less than 0.1 m/s were omitted and a stationarity test was performed according to Foken and Wichura (1996). The CO_2 fluxes were corrected for the sensor heating effects (Burba et al., 2006).

We are presenting data from the year 2006. The record was divided into four seasons: Winter from January to March and December, spring from April to mid-May, summer from mid-May to August and fall from September to November. In addition, division between the different land use sectors was made.

3. RESULTS AND DISCUSSION

The CO_2 concentrations were slightly higher, median values being between 375 and 383 ppm, during winter and spring compared to summer when the concentrations ranged from 354 to 367 ppm (Table 1). The somewhat higher values during colder months are most probably caused by enhanced domestic activity such as heating. The concentrations did not have a clear dependence from the land use sectors. The measured concentrations are consistent with other studies. Grimmond et al. (2002) measured a mean value of 384 ppm in Chicago in summer 1995 and a median concentration of 372 ppm was measured in Edinburgh in fall 2000 by Nemitz et al. (2002). The diurnal cycle of CO_2 concentration was similar in all sectors during the summertime. Summery concentrations increased during the night time and decrease rapidly after 5 am staying low until the evening. The increasing nocturnal concentrations are due to accumulation of both vegetation respiration and traffic emissions to the low boundary layer. The rapid decrease in the morning was observed even though the emissions still continued increasing (Fig. 1c). The decreasing is caused by the boundary layer growth due to the turbulent mixing and maybe also entrainment of low CO_2 air to the boundary layer. In addition, the vegetation uptake decreases the daytime concentrations at summertime. The amplitudes of the diurnal cycles were 10 ppm in the vegetation and urban sectors and 18 ppm in the road sector. The summer diurnal cycles were similar to those measured at Vancouver by Reid and Steyn (1997) and at Chicago by Grimmond et al. (2002) during summertime. However, these studies showed amplitudes of 27 and 35 ppm, respectively, which are higher than ours. The wintry diurnal cycle of CO_2 concentrations were similar to the summery in the direction of urban sector with amplitude of 13 ppm. The diurnal differences were small in the vegetation sector and the concentrations were around 374 ppm. In the urban sector, one peak of 388 ppm was detected between 7 am and 13 pm. The peak was now caused by the accumulation of traffic CO_2 emission in smaller volume due to the lower mixing heights before the sunrise.

Table 2: The median CO_2 concentrations and quartile deviations during different seasons and land use sectors.

	Urban	Road	Vegetation
Winter	383 ± 8	376 ± 7	375 ± 8
Spring	383 ± 6	382 ± 3	380 ± 4
Summer	364 ± 7.2	354 ± 8	367 ± 5
Fall	378 ± 19	373 ± 8	366 ± 6

The winter median CO_2 fluxes changed from 7.7 μmol/m^{2}s in the vegetation sector to 17.0 μmol/m^{2}s in the road sector. Slightly lower values were measured during spring and summer especially in the urban and vegetation sectors, when the fluxes changed between 3.8 and 16.5 μmol/m^{2}s (vegetation and road sector, respectively). The lowest fluxes were always measured in the vegetation sector where the anthropogenic CO_2 sources are expected to be limited. On average, the fluxes were always directed upwards even at summer when the vegetation acts as a sink of CO_2 during daytime. Our wintertime fluxes are consistent with the 18 μmol/m^{2}s measured at the downtown of Edinburgh (Nemitz et al., 2002) and our summertime fluxes are of the same order of magnitude as the 0 – 10 μmol/m^{2}s measured at Chicago (Grimmond et al., 2002). The diurnal cycle of CO_2 fluxes showed a clear dependence from traffic activity in the urban and road sectors (Fig. 1). The fluxes increased during the morning rush hour around 5 am and stayed elevated through the day, maximum values being about 30 μmol/m^{2}s in the road sector and somewhat lower in the urban sector. Deviations were small between the seasons, indicating equal emissions throughout the year from the road and urban sectors. The nocturnal fluxes were 10 μmol/m^{2}s at winter, while they had slightly lower values during other seasons. This is probably due to the enhanced domestic activity during the winter. Largest seasonal differences were measured in the vegetation sector. The daytime fluxes were between 10 and 20 μmol/m^{2}s outside the growing season, showing the effect of anthropogenic sources, and less than 4 μmol/m^{2}s during the

summer. On average, the fluxes had negative values during summer mornings when vegetation uptake exceeds the anthropogenic sources. The nocturnal fluxes were similar, about 6 μmol/m^{2}s, in the vegetation sector during all seasons.

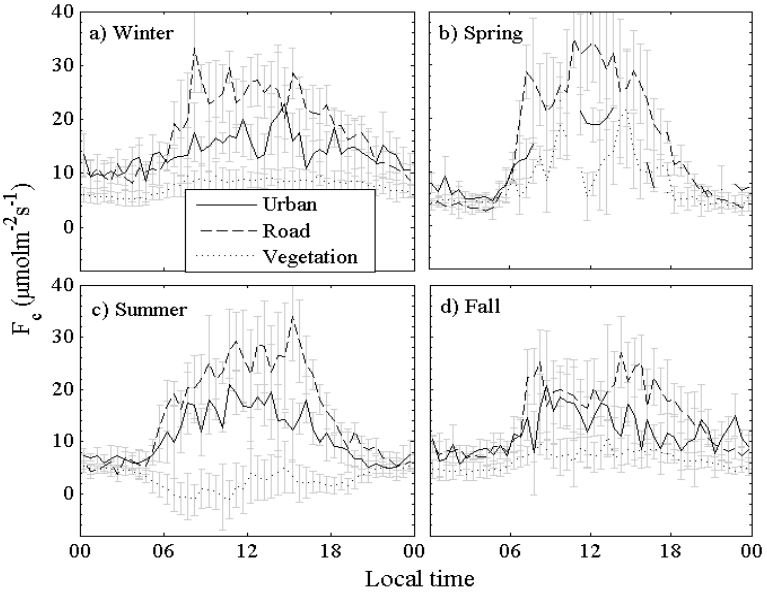

Figure 1. The diurnal cycle of half hour median CO_2 fluxes (F_c) at a) winter, b) spring, c) summer and d) fall for different land use sectors. Positive means upward and negative downward values. The error bar presents the quartile deviations of the fluxes.

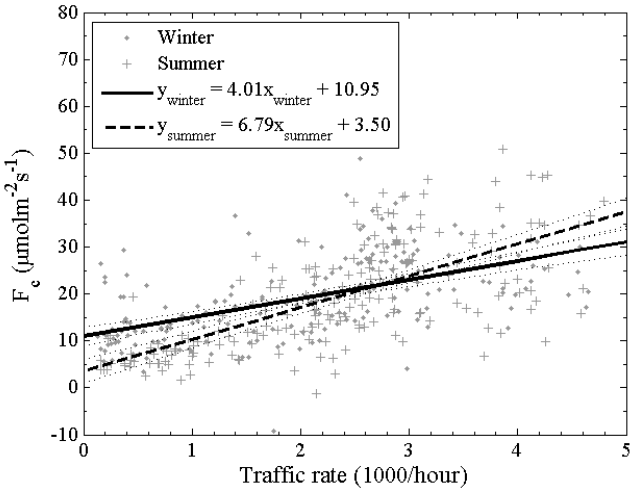

Figure 2. CO_2 exchange as a function of traffic rates for winter (Jan - Mar) and summer (Jun - Aug), separately. The lines are the linear fittings made to data points and the dotted lines show 95 % confidence bands for the measured flux.

The effect of traffic to the net CO_2 exchange was studied by the means of regression analysis. The hourly flux values were plotted against traffic rates for two periods from January to March and from June to August (Fig. 2). The traffic rates were obtained from one of the main roads of Helsinki and only flow situations from the road sector were taken into account. A linear regression was made to the data points and dependence between these two was found. The correlation was higher at summer (R^2 = 0.47) than at winter (R^2 = 0.31). Also the slope had higher value during the summer. The offsets of the fittings can be considered to be the non-vehicle sources. The wintertime offset 11 μmol/m^{2}s was much higher than the summertime value 4 μmol/m^{2}s, which can be explained by higher domestic activity at wintertime. Similar analysis made at the center of Edinburgh by Nemitz et al. (2002) in fall 2000, gave an offset of 12 μmol/m^{2}s. This is consistent with our wintertime value.

4. CONCLUSIONS

A full year of CO_2 concentration and flux data was studied by dividing the data according to season and different land use sectors. On average, the surroundings of the measurement tower acted as source for CO_2. The effect of growing season was evident in CO_2 exchange. The nocturnal summer concentrations were increased by ecosystem respiration and decreased during the day due to vegetation uptake. Also the strength of the turbulent mixing and traffic emissions affected to the diurnal cycle of concentrations. The diurnal cycle of fluxes between different seasons were similar in urban and road sectors but deviated in the vegetation sector. Summer mornings showed negative fluxes due to the vegetation CO_2 uptake.

The measured differences between the different sectors clearly showed the effect of land use to CO_2 exchange. The emissions from vegetation cover were lower than from urbanized covers. Especially, the fluxes measured in the road sector were higher, showing the strong effect of traffic as a source of CO_2. This was further proved by linear regression analysis made between the fluxes and traffic rates during winter and summer.

5. ACKNOWLEDGEMENTS

This study was supported by REBECCA by University of Helsinki Environmental Research Centre (HERC) and Research Foundation of the University of Helsinki.

6. REFERENCES

Baldocchi, D., D. 2003. Assessing the eddy covariance technique for evaluating carbon dioxide exchange rates of ecosystems: past, present and future. *Global Change Biology* 9, 479-492

Burba, G., Anderson, D., Liukang Xu and McDermitt, D. 2006. Correcting apparent off-season CO2 uptake due to surface heating of an open path gas analyzer: progress report of an ongoing study. *AMS*

Coutts, A., Beringer, J. and Tapper, N. 2007. Characteristics influencing the variability of urban CO2 fluxes in Melbourne, Autralia. *Atmos. Env*. 41, 51-62.

Foken, T. and Wichura, B. 1996. Tools for quality assessment of surface-based flux measurements. *Agric. For. Meteorol.* 78, 83-105

Gratani, L. and Varone, L. 2005. Daily and seasonal variation of CO2 in the city of Rome in relationship with traffic volume. *Atmos. Env.* 39, 2619 – 2624

Grimmond , S., King, T., Cropley, F., Nowak, D. and Souch, C. 2002. Local-scale fluxes of carbon dioxide in urban environments: methodological challenges and results from Chicago. *Env. Pollution* 116, 243-254.

Lilleberg, I. and Hellman T. 2006. *Traffic rates in Helsinki in 2005 (in Finnish)*. Helsinki City Planning Department.

Myllynen, M., Aarnio, P., Koskentalo, T. and Malkki, M. 2006. *The Air Quality in Helsinki Metropolitan Area year in 2005 (in Finnish)*. YTV Helsinki Metropolitan Council.

Nemitz, E., Hargreaves, K., McDonald, A., Dorsey, J. and Fowler, D. 2002: Micrometeorological measurements of the urban heat budget and CO2 Emissions on a city scale. *Environ. Sci. Technol.* 36, 3139-3146

Reid K. and Steyn, D. 1997. Diurnal variations of boundary-layer carbon dioxide in a coastal city – observations and comparison with model results. *Atmos. Env.* 31, 3101-3114

PRELIMINARY RESULTS OF SUSPENDED PARTICLES MEASUREMENTS BY GRIMM ANALYZERS IN INDUSTRIAL AGGLOMERATION IN CZECH REPUBLIC

Josef Keder, Czech Hydrometeorological Institute

ABSTRACT

During the period September 2005 – October 2006, measurements of suspended particles fractions PM1, PM2.5 and PM10 have been provided using GRIMM Model 180 analyzer at two places in the Czech Republic. The concentration time series were checked, revised and supplemented by meteorological data as temperature, wind, humidity and global radiation. A comparison with the PM10 data from the collocated beta-absorption monitor has been provided with the aim to find possible correction factors. Time changes of proportions among separate PM fractions were studied and related to the weather elements. Distinct patterns in the data, changing in time and correlated with the meteorological conditions, were found and interpreted in relation to the human health risk.

1. INTRODUCTION

Particles are considered as one of the most problematical pollutants affecting the human health. They comprise typical air pollution burden especially in the urban environment, where they are emitted primarily from the mobile sources and in the industrial regions as well. Health risk depends by particulate matter concentration and particles size, morphology and chemical composition (Pope and Dockery, 2006). The air quality standards regulate PM10 concentrations first of all. In recent years, however, the PM2.5 and PM1 particles, depositing in the lower respiratory tract and being assumed as the main cause of increased morbidity and mortality among population, were studied with the increased intensity.

2. METHODOLOGY

Measured data from GRIMM Model 180 analyzer (GRIMM Aerosol Technik, 2003), gathered at two places in the Czech Republic during the period September 2005 – October 2006, were analyzed. The GRIMM analyzers were installed at automatic monitoring stations located in Prague (Czech Republic capital) and in highly industrialized town Ostrava. PM10 concentrations measurements by means of Thermo ESM Andersen FH 62 I-R analyzers are provided at both stations at regular basis. Parallel meteorological data such as air temperature and humidity, wind and global solar radiation are available as well at these stes. The analysis has been provided for the hourly means of all measured quantities.

3. RESULTS AND DISCUSSION

Hourly mean particle concentrations in fractions PM10 and PM2.5, measured by GRIMM analyzers, were compared with those from regular network. Example of such comparison gives a scatter graph at picture 1, where comparison of PM10 data from Prague was depicted. The good correlation of both methods is obvious, but GRIMM analyzer significantly underestimates PM10 mass concentration values. Similar results were obtained for the PM2.5 fraction.

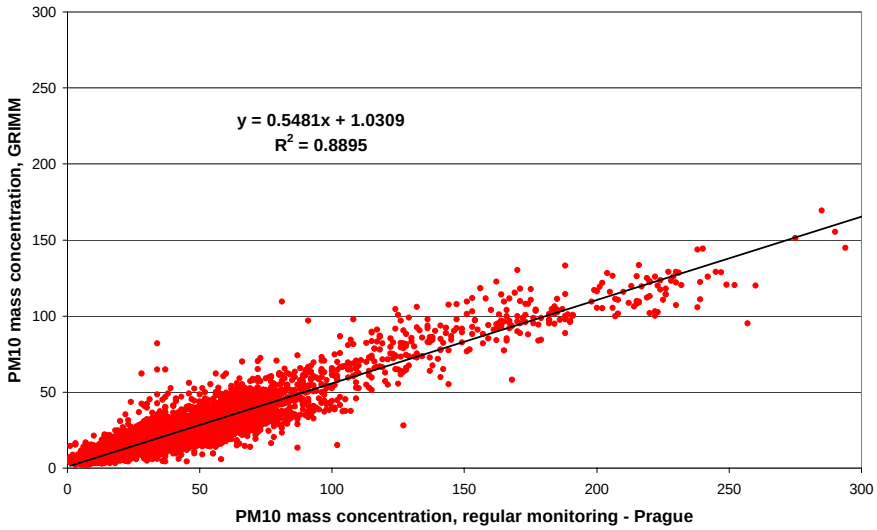

Fig. 1.: Comparison of PM10 concentration measured by GRIMM and a standard network analyzer

For further analysis, proportions of particular fractions measured by GRIMM were determined, where e.g. GM1/GM10 stays for the share of PM1 in total PM10 concentration. Changes of share of PM1 and PM2.5 in PM10 with air temperature and relative humidity are represented by means of boxplots at pictures 2 and.3. It

is apparent that the share of fine fraction in total PM10 concentration increases when air temperature decreases. For low temperatures, practically the whole PM2.5 fraction consists of the finest PM1 particles, which are the most dangerous form the aspect of health effects (Fig. 2).

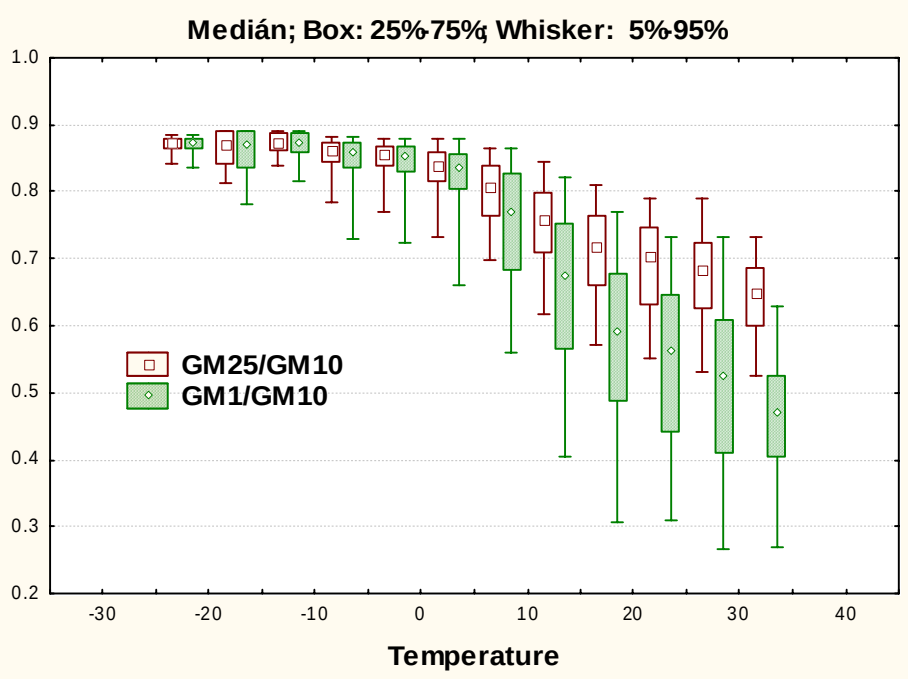

Fig. 2.: Dependence of share of PM1 and PM2.5 in total PM10 at air temperature in Prague

Similarly, the picture 3 shows that the share of both fractions in the total PM10 increases with increasing relative humidity and that the share of PM1 in PM2.5 increases as well. In range of relative humidity between 80 and 90% practically all PM2.5 consists of PM1.

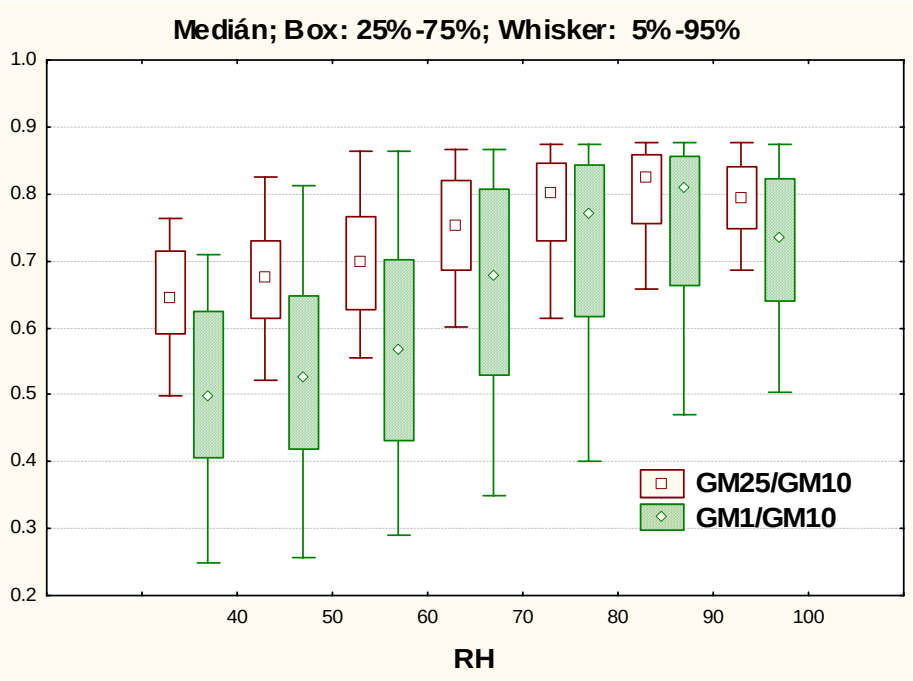

Fig.3.: Dependence of share of PM1 and PM2.5 in total PM10 at relative humidity in Prague

For the purpose of health protection and for considerations on particle origin there is necessary to answer the question if and how the share of particular fraction in PM10 changes in time. The results of multicomponent analysis showed that this share has been changing at both locations during the day and from one month to another as well. Four typical profiles of share of PM1 and PM2.5 fractions in PM10 were found by means of cluster analysis, marked from 1 to 4. Each hourly profile was then allocated into one profile class. The share

of fine fraction in total PM10 increases with the increasing class number and for class 4 practically the whole PM10 consists of PM1. Thus, the rate of danger for the human health increases with class number.

Figure 4 shows the daily changes of profile classes in Ostrava for winter (January) and summer (August) month. The most dangerous profile class dominated in Ostrava over the whole January 2006, without any indication of the daily course. The different picture showed August, when amount of less serious classes increased and daily course of them is also apparent. The described approach enables to map the changes of burden by particular PM fractions during the whole year and study their relation to meteorological parameters and emission sources types.

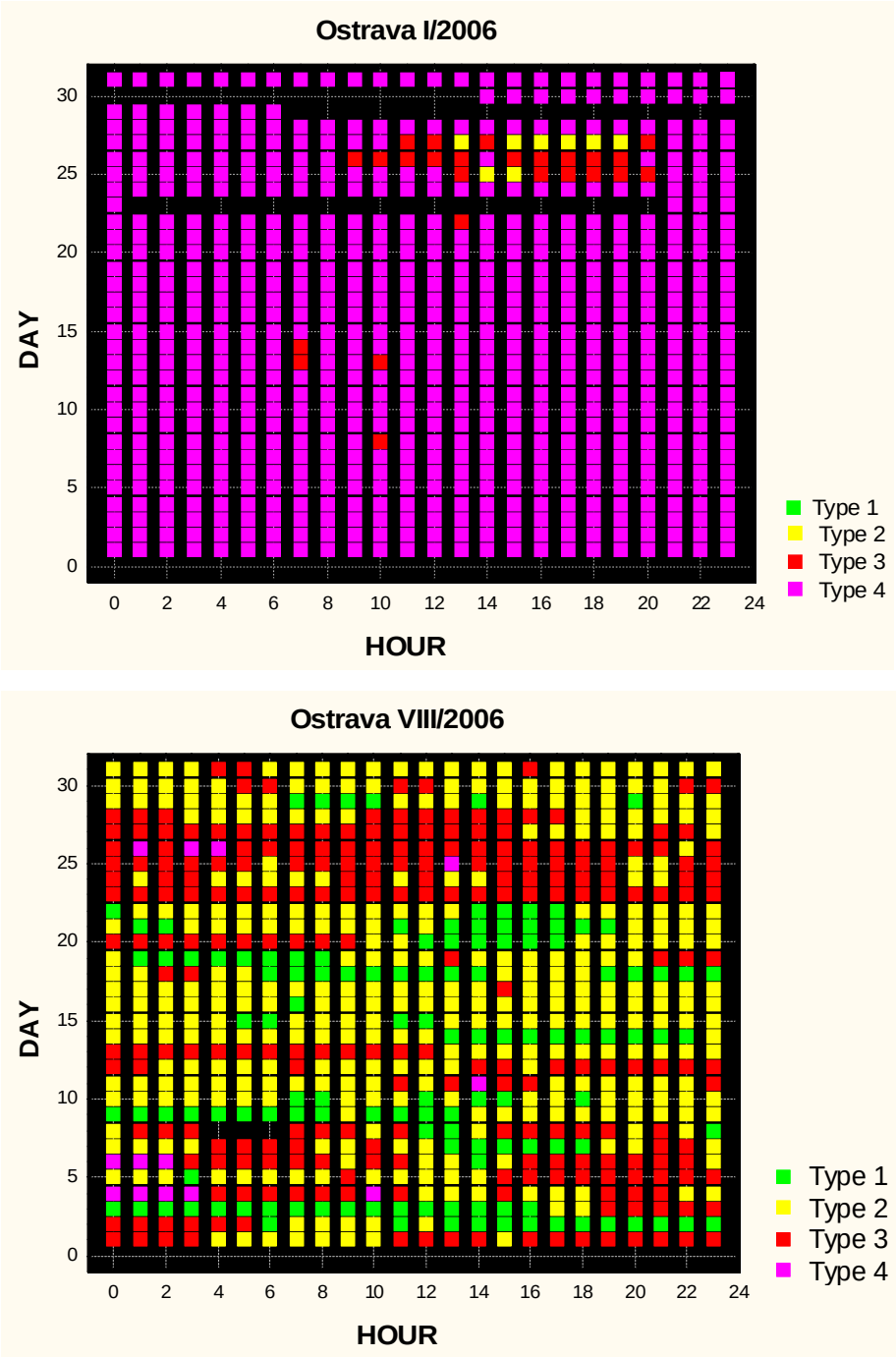

Fig. 4.: Time changes of typical profiles of PM fractions share in PM10 in Ostrava in winter and summer month

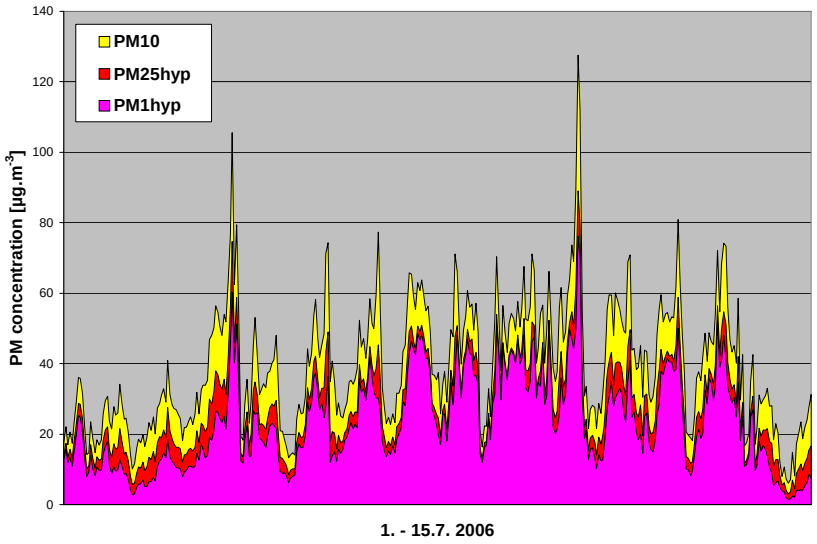

Fig. 5.: Disaggregation of operationally measured PM10 mass concentrations measured by means of fraction proportions determined from GRIMM. Ostrava, July 2006

Clearly, not only the proportion of fractions but also their mass concentration is crucial from the viewpoint of health effects. Figure 5 gives an example of combination of parallel GRIMM and standard analyzer measurement. The PM10 mass concentration from standard analyzer has been disaggregated among particular fractions by means of coefficients derived from the share of PM1 and PM2.5 fractions measured by GRIMM. The PM1 and PM2.5 concentrations derived from PM10 ones are marked as "hypothetical". If the GRIMM analyzer were set for measurements of broader spectrum of fractions, the parallel measurements provided by both analyzers would enable to assess particulate mass concentrations in separate spectral bands and determine their time changes.

4. CONCLUSIONS

Following conclusion were derived from the parallel measurements of particle concentrations by GRIMM analyzers and routine PM measurements, provided at two monitoring stations in Czech Republic:

- The PM10 mass concentrations measured by GRIMM analyzer are underestimated significantly, nevertheless the data are homogenous and well correlated with the routine analyzer measurements
- It is possible to derive correction formulae for the recalculation of GRIMM data and disaggregate the PM10 data from regular monitoring into particular fractions, using the fractions proportions derived from GRIMM
- Share of particular fractions (PM1 and PM2.5) in total PM10 concentration showed significant time changes and was related to the meteorological conditions
- It was possible to define typical profiles of such proportions and to highlight the presence of structures in measured data that way
- The share of particles, depositing in the low respiratory tract (PM1 and PM2.5) at the total PM10 concentration increased with the decrease of air temperature and increase of relative humidity. This is very serious fact in relation to the human health protection.
- It has been found that particle size distribution might change suddenly when wind speed increase over 4m.s^{-1}. This might be a consequence of particle resuspension which occur at this wind speed threshold.

5. ACKNOWLEDGEMENTS

This work has been financially supported by the Czech Ministry of Environment from granted research project VaV SM-9-86-05.

6. REFERENCES

GRIMM Aerosol Technik GmbH & Co. KG, 2003. GRIMM Environmental Dust Monitor #180 User Manual www.grimm-aerosol.com

Pope III, C.A., Dockery, D.W. 2006. Health Effects of Fine Particulate Air Pollution: Lines that Connect. Air & Waste Manage. Assoc. 56:709–742

APPLICATION OF A NETWORK OF MW-RADIOMETERS AND SODAR FOR THE VERIFICATION OF METEOROLOGICAL FORECASTING MODELS

D. Pernigotti, A. Rossa, M. E. Ferrario, M. Sansone

Institution for all authors: ARPAV-CMT, Via Marconi 55, 35037 Teolo (PD), Italy.
Corresponding author: dpernigotti@arpa.veneto.it

Abstract
The Centro Meteorologico di Teolo (CMT) of the Regional Agency for Protection and Prevention of the Environment of the Veneto Region (ARPAV) has recently installed on its territory a boundary layer profilers network, which consists of four passive microwave radiometers (1 Radiometer Physics GmbH, 3 Kipp & Zonen) and 4 SODAR (Metek).
In the framework of the contribution of ARPAV to the COST728 this paper will present the application of the radiometers and SODAR data for the verification of profiles of temperature and wind for various MetM: ECMWF model, COSMO Model in the Italian (LAMI) and Swiss (aLMo) Suite. In this paper comparisons of profiler data acquired in the year May 2005-April 2006 with the analysis made with the MetM are presented. In particular, the potential of the profiler network to detect and characterize the ability of MetM to describe the PBL for pollutant dispersion applications is discussed.

1. INTRODUCTION

The Centro Meteorologico di Teolo (CMT) of the Regional Agency for Protection and Prevention of the Environment of the region Veneto (ARPAV) has recently installed a network of four passive radiometers and four SODAR for air quality monitoring purposes. The instruments are all located in Veneto, as reported in Figure 1. The network, in the framework of the project DOCUP (D*OCumento Unico di Programmazione*) co-funded by the European Union, Italy, and the region of Veneto, is the first of its kind in Italy. The Profilers data have more time and vertical resolution when compared to radio-sondings, which allows for a great value of these data for MetM verification in the Planetary Boundary Layer (PBL), i.e. for the region where all application for pollutant dispersion modelling take place.

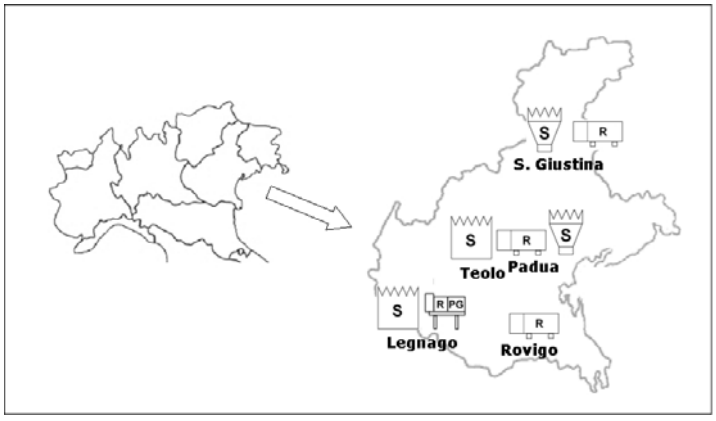

Figure 1: Profiler Network on north/east Italy

2. DATA SET

The MetM analysis uesed are extracted form the operational database of ECMWF (IFS model), ARPA-SIM (Cosmo Model, LAMI suite) and MeteoSwiss CSCS (Cosmo Model, aLMo Suite). All data are given at the models levels, then interpolated on the vertical coordinate of the instrument measurement. The IFS model is a Global Model with analysis stored at ECMWF with time resolution of 6 hours whilst Lokal Moedell is a Limited Area Model (LAM) with analysis stored at ARPA-SIM and CSCS with 1h time resolution.

	IFS till 31/02/06	IFS	LAMI till 25/1/06	LAMI	aLMo
Horiz. Resol.	0.5° (50km)	0.25° (25km)	7km	7km	7km
Vertical lev.	60	91	35	40	45
V. lev <1000m	11	13	9	14	10
Temp. Resol.	6h	1h	1h	1h	1h

Tab. 1: Some details on the MetM used for verification

The 3 MTP5-HE Radiometers ("R" in figure 1) are manufactured by Attex in Russia and distributed by Kipp & Zonen. As shown in Kadygrov et al. (2005) this instrument reports a good agreement within 0.5-0.8K with a co-located radio sounding found in Payerne, Switzerland, on 63 profiles. Ferrario et al (2006) confirmed this data for the ARPAV MTP5-HE radiometers. All instruments are set to have the first level at 50m.

The radiometer ("RPG" in figure 1) is manifactured by Radiometer Physics GmbH. It recieves radiation emitted by the atmosphere in 14 channels (molecular oxyigen and water vapour lines) and converts this data to profiles for themperature and humidity (T. Rose et al.,2005) via neural algorithm optimized for the measuring site. The instrument installed in Legnago makes also a vertical scan every 20' for temperature to increase vertical resolution (50-75m up to 2000m) in the PBL, where the declared accuracy is 1K.

The SODAR ("S" in figure 1) are two PCS2000-24 and two PCS2000-64 manifactured by Metek. This is well known technology (I. Antonious et al., 2003) and the manifacturer declared accuracy of the data is of 0.3m/s for wind intensity and 5-8° for wind direction. This kind of instrument have always the problem of the vertical range, which is dependent by the atmospheric stability, giving a strong decrase on the number of sampling incrising the altitude. All SODAR are set with first level at 40m and temporal resolution of 15'.

	SODAR				MTP5-HE			HATPRO
	Padova	S.Giustina	Legnago	Teolo	Padova	S.Giustina	Rovigo	Legnago
Vert. resol	20m	20m	20m	20m	50m	50m	50m	50-75m
Temp.resol	15'	15'	15'	15'	5'	5'	5'	20'
V. range	200m	220m	200m	440m	1000m	1000m	1000m	2000m
#data	75%	73%	66%	85%	97%	70%	79%	63%

Tab. 2: Some parameters on instruments settings and data availability, Vertical range for SODAR is the altitude were availability go down to 30% of the one of first level (40m)

The measuring sites are flat and rural (Legnago), flat and urban (Padua and Rovigo), on smooth hills (Teolo) and in a closed valley with very very light winds and strong inversions (S. Giustina, Val Belluna).

3. SCORES FOR TEMPERATURE

As reported in the works made in the framework of the FUMAPEX Project (S. Jongen and G. Bonafè, 2006; B. Fay et al.,2005) a good simulation of the thermal profile in the levels near ground is very important for air quality assessment purposes.
The MW-Radiometers can be very useful in assessing the ability of MetM analysis to simulate the temperature profile in the PBL. The results reported in Tab.3 show that the models' analysis is good for correlation (R) in Padua, Legnago and Rovigo, whilst it is not so good for S. Giustina; the BIAS is quite important in Padua and S. Giustina as can be also seen in Fig. 2, but this can be related to the instrument site setting (see M.E. Ferrario et al., 2006); the RMSE is big in all sites and in the case of Legnago and Rovigo (where the BIAS is small) this can be partially related to the inability of models to correctly simulate the temperature in the lowest levels. To confirm this the statistical scores in the first 300m for Rovigo and Legnago were calculated, giving a slightly grater RMSE.

	Padova			Legnago			Rovigo			S. Giustina		
	IFS	LAMA	aLMo	IFS	LAMA	aLMo	IFS	LAMA	aLMo	IFS	LAMA	aLMo
distance	13.9	2.9	2.9	22.3	3.8	3.8	18.7	4.3	4.3	9.9	2.2	6.4
# data	1409	8315	8455	918	5405	5539	1031	5972	6145	1156	6810	6913
BIAS (°)	-2.0	-1.2	-1.5	1.4	0.7	0.5	0.1	-0.2	-0.5	-2.5	-2.2	-0.9
RMSE	2.5	1.8	2.1	2.6	2.3	2.2	2.6	2.7	2.7	10.3	10.0	9.9
R	0.99	0.99	0.98	0.94	0.95	0.94	0.94	0.95	0.95	0.70	0.71	0.69

Tab. 3: Average of statistical parameter from 50m to 1000m above ground, 'distance' is the distrance from model point to the radiometer site.

Number and strength of nocturnal inversions are particular important for pollutant dispersion, expecially in the PO-Valley (S. Jongen and G. Bonafè, 2006). The radiometers' data report 37% of total time with inversions in Padua, 49% in Rovigo and 60% in Legnago. This variability in not well reproduced in the LM model data, that give inversion always around 45% of the time for LAMA and 35% for aLMo. The IFS model is doing better, with 37% of the time with inversion in Padua, 44% in Rovigo, 51% in Legnago. The Fig. 1 show the histograms for the inversions distribution, showing that all models underestimate the strength of the strongest inversions, which happen mostly in S. Giustina and Legnago; in these cases LAMA is doing better then IFS whils aLMo is performing the worse.

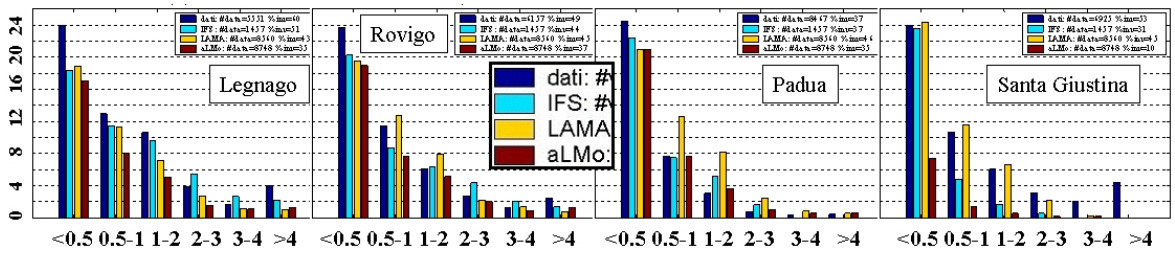

Fig. 1: Histogram of temperature inversion strength (maxT(50,1000)-T(50)) in degrees in % on the total data**.**

Fig. 2 confirms that in all sites LAMA and IFS report the inversion of midnight, whilst for aLMo this is allways too weak or absent as in the case of S. Giustina.

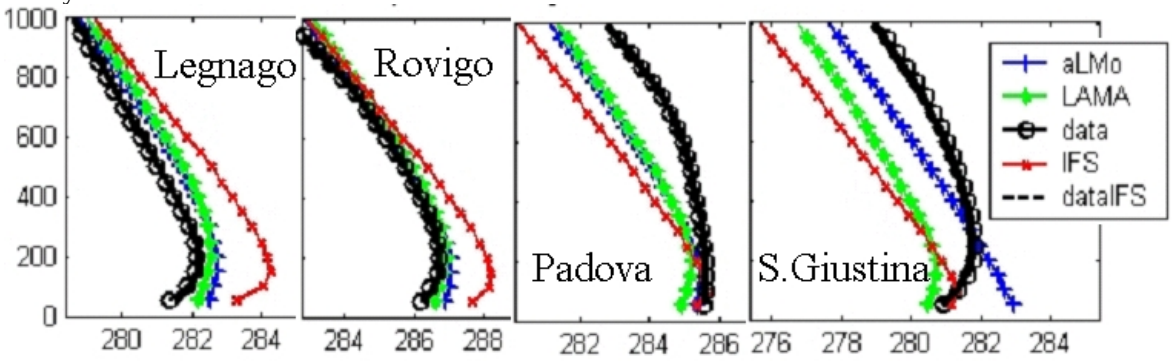

Fig. 2: Average temperature profile for 00UTC for various stations and models

4. SCORES FOR WIND

The availability of SODAR data is normally decreasing very rapidly with the height, as can be seen in Tab. 2 on the vertical range, therefore for the wind the verification is limited for all sites to about 200m, except for Teolo where the vertical range goes up to 440m.

	Padova			Legnago			Teolo			Sgiustina		
	IFS	LAMA	aLMo	IFS	LAMA	aLMo	IFS	LAMA	aLMo	IFS	LAMA	aLMo
distance	14.2	3.5	3.5	21.9	4.3	4.3	22.3	2.8	2.9	9.4	2.6	6.8
#data min	337	2155	2190	307	1817	1851	357	2094	2149	353	2052	2110
BIAS	0.21	0.30	0.03	-0.39	-0.41	-0.38	-0.27	0.52	0.30	1.49	2.26	1.20
RMSE	2.28	2.36	2.31	2.53	2.47	2.50	2.49	2.72	2.56	2.87	4.42	3.07
R	0.58	0.61	0.62	0.60	0.66	0.66	0.59	0.61	0.63	0.09	0.05	0.06
DIST	3.12	2.92	2.91	3.37	3.11	3.10	3.35	3.45	3.18	3.27	4.12	3.16
Perc30	0.46	0.53	0.50	0.51	0.57	0.57	0.46	0.47	0.51	0.22	0.19	0.20
Perc60	0.71	0.75	0.74	0.73	0.76	0.77	0.65	0.69	0.71	0.39	0.38	0.38

Tab. 4: average for statistical scores from 40m to 'vertical range' of SODAR (see tab. 2). 'distance' is the distance in km from model point to SODAR, '# data min' is the number of data available at the 'vertical range' height, 'DIST' is the vectorial distance of model from data averaged over the year. Perc30 and Perc60 are the number of success of the model predicting the wind direction in a range of 30° and 60°.

The data reported in Tab. 4 and in Fig. 3 show that there are not significant differences between models even when the topography is not very simple as in Teolo. The case of S.Giustina has to be considered apart as it is in a closed valley, where all models do very bad in analyzing both wind intensity and direction; in particular LAMA analysis does particularly bad, probably because the grid point of the model is not the best for representing that valley. The results are not very different compared with the results obtained in Pernigotti et al. (2005) where the verification for wind was carried for one year with the surface stations, only RMSE seems to be grater when using the wind profile (about 1.5m/s for surface stations, around 2.5 m/s here).

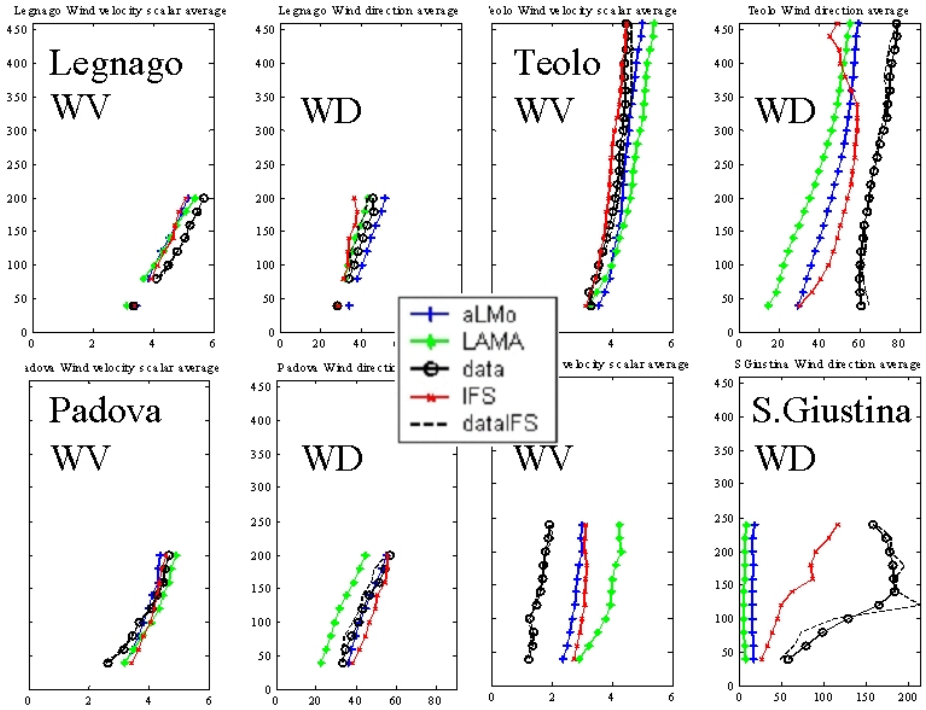

Fig. 3: profiles for annual scalar average for wind intensity (m/s) ;vectorial average for wind direction

5. CONCLUSIONS

The present study show the potential use of the network of profilers for the verification of MetM, especially for air quality application.

The results for wind show that there is not a clear and significant improvement on the long-term analysis with the use of a LAM model instead of a Global Model nor in the flat nor in a mountains valley. Further improvement in complex topography are probably possible with LAM at higher resolution (2km), which seems to be achievable for Lokal Modell in the near future. The use of SODAR data on case study could possibly give more hints on the ability of models in reproducing the wind temporal variability.

The result for temperature profile and inversion analysis is quite surprising, giving that IFS seems to be more able to reproducing the variability of the PBL even in a flat terrain, which could be explained with the grater vertical resolution of this GM compared with LM.

6. AKNOWLEDGMENTS

This work was supported by the European Community, Italian Government and Padua Municipality trough the DOCUP Project and the 'Air pollution in the city of Padua' Project.

Particular thanks are due Jean-Marie Bettems and Emanuele Zala at MeteoSwiss for the aLMo data and to Enrico Minguzzi of ARPA.SIM for the LAMA data.

7. REFERENCES

Ferrario, M.E., Rossa, A.M., Pernigotti, D., Sansone. M., Benassi, A. 2006. Presentation and first assessment of a radiometer network in the Italian region Veneto. Proc. of the Int. Conf. on Urban Climate, Goteborg, 10-16 June 2006.

Fay, B., L. Neunhäuserer, Palau, J. L., Pérez-Landa, G., Dieguez J.J., Ødegaard, V., Bonafè, G., Jongen, S., Rasmussen, A., Amstrup, B., Baklanov, A., Damrath, U. 2005. Evaluation and intercomparison of operational mesoscale models for FUMAPEX target cities. Deliverable D3.4, project FUMAPEX (EVK4-CT-2002-00097).

Rose, T., Crewell, S., Löhnert, U., Simmer, C. 2005. A Network suitable microwave radiometer for operational monitoring of the cloudy atmosphere. Atmospheric Research 75 (2005) 183-200.

Kadygrov, E., Khaikine, M., Miller, E., Shaposhnikov A., Troitsky, A. 2005. Advanced atmospheric boundary layer temperature profiling with mtp-5he microwave system. Teco 2005 Posters.

Jongen, S., Bonafè, G.2006. LAMI verification for air quality forecast and assesment purposes: case studies, spezial measurement campaigns, long term evaluation. ARPA-SIM Internal Report.

Pernigotti, D., Sansone, M., Ferrario, M., 2005. Validation of one-year LAMI model re-analysys on the Po-Valley, northern Italy. Comparison to CALMET model output on the sub-area of the Veneto Region. Proceedings of the Tenth International Conference on Harmonisation within Atmospheric Dispersion Modelling for Regulatory Purposes, HARMO 10, Sissi (Crete, Greece) 17-20 October 2005.

DOCUMENTATION OF THE DIURNAL CYCLE OF PM10 CONCENTRATION FOR THE URBAN SITE OF VENICE-MESTRE

Rossa Andrea, Pernigotti Denise, Ferrario Massimo E., Sansone Maria, and Benassi Alessandro
Institution for all authors: ARPAV-CMT, Via Marconi 55, 35037 Teolo (PD), Italy.
Corresponding author: arossa@arpa.veneto.it

ABSTRACT

Stable boundary layer conditions are long known for causing increasing concentration of pollutant concentrations. In a recent study by the authors, emphasis was given to the documentation of the diurnal cycle of Particulate Matter with diameter < 10μm (PM10) in relation to the atmospheric stability for a high-concentration episode. In this contribution a four-year data set of two-hourly PM10 concentration values measured at the traffic site of Venice-Mestre is analyzed with a specific focus on the intra-diurnal variations. Also, atmospheric static stability observations measured with a radiometer are analyzed when available.
It was found that daily variations of the PM10 concentration often are of the same magnitude, or larger, than the average daily values static stability does play role in the accumulation of PM10, but there seems not to be a linear relation neither with the absolute values nor with the increase of PM10 concentration; a relatively moderate static stability seems to be sufficient to allow significant accumulation, while marked decrease is observed also in strongly stable conditions. PM10 peak concentrations mostly occur in the late evening and early night hours, while the minimum values are more evenly distributed during the day, with preferred occurrence in the early morning and mid-afternoon. On a quantitative note, PM10 intra-diurnal variations between maxima and minima reach 100 $\mu g/m^3$ and obviously depend on the peak concentrations; hourly rates are estimated to reach 20 $\mu g/m^3$/h and more.

INTRODUCTION

Inversions are tied to very stable conditions and therefore inhibit vertical mixing. They are, therefore, long known for causing increasing concentration of pollutant concentrations (e.g. MILIONIS and DAVIES, 1994 and references therein). Presence of a temperature inversion or stable stratification at ground level causes the response of PM10 concentrations to the morning traffic in a much more pronounced way (JANHÄLL et al., 2006), diurnal behaviour of PM10 and PM2.5 are influenced by temperature inversions on episodic basis. In response to the unfortunate climatology of the Po Valley in northern Italy, the Meteorological Centre of Teolo (CMT) of the regional agency of environmental protection of the region Veneto (ARPAV), has recently installed a boundary layer profiler network (Pernigotti et al. 2007), which consists of one HATPRO radiometer, three MTP5-HE radiometers and four PCS-2000 SODAR, mostly funded by the DOCUP 2000-2006 Project. The network is the first of its kind in Italy and its principal applications are in the field of environmental emergency management and regional air-quality short time forecasting.
In a recent study by Pernigotti et al. (2007, P07) the CMT profilers were applied to analyze the diurnal PM10 concentrations in a pollution episode that occurred in particularly stable conditions. In such regimes they found that the intra-diurnal PM10 concentration variations can be much stronger than day-to-day variations of daily averages reaching 100-150$\mu g/m^3$ in just 4 – 6 hours (see Fig. 4 of P07). They propose a schematic mechanism which depends on the daily emission cycle for the interpretation of the diurnal cycle of PM10 concentration in anticyclonic conditions. It accounts for the fundamentally different removal mechanisms of the particulate matter from the atmosphere in stable and unstable conditions, i.e. for the morning and evening emission peaks, respectively. In more detail:

- The peak concentration occurs at around midnight and subsequently decreases during the night when emissions are significantly reduced, and probably trough deposition and chemistry of this pollutant. This reduction takes place while the boundary layer stability is still increasing, which yields an anticorrelated behaviour.
- The morning emission peak occurs in stable conditions so that the PM10 concentration increases (JANHÄLL et al., 2006), but is counteracted by the destabilization of the boundary layer during the morning hours. Consequently, the resulting concentration signature, which does not always show as a distinct maximum, is much lower compared to the peak of the night and occurs before noon.
- The minimum concentration values are reached mid afternoon when the emissions are lower and stability is at its minimum.
- The main and sharp build-up of the PM10 concentration values comes about when the evening emissions due to traffic, including re-suspension, and other sources are coincident with the stabilization of the boundary layer and are not diluted through vertical mixing.

This mechanism does not account for aerosol chemistry, which plays an important role in the production of secondary PM. In this contribution the diurnal variability of PM10 concentration is further documented for the traffic station of Venice-Mestre analyzed in P07, which features two-hourly measurements since 2003.

Particular attention is given to the time of the day when the maximum and minimum concentration values are attained. In section 2 the data set and the approach are described, results are presented in section 3, while a summary and an outlook on further work follows in the final section.

DATA SET AND APPROACH

In this study we focus on the relation between static stability and PM10 concentration evolution at the Venice-Mestre site. The closest thermal profile is measured in Padua, a city some 25km west of Venice, with an MTP5-HE radiometer, manufactured by Attex (Russia) and distributed by Kipp & Zonen (NL). It is a well proven and robust instrument that measures temperature up to 1000m with a vertical resolution of 50m and a time resolution of 5'. Data availability in the first year of deployment is quite high for the Padua site with 97% with a nominal accuracy of 0.3-0.4K for adiabatic and 0.8-1.2K for inversion conditions (FERRARIO et al., 2006). The particulate matter with diameter lower than 10 μm (PM10) are measured every two hours with an ENVIRONNEMENT MP101M, using the method of beta-ray attenuation; the daily average are validated trough comparison with a near by gravimetric instrument. The MP101M is located in the centre of Venice-Mestre, a city close to Venice. For this study a four-year time series of two-hourly measurements are available, as well as temperature profiles for a full year starting 1 Apr 2005.

RESULTS

A high-concentration episode, the strongest of the analyzed data set, occurred in Venice-Mestre in the Christmas week 2005 when a stable high pressure system persisted for several days (see P07 for more details). Figure 1 shows the PM10 concentration evolution for this period with values below 50 μg/m^3 at the 19th that increased over the next days to 150 μg/m^3 around noon, and peaks over 200 μg/m^3 during the night. Eventually, on the 26th the synoptic conditions changed and brought the episode to an end. One very obvious feature of this evolution is the pronounced diurnal cycle, both of the PM10 concentration and the PBL stability.

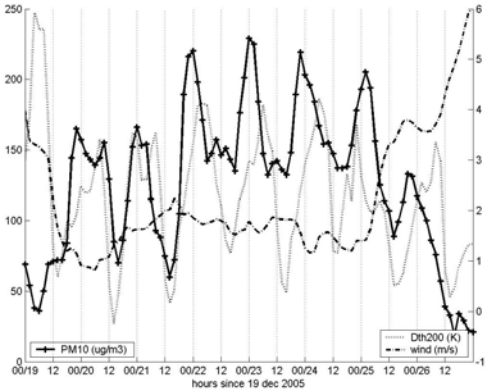

Figure 1 :19-26 dec 2006, 2h-ly data, left axis for PM10, right axis for difference of potential temperature between 200m and ground level in K, and wind at 100m above ground in m/s.

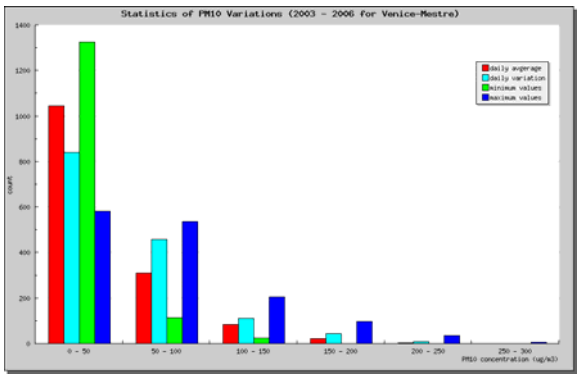

Figure 2 Daily average, maximum daily variation, minimum, and maximum values of PM10 concentration measured at the traffic station Venice-Mestre for the period 1 Jan 2003 – 31 Dec 2006. The measurements are made for two-hourly intervals**.**

Figure 2 summarizes a more systematic documentation of the two-hourly PM10 concentration values of the traffic station Venice-Mestre by looking at an intensity histogram for the period 1 Jan 2003 – 31 Dec 2006. The daily average values (red, leftmost bar) peak for the lowest class of concentration values between 0 and 50 μg/m^3 with a count of over 1000 of a total of 1460, leaving a significant number of days with average values above 50 μg/m^3 (about 300), above 100 μg/m^3 (still about 80), and episodes with concentrations above 150 μg/m^3. The minimum (green, second from the right bar) and maximum (blue, rightmost bar) show that for about one third of the time the concentration does not relax below 50 μg/m^3, while for about one forth of the days maximum daily values are well over 100 μg/m^3. It is noteworthy that the significant daily variations present in the 2005 Christmas episode seem not to be exceptional, in that a substantial number of days are found in which daily variations are of similar magnitude, or larger, that the daily average concentration values. This seems to be especially true for concentrations above 50 μg/m^3.

The timing of the peak and minimum values in the Christmas episode is another salient aspect of the diurnal PM10 concentration that is found in the entire in the entire data set (Fig. 3). As a matter of fact the largest part of the peak values with an amplitude of at least 30 µg/m^3 are attained in the evening and night hours between 20 and 02 (local time). There is a minimum of the peaks at 06 stability is largest, and in the afternoon, when atmospheric mixing is largest. The minimum values, on the other hand, have a less distinct diurnal distribution, but tend to cluster in the early morning and mid-afternoon hours.

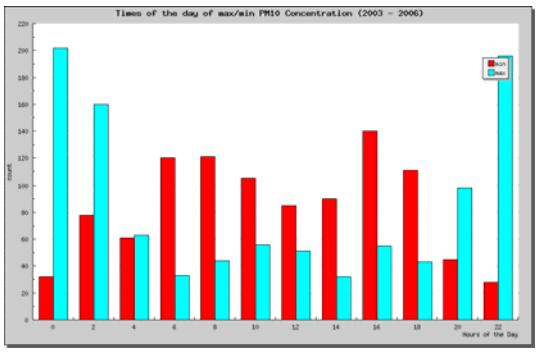

Figure 3 Histogram of time of the day of relative minimum (red, left bars) and maximum (cyan, right bars) values of PM10 concentration (counted extrema > 30 µg/m^3).

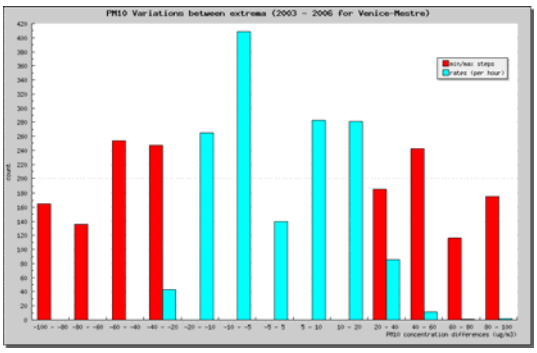

Figure 4 PM10 variations between adjacent minima and maxima (> 30 µg/m^3). Red bars (left) denote the absolute variation, while the cyan bars (right) denote the rate of change per hour of the same variations.

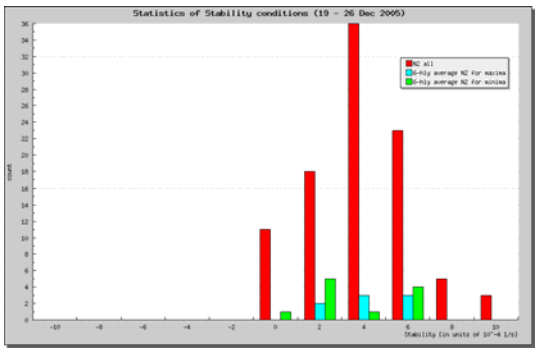

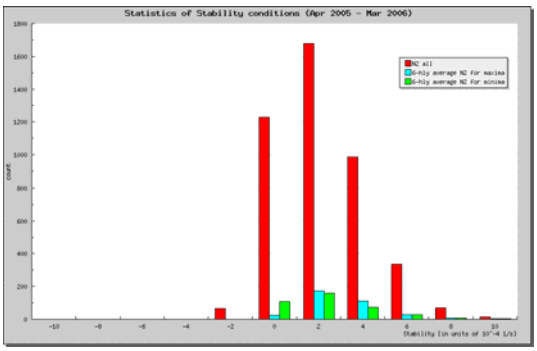

Figure 5 Atmospheric static stability in terms of the Brunt-Vaisala frequency N^2 in 10^4/s for the Christmas 2005 episode (left panel) and the year 1 Apr 2005 – 31 Mar 2006 (right panel). The red and leftmost bars denote all stability values, while the cyan/middle and the green/rightmost bars denote static stability at the time of minimum and maximum PM10 concentration, respectively.

Figure 5 summarizes the static stability conditions for the Christmas 2005 episode as well as for the year 1 Apr 2005 – 31 Mar 2006 evaluated between the ground and 200m height from the temperature profiles measured by the radiometer of Padua. Firstly, it can be seen that there seem to be relatively few conditions which are statically unstable, while the most populated stability classes are between 0 and 4 times 10^{-4} and even very stable situation very rarely reach 10 times 10^{-4}. The static stability values for the times of peak concentrations are very similar to those found for minimum concentration, except for the weakly stable class 0, when very few maxima occur. Most PM10 peaks, however, occur in moderately stable condition, while minimum concentration values can be found even in strongly stable conditions. This is in agreement with the conclusions of P07 who claim that the diurnal PM10 cycle cannot be explained with atmospheric parameters alone but need to take into account the emission cycle which, in the case of a traffic station features a distinct morning-evening-peak behaviour. As a last part of the documentation of the diurnal cycle we look the intensity of the PM10 accumulation and dilution between extrema. Figure 5 shows that in absolute values variations between 40 and 100 µg/m^3 are almost equally frequent, while the PM10 rate of change per hour are confined by 20 µg/m^3/h in both directions, which occasionally larger values.

The mean daily average PM10 concentration (all in µg/m^3) for the entire four-year period is 42 with a variance of 34. The mean daily minimum 19 with a variance of 25, while the mean peak concentration is 71 with a variance of 52 with a fair correlation of 0.66 between the two series. The mean daily variation of

PM10 amounts to 52 with a variance of 40 and correlates very well with the peak concentrations featuring a coefficient of 0.88. Looking for a relation between PM10 concentration and static stability seems not to be straight forward. For the Christmas 2005 episode the correlation between the PM10 increase that leads to the peak values and the six-hourly average of the static stability preceding the peak yields a correlation coefficient of 0.88. The PM10 drops that lead to the minimum values with the same stability measure yields 0.64. Analysis for the year 1 Apr 2005 – 31 Mar 2006, on the other hand, gives moderate correlation coefficients of 0.26 and 0.09 for the static stability and the peak and minimum values, respectively.

SUMMARY AND OUTLOOK

In the present paper the two-hourly PM10 concentration measurements for the traffic station Venice-Mestre is documented with a particular focus on the diurnal cycle. Features found in Pernigotti et al (2007) in an episode could be recognised in the four years worth of data. In particular:

- there are a significant number of days (about 400 in 4 years) with PM10 concentrations above 50 $\mu g/m^3$;
- daily variations of the PM10 concentration often is of the same magnitude, or larger, than the average daily values;
- static stability does play role in the accumulation of PM10, but there seems not to be a linear relation neither with the absolute values nor with the increase of PM10 concentration; rather, a relatively moderate static stability appears to be sufficient to allow significant accumulation, while marked decrease is observed also in strongly stable conditions;
- PM10 peak concentrations mostly occur in the late evening and early night hours, while the minimum values are more evenly distributed during the day, with preferred occurrence in the early morning and mid-afternoon;
- PM10 variations between maxima and minima reach 100 $\mu g/m^3$ and clearly depend on the peak concentrations; hourly rates are estimated to reach 20 $\mu g/m^3/h$ and more.

From this perspective it becomes evident that explaining the diurnal variations of PM10 concentration is more complex that trying to relate day-to-day variations. The emission cycle as well as aerosol chemistry are likely to play a fundamental role in governing the significant variability of the intra-diurnal PM10 concentration variability.

ACKNOWLEDGMENTS

This work was supported by the European Community, Italian Government and Padua Municipality trough the DOCUP Project and the 'Air pollution in the city of Padua' Project. Particular thanks are due to Massimo Bressan of the ARPAV-Padua Department for the data of radiometer and SODAR and to the ARPAV-Venice Department for the data of PM10 concentrations.

REFERENCES

FERRARIO, M.E., A. M. ROSSA, D. PERNIGOTTI, M. SANSONE, A. BENASSI, 2006: Presentation and first assessment of a radiometer network in the Italian region Veneto -- Proc. of the Int. Conf. on Urban Climate, Goteborg, 10-16 June 2006.

JANHÄLL, S., K. F. G. OLOFSON, P. U. ANDERSSON, J. B.C. PETTERSSON, M. HALLQUIST, 2006: Evolution of the urban aerosol during winter temperature inversion episodes.-- Atmospheric Environment. **40**, 5355-5366.

MILIONIS, A.E., T. D. DAVIES, 1994: Regression and stochastic models for air pollution—II. Application of stochastic models to examine the links between ground-level smoke concentrations and temperature inversions -- Atm. Env. **28**, 2811-.2822.

PERNIGOTTI, D., A. ROSSA, M. FERRARIO, M. SANSONE, A. BENASSI, 2007: Influence of PBL stability on the diurnal cycle of PM10 concentration. Submitted to Meteorologische Zeitschrift.